Rab4 and Rab10 Oppositely Regulate AMPA Receptors Exocytosis and Structural Plasticity in Single Dendritic Spines

by

Jie Wang

Department of Neurobiology
Duke University

Date:_____

Approved:

_____
Ryohei Yasuda, Supervisor

_____
Scott Soderling, Co-supervisor

_____
Fan Wang

_____
Anne West, Chair

Dissertation submitted in partial fulfillment of
the requirements for the degree of Doctor of Philosophy
in the Department of Neurobiology in the Graduate School of
Duke University

2016

ABSTRACT

Rab4 and Rab10 Oppositely Regulate AMPA Receptors Exocytosis and Structural Plasticity in Single Dendritic Spines

by

Jie Wang

Department of Neurobiology
Duke University

Date:_____
Approved:

_____
Ryohei Yasuda, Supervisor

_____
Scott Soderling, Co-supervisor

_____
Fan Wang

_____
Anne West, Chair

An abstract of a dissertation submitted in partial
fulfillment of the requirements for the degree of Doctor of Philosophy
in the Department of Neurobiology in the Graduate School of
Duke University

2016

Abstract

Membrane trafficking in dendritic spines is critical for regulating the number of channels and spine structure during synaptic plasticity. Here I report two small Rab GTPases, Rab4 and Rab10, oppositely regulate AMPA receptors (AMPARs) trafficking and structural plasticity of dendritic spines. Combining two-photon glutamate uncaging with two-photon fluorescence lifetime imaging microscopy (2pFLIM), I found that Rab4 is transiently activated whereas Rab10 is persistently inactivated in the stimulated spines during structural long-term potentiation (sLTP). Inhibition of Rab4 signaling has no effect on GluA1 endocytosis but inhibits activity-dependent GluA1 exocytosis. Conversely, disruption of Rab10 signaling inhibits GluA1 endocytosis while enhancing activity-dependent GluA1 exocytosis. In summary, these results uncover a new mechanism to establish the specificity and directionality of AMPARs trafficking and sLTP via distinct regulations of Rab4 and Rab10 signaling.

Dedication

This dissertation is dedicated to my dear parents for their love and supports all the time.

Contents

List of Figures

List of Abbreviations

2p	two-photon
ACSF	artificial cerebrospinal fluid
Akt	protein kinase B
AMPARs	α-amino-3-hydroxy-5-methyl-4-isoxazole-propionic acid receptors
AP2	assembly polypeptide 2
AP5	D-(-)-2-Amino-5-phosphonopentanoic acid
ATD	amino-terminal domain
BBF	basal binding fraction
BF	binding fraction
CA	constitutive activated
CA1	cornu ammonis 1
CA3	cornu ammonis 3
Ca^{2+}	calcium
CaMKII	calcium/calmodulin-dependent kinase II
CCVs	clathrin-coated vesicles
C. elegans	*Caenorhabditis elegans*
CN21	derived from CaM-KIIN amino acids 43–63
CNS	central nervous system
CNIH-2	cornichon-2

CNIH-3	cornichon-2
CREB	cyclic adenosine monophosphate response element–binding protein
CTD	carboxyl-terminal domain
DAG	diacylglycerol
DG	dentate gyrus
DMSO	dimethyl sulfoxide
DN	dominant negative
EC	entorhinal cortex
EEA1	early endosome antigen 1
Elk-1	E26-like transcription factor-1
EPSC	excitatory postsynaptic current
ER	endoplasmic reticulum
ERK	extracellular signal-regulated kinase
F-actin	filamentous actin
FLIM	fluorescence lifetime imaging microscopy
FRAP	fluorescence recovery after photobleaching
FRET	förster resonance energy transfer
GAP	GTPase-activating protein
GDI	GDP dissociation inhibitor
GDF	GDP dissociation inhibitor displacement factor

GDP	guanosine diphosphate
GEF	guanine nucleotide exchange factor
GGT	geranylgeranyl transferase
GLR-1	glutamate receptor 1 homolog in *Caenorhabditis elegans*
GluA1	glutamate receptor 1
GLUT4	glucose transporter type 4
GTP	guanosine triphosphate
IUE	*in utero* electroporation
LatA	latrunculin A
LBD	ligand-binding domain
LTD	long term depression
LTP	long term potentiation
MAPK	mitogen-activated protein kinases
mCh	monomeric Cherry
MDCK	Madin-Darby Canine Kidney
mEGFP	monomeric enhanced green fluorescent protein
M6PRs	mannose-6-phospate receptors
MEK	mitogen-activated protein kinase kinase
Mg^{2+}	magnesium
MNI-glutamate	4-methoxy-7-nitroindolinyl-caged-L-glutamate

mTurquoise2	monomeric Turquoise2
mVenus	monomeric Venus
HDR	Homology-directed repair
NMDA	*N*-Methyl-D-aspartic acid
NMDARs	*N*-methyl D-aspartate receptor
PAM	protospacer adjacent motif
PBS	phosphate-buffered saline
PH domian	pleckstrin homology domain
PI3K	phosphoinositide-3-kinase
PIP_2	phosphoinositide-4, 5-biphosphate
PIP_3	phosphoinositide-3, 4, 5-trisphosphate
PKC	protein kinase C
PSD	postsynaptic density
Rab11-FIP2	Rab11 family interacting protein 2
Rabep1	Rab GTPase-binding effector protein 1
RasGRS	Ras-guanine-nucleotide releasing factor
RBD	Rab binding domain
RCP	Rab coupling protein
REP	Rab escort protein
RILP	Rab-interacting lysosomal protein
RT	room temperature

SEP	superecliptic pHluorin
sgRNA	single-guide RNA
sLTP	structural long term potentiation
ssODNs	single-strand oligodeoxynucleotides
TARPs	transmembrane AMPAR regulatory proteins
TeTxLC	tetanus toxin light chain
TGN	*trans*-Golgi network
TMD	transmembrane domain
TrkB	tyrosine receptor kinase B
TTX	tetrodotoxin
UTR	untranslated region
VDCCs	voltage-dependent calcium channels
WT	wild type

Acknowledgements

I would like to express my deepest gratitude to my advisor Dr. Ryohei Yasuda for his guidance throughout my graduate school. His passion for science, creativity, critical thinking and diligence set a good example of scientist for me to learn from. Particularly, his optimistic attitude and open mind in science have great influence on me. Although I am an "immature" graduate student, he always encourages and supports me to explore various directions in science. From those explorations and following discussions, I learned not only the techniques, but also the way of thinking and solving problems, both of which make me more confident as a scientist.

I am also deeply grateful to my thesis committee members, Dr. Scott Soderling, Dr. Fan Wang, Dr. Anne West and the former member Dr. Sridhar Raghavachari, for their valuable inputs and helps during my entire graduate school. I benefited a lot from their insightful and critical feedbacks for my thesis project, as well as their sincere advices for my career development. I will always remember those "prelim days" when they helped the "naïve me" to format my proposal and refine my presentation with great patience. I will also remember those "inspiring" committee meetings when I felt a little directionless about my project. Without their caring and help, this thesis cannot be finished.

I would like to thank all the Yasuda Lab members that overlapped with me for their helps and supports: Jui-yun Chang, Lesley Colgan, Paul Evans, Nathan Hedrick,

Mo Hu, Rishabh Kasliwal, David Kloetzer, Tal Laviv, Kathy Liu, Takayasu Mikuni, Corey Moran, Tavita Garrett, Jun Nishiyama, Ana Oliveira, Eugene Park, Paul Evans, Paula Parra-Bueno, Michael Patterson, Rohit Ramnath, Monica Reum, Jaime Richards, Mikihiro Shibata, Myung Shin, Michael Smirnov, Ye Sun, Erzsebet Szatmari, Ada Tang, Airong Wang, Hong Wang, Boram You and Shenyu Zhai. Particularly, I would like to thank Paula Parra-Bueno for doing the electrophysiology experiment; Erzsebet Szatmari for doing the western blot experiment in Figure 12; Kathy Liu for helping me do the localization experiment in Figure 33 and encouragement; Tal Laviv for doing the in utero electroporation for electrophysiology experiment; "Lab sister" Jui-yun Chang for discussion and spiritual support; Jun Nishiyama for teaching me molecular cloning and dissociated neuron culture techniques; Nathan Hedrick, Rohit Ramnath and Michael Patterson for teaching me how to do two-photon microscopy imaging when I first joined the lab; Jaime Richards for technician support and David Kloetzer for awesome lab management, help and encouragement.

I would like to thank all my colleagues at both Duke University and Max Planck Florida Institute for helps and supports. Particularly, I would like to thank Boris Kantor and Marguerita Klein at Duke University Viral Vector Core for lentivirus production; Long Yan at the light microscopy facility of Max Planck Florida Institute for confocal training and two-photon microscopy training; Ute Hochgeschwender at Duke

University for generating Rab10 transgenic mice; Minida Dowdy and Jenny Yu at Max Planck Florida Institute for the verification and breeding of Rab10 transgenic mice.

I would like to thank my friends in the neurobiology family at Duke, particularly Catherine Hueston and the Hueston family, Rohit Ramnath, Nathan Hedrick, Bin Yin, Yilei Cai, Cynthia Hsu, Ted Stanek, Jessica Bolton, Manu Raghavan and Anders Nelson. I feel really lucky to have so many awesome friends in the department when I first came to the US, an entirely different culture. With them, I accomplished many "first times in life": the first camping, the first Christmas, the first pumpkin carving, the first Duke basketball game, the first American wedding, and the first alcohol drinking…They made me feel like in a family during my first days in the US, which will be my forever memories in life.

I would like to thank my parents for their unconditioned love and supports all the time. Their encouragements give me the courage to pursuit my dream bravely. I would also like to thank my boyfriend Yi Miao, whose spiritual support, calmness and encouragement over long distance helped me go through the most difficult moments with confidence.

Chapter 1. Introduction

1.1 Long-term potentiation of synaptic transmission

1.1.1 History of LTP

How do our brains encode and store memory? This fascinating question has attracted attentions of neuroscience community since long time ago. In the 19th century, Ramón y Cajal proposed that memory was stored by strengthening the communications between neurons instead of increasing the number of neurons (Cajal, 1894). In 1949, Hebb proposed that repeatedly or persistently presynaptic stimuli could cause an increase in the synaptic efficacy (Hebb, 2005), which is the famous Hebbian theory -- "neurons that fire together, wire together".

Due to technique limitation, it was not until 1966 that long term potentiation (LTP) was discovered, which provided the experimental evidence for the abovementioned theories. In the hippocampus of anesthetized rabbit, Terje Lømo found that brief trains of stimuli in the presynaptic perforant pathway results in increased efficiency of transmission in the postsynaptic dentate gyrus cells (Lømo, 2003). In 1973, Terje Lømo and Timothy Bliss published the first paper about the characterizations of LTP (Bliss and Lømo, 1973). Later, LTP could be reliably induced in acute slices prepared *in vitro* (Andersen et al., 1977), which initiated various mechanistic studies such as pharmacological and genetic manipulations on LTP (Malenka, 2003). Although LTP was first discovered in the hippocampus, later researches proved the existence of

LTP in many other brain regions, such as cortex, cerebellum and amygdala (Clugnet and LeDoux, 1990; Laroche et al., 1990; Salin et al., 1996; Stripling et al., 1988). For decades, there was a vigorous debate over the pre- or post- synaptic locus of LTP expression. Nowadays most neuroscientists agree that both mechanisms are involved. The simplest presynaptic mechanism is to increase the probability of neurotransmitter release, whereas the simplest postsynaptic mechanism is to enhance AMPA receptors (AMPARs) function or increase AMPARs number (Malenka and Nicoll, 1999).

In 1970s and early 1980s, three key features of LTP were elucidated (Bliss and Collingridge, 1993; Malenka, 2003). Firstly, LTP is cooperative, which means that a threshold stimulus intensity during high-frequency stimulation is required to induce LTP (McNaughton et al., 1978). This property can be explained in the NMDARs-dependent LTP: the postsynaptic neurons must be sufficiently depolarized to pump out Mg^{2+} from NMDARs and allow Ca^{2+} influx to induce LTP. Secondly, LTP is input-specific. LTP is only induced at one set of synapses while nearby synapses without a history of activation show no potentiation (Andersen et al., 1977). However, following studies found that there is no "input specificity" at a distance of less than 70 μm (Engert and Bonhoeffer, 1997). Thirdly, LTP is associative, which means that sub-threshold stimuli can also induce LTP if there is a concurrent strong LTP-inducing stimuli at the nearby synapses of the same neuron (Levy and Steward, 1979; McNaughton et al., 1978).

These three interesting properties ensure LTP to be the dominant cellular mechanisms for learning and memory.

1.1.2 Schaffer collateral LTP of hippocampus

1.1.2.1 Structure and circuit of hippocampus

Hippocampus is the key structure for learning and memory. It is located in the medial temporal lobe of the brain with a similar shape to sea horse. One distinct feature of hippocampus is the "trisynaptic circuit" including the perforant path-dentate gyrus-CA3-CA1 pathway (Andersen et al., 1971). The major external inputs to hippocampus come from the layer II entorhinal cortex (EC) through the perforant pathway and arrive at the dentate gyrus (DG). Granule cells in the DG project axons to the CA3 pyramidal neurons via the mossy fiber pathway, which is further relayed by the Schaffer collaterals pathway and terminate at the CA1 pyramidal neurons. In turn, CA1 pyramidal neurons project to the subiculum, which projects to the deep layer of EC and is the final stage of the pathway (Figure 1).

Since my thesis project is about the structural plasticity in the hippocampal CA1 pyramidal neurons, I will mainly focus on LTP at the CA3-CA1 synapses of rat hippocampus. Morphologically, both CA3 and CA1 pyramidal neurons have the basal and apical dendrites, as well as an apical tuft. The basal dendrites are in general shorter than the apical dendrites, and the apical dendrites usually bifurcate before reaching the tuft. However, there are several morphological differences between CA1 and CA3

neurons. Firstly, the soma of the CA1 pyramidal neurons is triangle shaped while that of CA3 pyramidal neurons is more round shaped. Secondly, the branches of CA3 pyramidal neurons apical dendrites are closer to the soma than those of CA1 pyramidal neurons. Thirdly, CA3 pyramidal neurons have many "petal shaped" large spines in the first 100 μm of the apical dendrite (Figure 2)(Spruston, 2008).

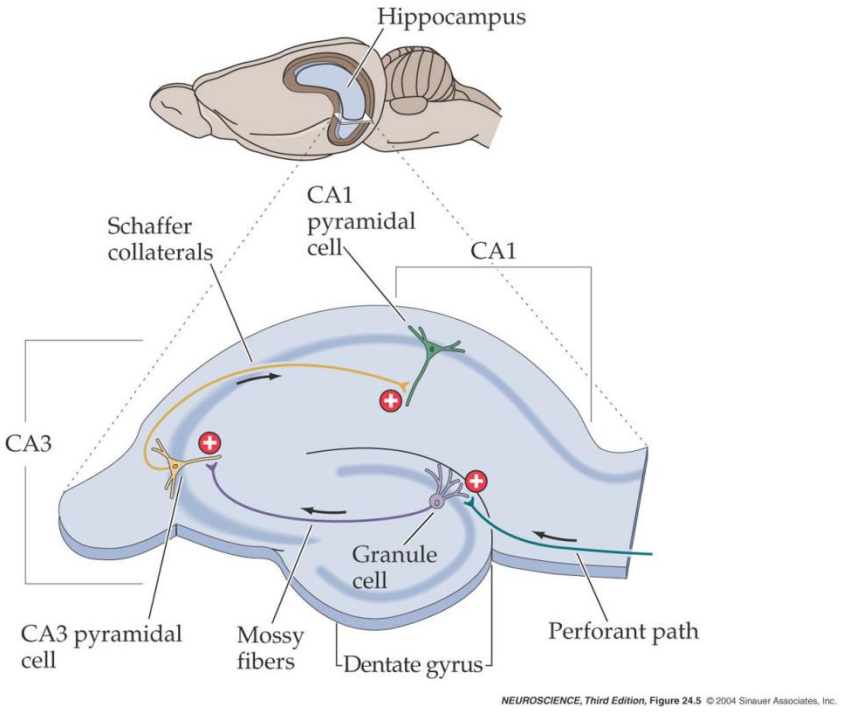

Figure 1 Diagram of rodent hippocampus with major regions, pathways and connections.

Adapted from (Purves et al., 2004).

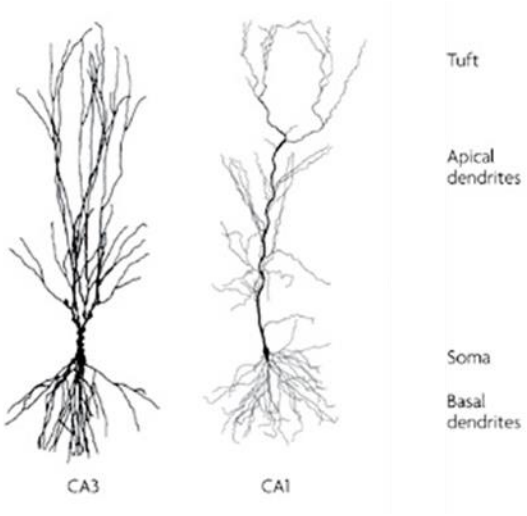

Figure 2 The structures of CA3 and CA1 pyramidal neurons in the hippocampus of rat

Modified and adapted from (Spruston, 2008)

1.1.2.2 Induction of LTP at hippocampal CA3-CA1 synapses

LTP can be induced by high-frequency stimulation of synapses or paring the postsynaptic depolarization with low frequency stimulation (Malenka and Nicoll, 1999). In basal low-frequency synaptic transmission, AMPA receptors (AMPARs) mediate the majority of basal postsynaptic response while NMDA receptors (NMDARs) contribute little. However, in high-frequency synaptic transmission, NMDARs activation is required to trigger LTP. The experimental evidence is: NMDARs antagonist has little effect on basal synaptic transmission but completely blocks LTP (Bliss and Collingridge, 1993; Malenka and Nicoll, 1999; Nicoll and Malenka, 1995). There are two requirements to activate NMDARs during LTP. Firstly, the postsynaptic cells need to be sufficiently

depolarized to remove the Mg^{2+} blocking the NMDARs. Secondly, L-glutamate binds to NMDARs, which opens NMDARs to trigger Ca^{2+} influx and LTP.

It is a general consensus that postsynaptic rise of Ca^{2+} plays an important role in the induction of LTP. Intracellular injection of Ca^{2+} chelators can block the induction of LTP, while photolysis of postsynaptic caged Ca^{2+} can mimic LTP (Lynch et al., 1983; Malenka, 1988; Malenka et al., 1992). The major sources of intracellular Ca^{2+} include Ca^{2+} influx through NMDARs and voltage-dependent Ca^{2+} channels (VDCCs), as well as Ca^{2+} release from intracellular source (Kumar, 2011). In CA1 hippocampal synapses, although the VDCCs, intracellular source and other glutamate receptors can regulate the Ca^{2+} level in the dendritic spines (Dingledine et al., 1999; Jaffe et al., 1994; Korkotian and Segal, 1999), NMDARs-mediated Ca^{2+} influx is the major source for LTP induction. So from now on, I will mainly focus on the NMDARs-dependent LTP in CA1 hippocampal synapses.

1.1.3 Signal transduction mechanisms of LTP

The signaling pathways underlying the NMDARs-dependent CA3-CA1 LTP have been intensively studied. NMDARs are embedded in the postsynaptic density (PSD), which contains various scaffolding proteins and signaling molecules (Sheng and Kim, 2002). At the resting membrane potential, NMDARs are blocked by extracellular Mg^{2+}. During LTP induction stimuli, Mg^{2+} is pumped out by postsynaptic depolarization. Simultaneously, L-glutamate binding activates NMDARs and triggers Ca^{2+} influx, which

further triggers various protein cascades and leads to LTP expression. In this section, I will focus on several key proteins involved in LTP.

1.1.3.1 CaMKII in LTP

Ca^{2+}/calmodulin-dependent protein kinase (CaMKII) is a Ser/Thr protein kinase, and is highly abundant in hippocampus, comprising about 2% of the total protein (Erondu and Kennedy, 1985). Previous studies have shown that CaMKII is necessary for LTP. Pharmacological inhibitions of CaMKII by various inhibitors, such as KN62 and CN21, block LTP (Ito et al., 1991; Sanhueza et al., 2011). Furthermore, genetic deletions of CaMKII subunits impair LTP, as well as learning and memory in mice (Borgesius et al., 2011; Silva et al., 1992a; Silva et al., 1992b). In addition, CaMKII is also sufficient for LTP. Perfusion of activated CaMKII into CA1 cells mimics the effects of LTP, and occludes further LTP, indicating that CaMKII and LTP share the same mechanism to affect synaptic efficacy (Lisman et al., 2002; Lledo et al., 1995; Pettit et al., 1994).

Structurally, CaMKII is a dodecamer with each subunit composed of three domains, a catalytic domain, an autoinhibitory domain, a variable segment and a self-association domain (Lisman et al., 2002). The autoinhibitory domain contains a pseudosubstrate region that can bind to the catalytic domain at the substrate-binding site and inhibit CaMKII activity. In absence of Ca^{2+} and cammodulin, autoinhibitory domain binds to the catalytic domain, locking CaMKII in the "closed" state. After NMDARs activation, Ca^{2+} binds to calmodulin, which in turn binds to CaMKII at a

region overlapping with the pseudosubstrate region, and releases CaMKII into the activated "open" state (Lisman et al., 2002). One interesting feature of CaMKII is the autonomous phosphorylation mediated by the T286 phosphorylation, which makes CaMKII activity persistent even after Ca^{2+} and calmodulin dissociation (Miller and Kennedy, 1986). T286A knock-in mice shows deficits in hippocampal LTP and spatial learning in the Morris water maze, demonstrating that T286 phosphorylation is important for LTP and learning and memory (Giese et al., 1998).

Activated CaMKII can be translocated to the PSD and bind to the C-terminal of NMDAR NR2B subunit, which locks CaMKII in an active conformation (Bayer et al., 2001). In addition, CaMKII can also interact with other proteins in PSD, such as densin 180, α-actin, SAP97 and multiple PDZ domain protein (Krapivinsky et al., 2004; Lisman et al., 2012; Nikandrova et al., 2010; Strack et al., 2000; Walikonis et al., 2001). It is possible that translocation of the activated CaMKII into PSD increases the anchoring sites for AMPARs by interacting with AMPAR-binding proteins. Furthermore, CaMKII can directly regulate AMPARs function and trafficking during LTP. Firstly, CaMKII can phosphorylate AMPARs subunit GluR1 at Ser831 and increase AMPAR conductance. Secondly, CaMKII can increase AMPRs insertions to synapse via phosphorylation of stargazin (Lisman et al., 2012). I will describe regulations of AMPARs by CaMKII in details in Chapter 1.3.

1.1.3.2 Ras-ERK pathway in LTP

Ras-ERK is a major postsynaptic signaling pathway in synaptic plasticity. As small GTPases, Ras cycles between the guanosine-5'-triphosphate (GTP)-bound "active" state and the guanosine diphosphate (GDP)-bound "inactive" state. Specific guanine nucleotide exchange factors (GEFs) converts GDP-bound Ras into GTP-bound form. Conversely, specific GTPase-activating proteins (GAPs) convers GTP-bound Ras to GDP-bound form. Ras signaling is required for hippocampal LTP, as dominant negative Ras blocks LTP while constitutive active Ras mimics and occludes LTP (Zhu et al., 2002). However, H-Ras knockout mice showed enhanced LTP (Manabe et al., 2000).

Ras activity is regulated by several Ras GEFs and GAPs located in the spines. For example, Ras-guanine-nucleotide releasing factor (RasGRF), an abundant and neuron specific Ras GEF, can relay the Ca^{2+} elevation to activate Ras (Cullen and Lockyer, 2002; Farnsworth et al., 1995). SynGap, a specific Ras GAP that binds to PSD95, negatively regulates Ras activity at excitatory synapses (Chen et al., 1998; Kim et al., 1998). Neurofibromin, a Ras GAP interacting with NMDAR complex in the postsynaptic region (Ballester et al., 1990; Husi et al., 2000), can inactivate Ras in dendritic spines, and its mutation is related with learning and memory deficit (Costa et al., 2002; Oliveira and Yasuda, 2014).

Multiple effector pathways of Ras have been characterized, including phosphoinositide-3-kinase (PI3K) and ERK/MAPK pathways (Cullen and Lockyer,

2002). ERK/MAPK cascade is required for hippocampal LTP and various forms of mammalian learning (Atkins et al., 1998; English and Sweatt, 1997; Selcher et al., 1999; Selcher et al., 2003). It has been shown that AMPARs exocytosis is dependent on the Ras-ERK signaling pathway during structural LTP (Patterson et al., 2010).

1.1.3.3 PKC and PI3K in LTP

Protein kinase C (PKC) was the first identified kinase involved in LTP (Patterson and Yasuda, 2011). PKC injection into hippocampal pyramidal cells elicits features of LTP, indicating that PKC is sufficient for LTP (Hu et al., 1987). Following studies eliminated LTP with various non-specific PKC inhibitors, such as mellitin, polymyxin B, H-7, as well as inhibitory peptide of PKC, demonstrating that PKC is also necessary for LTP (Lovinger et al., 1987; Malinow et al., 1989; Reymann et al., 1988; Wang and Feng, 1992). There are fifteen PKC isoforms in human, which can be classified into conventional, novel and atypical categories based on their dependence of Ca^{2+} and diacylglycerol (DAG)(MELLOR and PARKER, 1998). Several PKC isoforms have been implicated in LTP. For example, conventional PKCγ-mutant mice exhibits diminished LTP, as well as mild deficits in spatial and contextual learning (Abeliovich et al., 1993a; Abeliovich et al., 1993b). In addition, the persistent activated atypical PKMζ is shown to be both necessary and sufficient for LTP maintenance (Ling et al., 2002; Pastalkova et al., 2006).

A more recently identified kinase contributing to LTP is PI3K. PI3K can convert phosphoinositide-4, 5-biphosphate (PIP_2) into phosphoinositide-3, 4, 5-trisphosphate (PIP_3). PIP_3 can further recruit various pleckstrin-homology (PH) domain-containing proteins, such as protein kinase B (Akt) and the serine–threonine kinase PDK1, which further initiate downstream signaling cascades (Cantley, 2002; Wymann and Pirola, 1998). Activation of PI3K is required for NMDAR-dependent LTP via direct interaction with AMPARs in hippocampal CA1 neurons (Man et al., 2003). Moreover, PI3K signaling is required for fear conditioning in the amygdala, as well as retrieval and extinction of contextual memory (Chen et al., 2005; Lin et al., 2001).

1.2 Structural plasticity of dendritic spines

1.2.1 History of dendritic spine study

Dendritic spines were first described by Ramón y Cajal as the contacting sites for neurons in the 19th century (y Cajal, 1888). With Golgi or methylene-blue staining, light microscopy imaging showed that cerebral cortex dendrites have numerous spinous protrusions, which initiated debates over the nature of those protrusions (Fox and Barnard, 1957; Sholl, 1956; y Cajal, 1934). In 1959, an electron microscopy study first proved that dendritic spines are in fact sites of synaptic contact (Gray, 1959). Before the advent of confocal microscopy imaging in living cells, it was thought that the dendritic spines are formed in the embryonic development, and remained stable after birth. However, time-lapse confocal imaging demonstrated the dynamics of the dendritic

protrusions in hippocampal slices (Bonhoeffer and Yuste, 2002; Dailey and Smith, 1996). In the last decade, two-photon laser scanning imaging with fluorescent proteins revealed that the spines are not static, but highly motile, and continuously change their morphology even in the adult brain *in vivo* (Holtmaat et al., 2005; Lendvai et al., 2000; Matus, 2000; Trachtenberg et al., 2002; Yoshihara et al., 2009; Zuo et al., 2005). Finally, reporters of cellular functions, such as Ca^{2+} indicators and GCaMP, have allowed the functional studies of spines in intact living cells (Grienberger and Konnerth, 2012; Helmchen et al., 1999; Nimchinsky et al., 2002; Svoboda et al., 1997; Takahashi et al., 2012).

1.2.2 Morphology and structure of dendritic spines

Dendritic spines are tiny and bulbous membrane protrusions emerging from the dendrites, which contact with the presynaptic axons at synapses and provide structural basis for synaptic transmission and memory storage. Morphologically, most spines contain a spine head (~0.1 fL) and a narrow spine neck (~0.1 μm in diameter and 0.5 μm in length). The spine heads have different shapes: “mushroom”, “thin” and “stubby” (Peters and Kaiserman-Abramof, 1969). The spine neck connects the spine head to the dendritic shaft, and functions as the electrical resistance and diffusional barrier for biochemical signals, isolating the spine head from its parent dendrite (Nishiyama and Yasuda, 2015).

Several kinds of receptors are expressed on the spine surface, including glutamate receptors and TrkB receptors, which sense the presynaptic signals and initiate the postsynaptic signal transduction. One important structure is PSD, an electron-dense region attached to the postsynaptic membrane. PSD is close to the presynaptic active zone, and contains various receptors, channels, and signaling proteins involved in the synaptic transmission and signal transduction. In CA1 hippocampal neurons, the areas of PSDs are proportional to the spine volume, number of AMPARs and NMDARs, as well as the area of the presynaptic active zone (Nimchinsky et al., 2002).

The primary cytoskeleton of dendritic spines is filamentous actin (F-actin), which determines the morphology of the spines. Actin undergoes continuous "treadmilling" between the filamentous F-actin and monomeric G-actin, which ensures the dynamic nature of dendritic spines (Cohen et al., 1985; Fischer et al., 1998; Star et al., 2002). Molecules that regulate actin polymerization and depolymerization, such as Rac1, Cdc42 and RohA, can rapidly modify the spine morphology (Nishiyama and Yasuda, 2015).

1.2.3 Structural LTP induced at a single spine

Due to their "bridge" position between axons and dendrites, dendritic spines have been proposed as mediators of the connective plasticity that underlies learning and memory. Activity-dependent remodeling of the dendritic spines is associated with learning and memory. Many studied have indicated that increases of neuronal activity produce more spines (Roberts et al., 2010; Xu et al., 2009). Furthermore, enlargement and

shrinkage of pre-existing spines are thought to be associated with LTP and LTD, respectively (Hayama et al., 2013; Matsuzaki et al., 2004; Oh et al., 2015).

LTP (sLTP) can be induced at a single dendritic spine by two-photon glutamate uncaging. In zero extracellular Mg^{2+} condition, repetitive quantum-like uncaging of glutamate (1 Hz, 1 min) induces a rapid enlargement of the stimulated spines in CA1 pyramidal neurons, which could be sustained for hours (Matsuzaki et al., 2004). There are several shared properties between sLTP and functional LTP. Firstly, the spine enlargement induced by glutamate uncaging is similar to that induced by high frequency electrical stimulation (100 Hz, 1 s) at the Schaffer-collateral pathway with Mg^{2+}, or low frequency electrical stimulation (2 Hz, 60 s) without Mg^{2+}. Secondly, spine enlargement of sLTP is associated with an increase in AMPARs-mediated currents at the stimulated synapse and is dependent on NMDARs and CaMKII activation, which is similar to functional LTP. Finally, sLTP is also input-specific: the spine enlargement and functional changes are only observed in the stimulated spines, whereas the nearby spines are not potentiated. One advantage of this technique is the robust spine enlargement, which is now considered a reproducible morphological correlate of LTP (Nicoll and Roche, 2013; Nishiyama and Yasuda, 2015).

1.2.4 Signaling computation in structural LTP by 2pFLIM

Signaling pathways involved in LTP have been intensively studied with pharmacological, biochemical and genetic methods as described in Chapter 1.1.3. The

application of 2pFLIM and 2p-glutamate uncaging at single spine resolution provides additional spatiotemporal information of the protein network activities during LTP.

Fluorescence resonance energy transfer (FRET) imaging has been used in cellular studies to report protein-protein interactions (Miyawaki, 2003). Combining with two-photon microscopy imaging, FRET sensors can be applied to study the spatiotemporal activities of proteins in light scattering brain tissue (Yasuda, 2006, 2012). Among different FRET methods, fluorescence lifetime imaging microscopy (FLIM) provides the most robust and quantitative measurement, which is independent of fluorophore concentrations and insensitive to wavelength-dependent light scattering (Yasuda, 2006). As illustrated in Figure 3, a protein of interest is tagged with the donor (GFP), and its binding domain is tagged with the acceptor (mCherry). Fluorophores are excited with a short laser pulse, and only the donor's lifetime is measured. When the donor and acceptor don't interact, the fluorescence decays in single exponential and donor's lifetime is τ_1. When the donor and acceptor bind together, the fluorescence decays in double exponential and donor's lifetime is τ_2. A mixture of free donor and acceptor-bound donor reports a decay time between τ_1 and τ_2. By fitting the fluorescence lifetime decay curve, the percentage of donor binding to acceptor can be calculated as binding fraction.

Combining 2pFLIM and 2p glutamate uncaging, the spatiotemporal dynamics of several proteins have been revealed as shown in Figure 4 (Bosch et al., 2014; Fujii et al.,

2013; Harvey et al., 2008; Lee et al., 2009; Murakoshi et al., 2011; Yasuda et al., 2006; Zhai et al., 2013). Upon glutamate uncaging (0.5 Hz, 45 pulses), Ca^{2+} influx (~ms) through the NMDARs binds to calmodulin, which further binds to and activates CaMKII. CaMKII activation is transient (~1 min) and restricted in the stimulated spines (Lee et al., 2009). Upon high frequency glutamate uncaging (20 Hz, 100 pulses), calcineurin (CaN) is activated (~1 min) in the stimulated spines, which spreads into the nearby spines. In contrast, after low frequency glutamate uncaging (5 Hz, 100 pulses), CaN is activated and restricted in the stimulated spines (Fujii et al., 2013).

Small GTPases H-Ras, Cdc42 and RhoA are all activated (~5 min) in the stimulated spines during sLTP (0.5 Hz, 30 pulses glutamate uncaging), but exhibit distinct spatial patterns. Ras activation spreads ~10 μm along the dendrite and invades into the nearby spines. RhoA activation diffuses out of the stimulated spine and spreads over about 5 μm along the dendrite. However, Cdc42 activation is compartmentalized in the stimulated spine, showing a steep gradient at the spine necks. Furthermore, inhibition of CaMKII signaling impairs the activations of H-Ras, Cdc42 and RohA, indicating that they are downstream of CaMKII (Harvey et al., 2008; Murakoshi et al., 2011). Cofilin is an actin binding protein. Cofilin-cofilin and cofilin-actin FLIM sensors report that cofilin accumulates in the stimulated spines by a stable interaction with F-actin during sLTP (Bosch et al., 2014).

Abovementioned studies showed that signaling induced the stimulated spines can be restricted in the stimulated spines, or spreads to the dendrites over 5 μm to 10 μm. However, signaling initiated in the spines can be integrated and transmitted to the nucleus. It has been shown that induction of sLTP in only three to seven dendritic spines is sufficient to activate ERK in the nucleus, and regulate downstream transcription factors, such as cyclic adenosine monophosphate response element–binding protein (CREB) and E26-like transcription factor-1 (Elk-1) (Zhai et al., 2013).

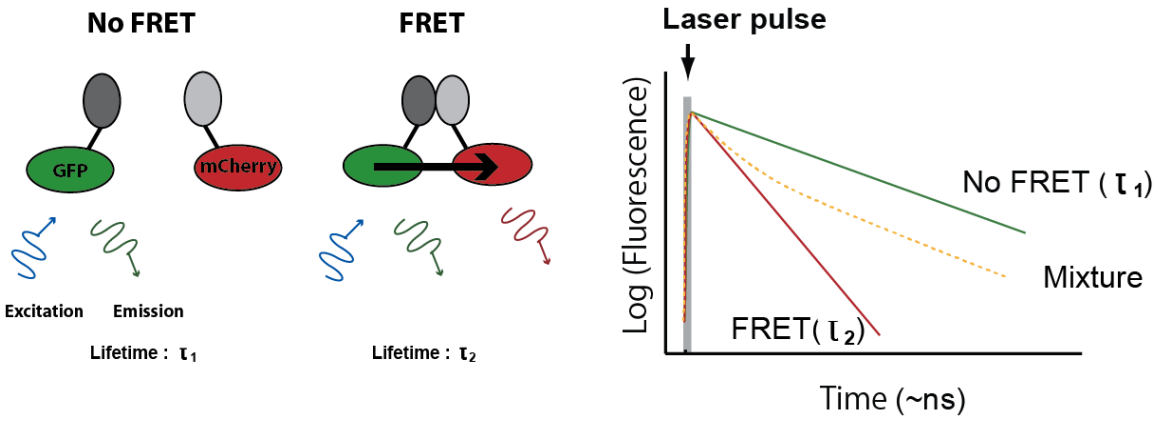

Figure 3 Schematic of FRET and FLIM

Redraw based on (Yasuda, 2012).

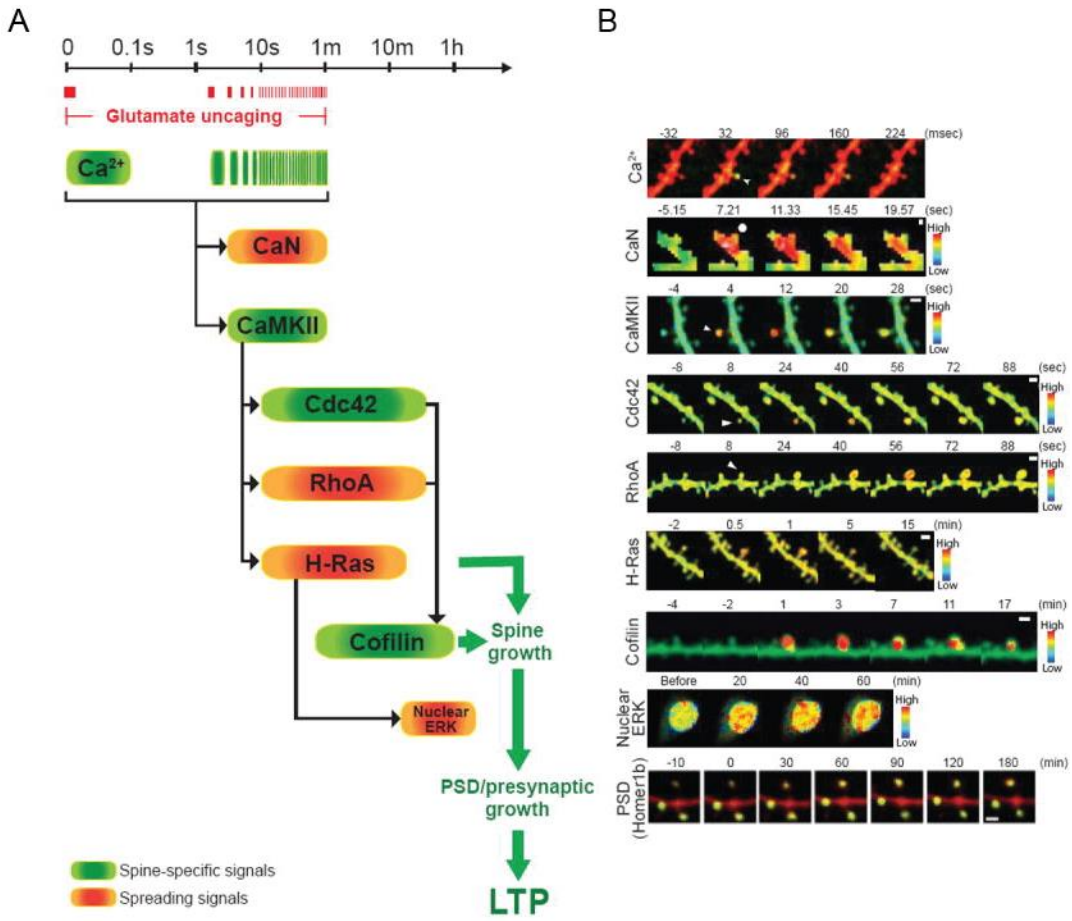

Figure 4 The spatiotemporal dynamics of protein networks during sLTP

(A) Schematic of the signaling timescale during sLTP. Green color indicates spine-specific signals whereas orange color indicates spreading signals.
(B) Representative images of the activation of different proteins during sLTP. Adapted from (Nishiyama and Yasuda, 2015).

1.3 AMPA receptors and LTP

AMPARs are the major ionotropic glutamate receptors that mediate the fast excitatory synaptic transmission in the mammalian brain. One simple way to change synaptic efficacy is to change either the function or the number of AMPARs (Sheng and

Kim, 2002). In this section, I will focus on the properties, phosphorylation, trafficking and auxiliary subunits of AMPARs.

1.3.1 Structure and function of AMPARs

AMPARs are tetrameric combiniations of subunits GluA1 to GluA4. In the hippocampus, AMPARs are mainly composed of GluA1-GluA2 and GluA2-GluA3 heteromers or GluA1 homomers (Lu et al., 2009; Sheng and Kim, 2002; Wenthold et al., 1996). GluA4 is mainly expressed in early development, whereas GluA1, GluA2 and GluA3 expression increases with development (Zhu et al., 2000).

In structure, each subunit of AMPARs contains four domains: the extracellular amino-terminal domain (ATD), the extracellular ligand-binding domain (LBD), the transmembrane domain (TMD), and an intracellular carboxyl-terminal domain (CTD) (Figure 5) (Sobolevsky et al., 2009; Traynelis et al., 2010). Firstly, ATD contains a signal peptide (14-33 residudes) that targets the receptor to the cell membrane and is removed afterwards. Secondly, LBD contains the binding site for agonist like glutamate, which is the first step for receptor activation. LBD have a"clamshell"-like shape with two amino acid segments called S1 and S2 lobes (Stern-Bach et al., 1994). The agonist binding pocket is located between the S1 and S2 lobes. Alternative splicing of LBD results in flip or flop isoforms, which determine the speed of receptor desensitization (Mosbacher et al., 1994; Sommer et al., 1990). Thirdly, AMPARs subunits have four transmembrane domains (M1-M4). Only the M1, M3 and M4 domains pass through the memebrane, and form the

core of the ion channel (Traynelis et al., 2010). However, the M2 domian does not cross the membrane, but either lies close to the intracellular face of the plasma membrane or loops into the membrane without spanning it (Hollmann et al., 1994). Finally, intracellular CTDs are the most structually and functionally divergent regions of all the subunits (Derkach et al., 2007). As shown in Figure 6, the CTDs vary both in length and sequence among different subunits. GluA1, GluA4 and a splice variant of GluA2 (GluA2L) have long CTDs, while GluR2, GluR3 and a splice variant of GluR4 (GluR4c) have short CTDs (Song and Huganir, 2002). CTDs are critical for the regulations of AMPARs function and trafficking. Firstly, CTDs contain several phpsphorylation sites and binding sites of various intracellular signaling proteins. Secondly, CTDs can also interact with scaffolding proteins that recruit signaling proteins or cytoskeletal protein (Collingridge et al., 2004; Derkach et al., 2007; Kim and Sheng, 2004; Nicoll et al., 2006).

In function, AMPARs open and close very fast, at a millisecond timescale, which makes them the ideal candidate to mediate the fast excitatory synaptic transmission in CNS (Platt, 2007). In the adult brain, post-transcriptional RNA editing can modify GluA2, and change glutamine (Q) codon at residue 607 to arginie (R). This conversion renders GluA2 impermeable to Ca^{2+} (Jonas and Burnashev, 1995; Kask et al., 1998). Most AMPARs contain the Ca^{2+} impermeable GluA2 subunit, so the major gated ions are Na^{+} and K^{+}. Upon agonist (like glutamate) binding, the S1 and S2 lobes move towards each other, close the shell and activate the receptor (Armstrong et al., 1998). Endogenous

polyamines can block the GluA2-lacking AMPARs in a voltage dependent manner (Bowie et al., 1998). After neuron depolarization, polyamines can strongly block GluA2-lacking AMPARs and prevent K^+ from fluxing out. So GluA2-lacking AMPARs have the inward rectification, which means that they preferentially pass inward current than the outward current (Derkach et al., 2007).

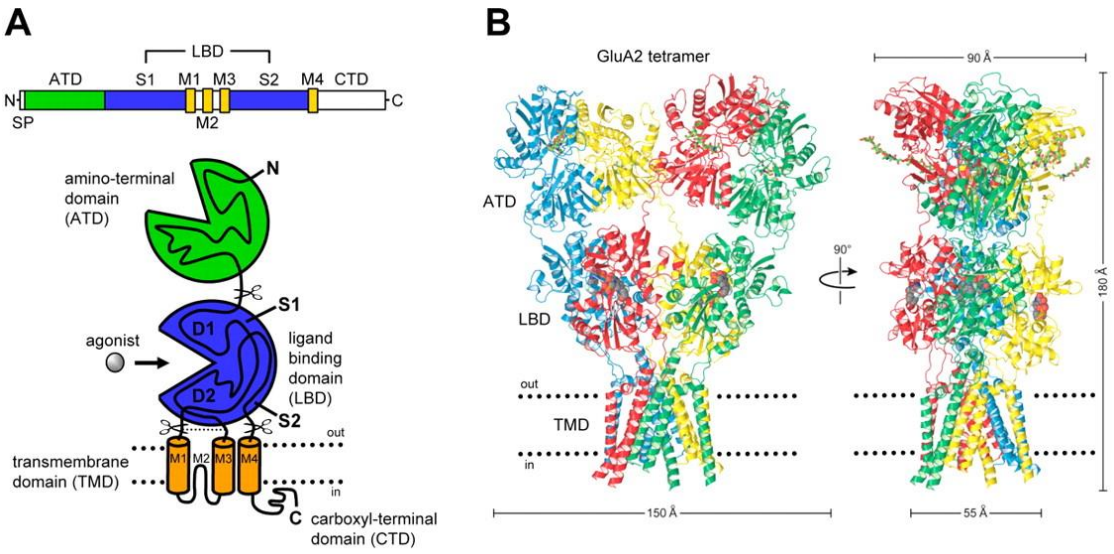

Figure 5 Structure and domain organization of AMPARs

(A) Schematic of the linear subunit domain and domain architecture.
(B) Crystal structure at 3.6 Å of the membrane-spanning tetrameric GluA2 AMPA receptor. Adapted from (Traynelis et al., 2010)

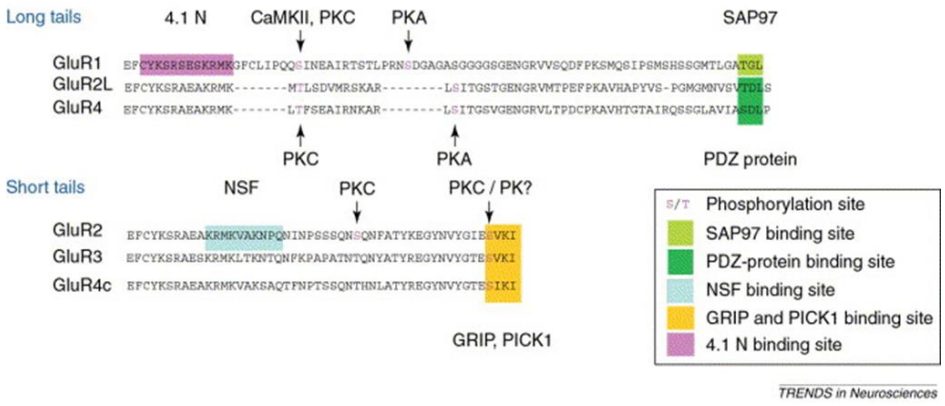

Figure 6 Carboxyl-terminal domains of AMPAR subunits

Adapted from (Song and Huganir, 2002).

1.3.2 AMPARs phosphorylation in LTP and LTD

GluA1-GluA4 subunits could be phosphorylated at serine, tyrosine and threonine residues by various kinases, such as CaMKII, PKC, PKA, PKG and JNK (Huganir and Nicoll, 2013). As shown in Figure 6, the most intensively studied ones are CaMKII, PKC (both at Ser831) and PKA (Ser845) phosphorylation sites on GluA1, and PKC site (Ser880) on GluA2. CaMKII phosphorylation of GluA1 at Ser831 site could decrease the activation energy required for intra-subunit conformational change and ion channel open, thus enhance the channel conductance of AMPARs (Derkach et al., 1999; Kristensen et al., 2011). It has been shown that phosphorylation and dephosphorylation of AMPAR subunits are critical for LTP and LTD expression. For example, induction of LTP in the hippocampus CA1 region is associated with an increase in single-channel conductance of AMPA receptors (Benke et al., 1998), and requires CaMKII phosphorylation of GluA1 at Ser831 site (Barria et al., 1997). Dephosphorylation of a

PKA site (Ser845) on GluA1 is one mechanism for NMDARs–dependent LTD expression (Kameyama et al., 1998; Lee et al., 1998). PKC phosphorylation of GluA2 at Ser880 is critical for the induction of cerebellar LTD (Chung et al., 2003). Furthermore, GluA1 knockin mice at S831 and S845 phosphorylation sites lacks NMDARs-dependent LTD and exhibits reduced LTP in hippocampal CA1 neurons. The mutant mice also has deficit in spatial memory retention (Lee et al., 2003). However, following studies have shown that the phosphorylation at those sites is not required for LTP expression, but are important for the modulation of LTP, lowing the threshold for LTP induction (Hu et al., 2007; Makino et al., 2011).

1.3.3 AMPARs trafficking

1.3.3.1 AMPARs trafficking in LTP and LTD

Tightly regulated AMPARs trafficking in and out of synapses underlies synaptic plasticity, learning and memory. In the hippocampal CA3-CA1 synapses, it is proposed that net insertion of AMPARs to the postsynaptic membrane leads to LTP, whereas net removal of AMPARs from the surface results in LTD (Barry and Ziff, 2002; Bredt and Nicoll, 2003; Malinow and Malenka, 2002; Sheng and Lee, 2001; Song and Huganir, 2002). In 1999, the recruitment of AMPARs into dendritic spines during LTP was directly visualized with time-lapse two-photon laser scanning microscopy (Shi et al., 1999). GFP-GluA1 was transiently introduced into neurons by Sindbis virus. LTP stimulation triggered a rapid delivery of GFP-GluA1 into dendritic spines, which required NMDARs

activation. This study provides a link between AMPARs recruitment and activity-induced forms of plasticity.

1.3.3.2 Subunit-specific AMPARs trafficking

Later studies discovered the subunit-specific regulations of AMPARs trafficking. As described in Chapter 1.3.1, the C-terminal domains of GluA1-GluA4 subunits are variable, which are tightly related with the subunit-specific membrane trafficking. It was found that GluA1-containing AMPARs (GluA1/GluA2) are inserted into synapses during LTP, which requires interactions between GluA1 and PDZ domain proteins. In contrast, GluA2-containing AMPARs (GluA2/GluA3) undergo continuous recycling (Hayashi et al., 2000; Shi et al., 2001). In addition, both GluA1 and GluA2 containing AMPARs are internalized during LTD (Anggono and Huganir, 2012; Kessels and Malinow, 2009). So for a long time, the dominant model in the field is that only GluA1-containing AMPARs are recruited to the synapses during LTP. To further support this model, GluA1 knockout mice showed impaired LTP in CA3- CA1 synapses, while GluA2 and GluA3 double knockout mice showed normal LTP (Meng et al., 2003; Zamanillo et al., 1999). However, a recent study questioned this subunit-specific model (Granger et al., 2013). Using a single-cell molecular replacement strategy to replace all endogenous AMPARs with transfected subunits, it was found that the GluA1 C-tail is not required for LTP. In addition, replacing all endogenous AMPARs with GluA2 or even kainite receptors showed normal LTP. These results lead the field to reevaluate the

mechanism of LTP. One possible explanation for the discrepancy is that Granger et al used a pairing protocol to induce LTP, which is close to the saturation of LTP. However, most of the previous studies used the tetanic stimulation protocol, which induces a lower level of LTP. It is possible that the C-terminal domains of AMPAR subunit are important for the threshold and magnitude of LTP induced by weaker stimuli (Huganir and Nicoll, 2013).

1.3.3.3 AMPARs exocytosis in LTP

Another controversial topic is the exact site of AMPARs exocytosis during LTP. There are two models for the AMPARs incorporations during LTP (Nicoll and Roche, 2013). In the first model, AMPARs are exocytosed extrasynaptically, and can move in and out of synapses by lateral diffusion. LTP induction can immobilize and capture AMPARs in the synaptic surface (Opazo et al., 2012). Using single-particle tracking, it was found that extrasynaptic AMPARs are mobile. However, raising intracellular calcium could trigger rapid receptor immobilization and local accumulation on the neuronal surface (Borgdorff and Choquet, 2002). A later study combined superecliptic pHluorin (SEP)-tagged AMPAR subunit and fluorescence recovery after photobleaching (FRAP) to determine the path that receptors reach the synapses. It was found that the majority of AMPARs incorporated into synapses during LTP is from lateral diffusion of GluA1-containing receptors. The intracellular GluA1-containing AMPARs are exocytosed primarily on dendrites (Makino and Malinow, 2009). In the second model,

LTP induction triggers direct AMPARs exocytosis from the intracellular pool to the spines (Kennedy et al., 2010; Patterson et al., 2010). Combing SEP-GluA1 and FRAP, Patterson et al. induced sLTP in single spines, and compared the SEP-GluA1 recover with or without prior bleaching. With prior bleaching, SEP-GluA1 recover indicates the intracellular exocytosis; without prior bleaching, SEP-GluA1 recover is mainly attributed to the lateral diffusion from the extrasynaptic pool. Interestingly, they found that spine recruitment of AMPARs is mainly supplied by the diffusion of preexisting surface receptors (70–90%) from the dendritic shaft, as well as exocytosis near spines (10–30%). Overall, these two models are not mutually exclusive, but implicate that AMPARs can be incorporated into synapses via multiple pathways.

1.3.4 AMPAR auxiliary subunits

In the past decade, a great progress has been made in the study of AMPAR auxiliary subunits (Jackson and Nicoll, 2011; Kato et al., 2010). These smaller auxiliary subunits can modulate the trafficking and properties of AMPARs (Huganir and Nicoll, 2013; Straub and Tomita, 2012). The first discovered and analyzed AMPARs auxiliary subunit is stargazin in stargazer mutant mice, which has epilepsy and cerebellar ataxia (Chen et al., 2000; Noebels et al., 1990). Stargazin can interact with both AMPARs and synaptic PDZ proteins, such as PSD-95. The interaction with AMPARs is essential for the delivery of AMPARs to the surface membrane of granule cells, whereas its binding with PSD-95 and related PDZ proteins through a C-terminal PDZ-binding domain is required

for AMPARs targeting to synapses (Chen et al., 2000). Later studies found that stargazin is a member of a family of transmembrane AMPAR regulatory proteins (TARPs) (Tomita et al., 2003). Several TARP family members, stargazin (γ2), γ3, γ4, and γ8, can interact and control surface expression of AMPARs, as well as the channel conductance and desensitization (Kott et al., 2007; Tomita et al., 2003). In addition, CaMKII and PKC can phosphorylate TRAPs in the C-terminal domains, which enhances AMPARs trafficking during LTP (Tomita et al., 2005). Other identified AMPAR auxiliary subunits include cornichon-2 and cornichon-3 (CNIN-2 and CNIH-3), CKAMP44, SynDIG1, GSG1L and so on (Kalashnikova et al., 2010; Schwenk et al., 2009; Von Engelhardt et al., 2010). They play different roles in AMPARs regulations. For example, cornichons increase surface expression of AMPARs, and alter channel gating by slowing deactivation and desensitization kinetics (Schwenk et al., 2009). However, CKAMP44 decreases AMPAR currents, enhances receptor desensitization, and slows recovery from desensitization (Von Engelhardt et al., 2010).

1.4 Small Rab GTPases

1.4.1 Structure and molecular circuitry of Rab proteins

Small Rab GTPases constitute the largest family of the small GTPases and the known membrane trafficking proteins (Fukuda, 2008; Stenmark, 2009). There are 11 identified members in yeast, 29 members in *C. elegans*, and more than 60 members in human and mice (Bock et al., 2001; Pereira-Leal and Seabra, 2001). Similar to the Ras

superfamily, Rab proteins consist of a six-stranded β sheet flanked by five α helices. The nucleotide-bound state of Rab proteins is tightly related with its localization and activity. The switch I and II regions can interact with the γ phosphate of GTP and determine the nucleotide-dependent functions of Rab proteins. Upon GTP binding, the switch regions undergo a conformational change from the disordered GDP-bound structure to a well-ordered structure (Gabe Lee et al., 2009). The C-terminal contains the most divergent "hypervariable domains" consisting of 35-40 amino acids, which target Rab proteins to the specific membranes through interactions with other proteins. Following the C-terminal is a CAAX box, which contains two cysteine residues that can covalently interact with the geranylgeranyl moieties. The geranylgeranyl tails are associated with the regulated membrane insertion of Rab proteins (Hutagalung and Novick, 2011).

As small GTPases, all Rab proteins function as molecular switches oscillating between two states, the GTP-bound "active" form and the GDP-bound "inactive" form (Stenmark, 2009). Conversion of the GDP-bound Rab into the GTP-bound Rab is catalyzed by the GEF. The GTP-bound Rab can further recruit diverse effector molecules, including lipid kinases, phosphatases, sorting adaptors, tethering complexes and motors (Eathiraj et al., 2005). Conversely, specific GAPs can catalyze the conversion from the GTP-bound Rab to the GDP-bound Rab. The newly synthesized Rab proteins, in the GDP-bound form, are presented by the Rab escort protein (REP) to the Rab

geranylgeranyl transferase (GGT), which attaches the prenyl-lipid group to the C-terminal of Rab proteins (Andres et al., 1993). The geranylgeranylated Rab proteins, in their inactive GDP-bound form, can bind to the cytosolic Rab GDP dissociation inhibitor (GDI), which regulate the cycling of Rab proteins. On the other hand, the GDI-displacement factor (GDF) can catalyze the dissociation of the GDP-bound Rab from GDI, and assist the subsequent targeting to the appropriate membrane (Figure 7) (Hutagalung and Novick, 2011; Pfeffer and Aivazian, 2004; Stenmark, 2009).

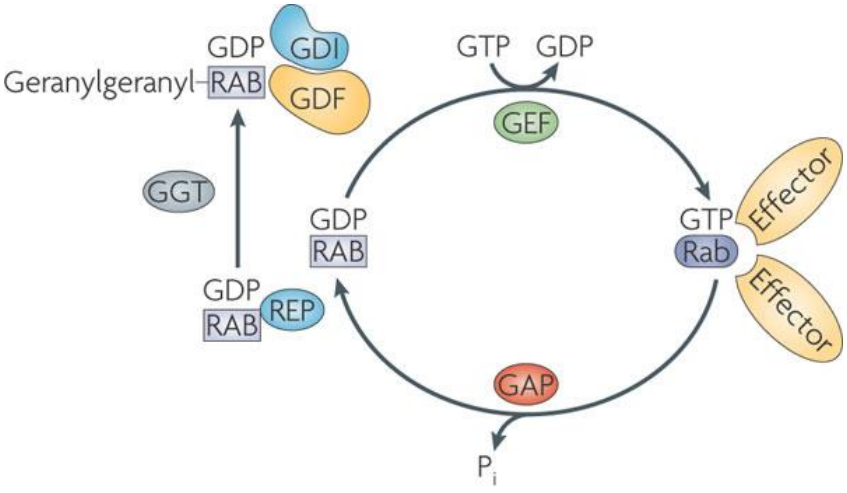

Figure 7 Rab proteins function as molecular switches and its circuitry

Adapted from (Stenmark, 2009).

1.4.2 Localization and function of Rab proteins

In humans, there are more than 60 members of Rab GTPases localized to distinct intracellular domains, and regulate different steps of membrane trafficking (Figure 8) (Stenmark, 2009; Zerial and McBride, 2001). For example, Rab1 regulates ER-Golgi

trafficking while Rab2 regulates the retrograde Golgi-ER trafficking. Rab6, Rab33 and Rab40 regulate the intra-Glogi traffic. Rab8, Rab10 and Rab14 mediate GLUT4 vesicle trafficking to the plasma membrane. Rab18 controls the formation of lipid droplets. Rab22 mediates the trafficking between TGN and the early endosome. Rab32 regulates mitochondria fission (Stenmark, 2009).

In the endocytic recycling pathway, Rab5 regulates endocytosis and the endosomal fusion of CCVs. After endocytosis, cargo proteins can be directly returned to the plasma membrane through a Rab4-mediated fast recycling pathway, or go through the slow recycling pathway mediated by Rab11 and Rab35. Alternatively, cargo proteins can be directed to the late endosome and lysosome for protein degradation, which are mediated by Rab9 and Rab7 (Stenmark, 2009).

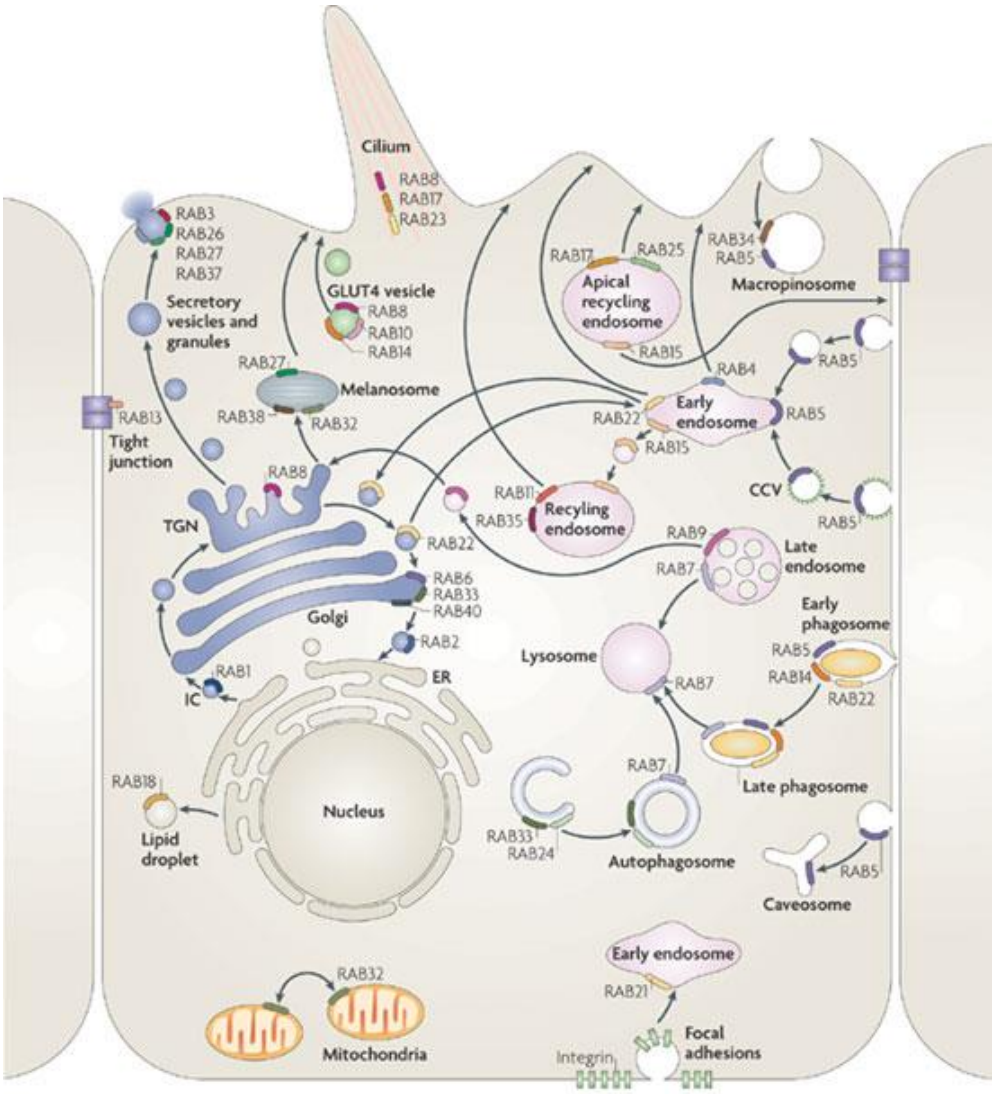

Figure 8 The intracellular localization of Rab proteins

Adapted from (Stenmark, 2009).

1.4.3 Rab proteins coordinate intracellular trafficking

Among the molecules mediating membrane trafficking, small Rab GTPases have been identified as the key coordinators of intracellular transport, which regulate

consecutive stages of vesicle budding, mobility, tethering and fusion by recruiting various effectors (Figure 9)(Hutagalung and Novick, 2011).

1.4.2.1 Rab proteins and vesicle budding

Vesicle budding and cargo selection are mediated by different coat proteins. The coat proteins can facilitate the formation of round buds from the flat membrane, and eventually cause the release of transport vesicles. In addition, coat proteins can selectively recognize the sorting signals of cargo proteins, and ensure the cargo-specific transport. Several classic coat proteins have been intensively studied, such as clathrin, COPI and COPII (Bonifacino and Glick, 2004). However, several Rab proteins have been shown to be involved in this process.

One example is Rab5, a Rab GTPase localized on the early endosome. It has been shown that the Rab5–GDI complex is required for ligand sequestration into clathrin-coated pits, and the subsequent clathrin-mediated endocytosis of transferrin receptors (McLauchlan et al., 1998). Another example is Rab9, which regulates the recycling of mannose-6-phosphate receptors (M6PRs) between the late endosome and the trans-Golgi network (TGN). GTP-bound Rab9 can directly bind to TIP47, an effector of Rab9, which recognizes the cytoplasmic domains of M6PRs and is required for the endosome-to-Golgi transport. The interaction with Rab9 can increase the affinity of TIP47 for M6PRs and facilitate the trafficking of M6PRs (Carroll et al., 2001).

1.4.2.2 Rab proteins and vesicle uncoating

After cargo sorting and vesicle budding from the donor membrane, coat proteins must be shed for vesicles to fuse with the acceptor membrane. One classic and intensively studied model is the AP2 adaptor complex and clathrin coat on endocytosis vesicles. AP2 can recruit clathrin to the newly formed vesicles and regulate the endocytosis of clathrin-coated vesicles (CCVs). Phosphorylation in the μ2 subunit of AP2 enhances its interaction with cargo and vesicles (Jackson et al., 2003). In addition, PIP2 recruits AP2 to the vesicles during clathrin-mediated endocytosis (Höning et al., 2005; Zoncu et al., 2007). It has been shown that Rab5 can regulate the clathrin uncoating through regulations of AP2. Rab5 is localized on CCVs and modulates the CCVs uncoating in two ways. Firstly, Rab5 can inhibit the phosphorylation of the μ2 subunit of AP2, which decreases its interaction with vesicles and promotes uncoating. Secondly, Rab5 can facilitate the turnover of PIP_2 by recruiting PI3K or PI phosphatases, thus decreasing the AP2 level and facilitating uncoating (Christoforidis et al., 1999; Semerdjieva et al., 2008; Shin et al., 2005).

1.4.2.3 Rab proteins and vesicle mobility

Rab proteins can also regulate vesicle trafficking along the actin filaments and microtubules. Rab proteins can interact with actin motors of the myosin V family through specific Rab effectors, which further drives vesicle trafficking along the actin filaments. For example, Rab11 can interact with Myosin Vb through its effector Rab11-

FIP2, and regulate the trafficking of various receptors from the recycling endosomes to the plasma membrane, both in neurons and non-neuronal cells (Hales et al., 2002; Wang et al., 2008). Rab27 on melanosomes can interact with myosin Va through its effector melanophilin, and mediate the trafficking of melanosomes to the plasma membrane (Wu et al., 2002).

Similarly, Rab proteins can also interact with microtubule motors of kinesin or dynein, and regulate vesicle trafficking along the microtubules. For example, GTP-bound Rab6 can directly interact with a kinesin, Rabkinesin-6 (kinesin family member 20A), and regulate directional membrane transport and dynamics of Golgi (Echard et al., 1998; Fontijn et al., 2001). Besides, Rab6 also indirectly interacts with microtubule motors through its effector Bicaudal D1, and controls the COPI-independent Golgi–ER transport (Matanis et al., 2002). Another example is Rab7, which regulates the trafficking between late endosomes and lysosomes. Rab7 can recruit the dynein-dynactin motor complex through interaction with its effector RILP, and mediate the trafficking of late endosomes to lysosomes (Jordens et al., 2001).

1.4.2.4 Rab proteins and vesicle tethering and fusion

To ensure the appropriate trafficking to final destinations, vesicles should be driven to the acceptor membrane by "tethering molecules". Rab proteins can mediate vesicle tethering by recruiting various effectors that can interact with molecules on the acceptor membrane. Two classes of these Rab-related "tethering molecules" have been

identified: long coiled-coil proteins and multi-subunit tethering complex. Moreover, Rab proteins can also regulate the SNARE-dependent vesicle fusion by directly interacting with SNARE proteins or indirectly with proteins associated with SNARE functions (Hutagalung and Novick, 2011).

One good example is Rab5 and its effectors, the early endosome antigen 1 (EEA1) and rabenosyn 5, which are important regulators in early endosome tethering and fusion. EEA1 binds to both the active Rab5 and the SNARE protein syntaxin 6 while rabenosyn 5 binds to both Rab5 and the SM protein VPS45, thus linking the Rab5-mediated vesicles to the fusion membrane (Callaghan et al., 1999; Nielsen et al., 2000; Simonsen et al., 1998).

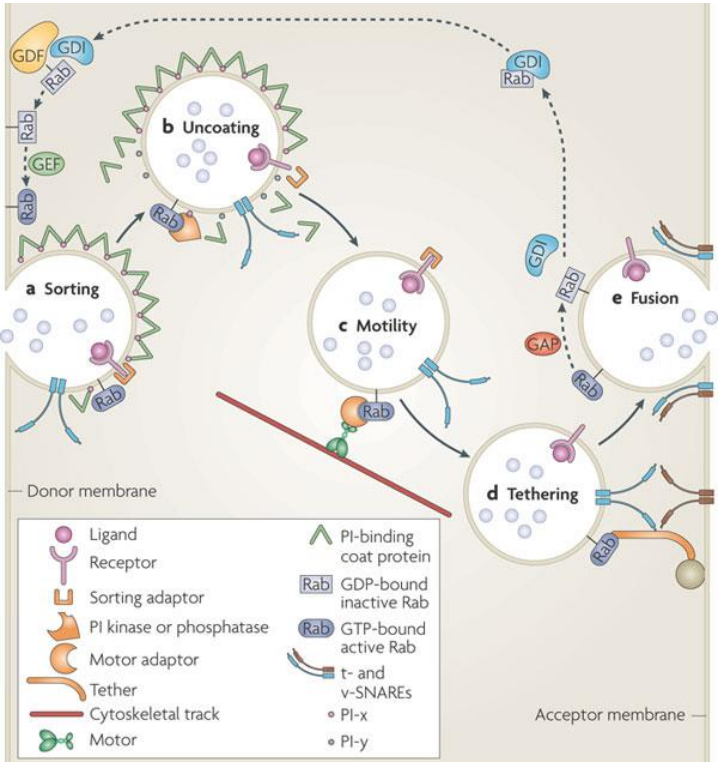

Figure 9 Rab proteins coordinate intracellular trafficking

Adapted from (Stenmark, 2009).

1.4.4 Rab4 and Rab10 in membrane trafficking

Previous cellular studies have shown that Rab4 regulates the fast recycling from early endosome to the plasma membrane (van der Sluijs et al., 1992). Rab10 mediates basolateral transport in Madin-Darby Canine Kidney (MDCK) epithelial cells (Babbey et al., 2006; Schuck et al., 2007), and is important for GLUT4 translocation to the adipocyte plasma membrane (Sano et al., 2007). In addition, Rab10 regulates the endoplasmic reticulum dynamics and morphology (English and Voeltz, 2013).

In the nervous system, Rab4 maintains the spine size (Brown et al., 2007), and its neuron specific effector GRASP-1 coordinates maturation of recycling endosomes (Hoogenraad et al., 2010). Rab10 is required for the axonal membrane trafficking during neuronal polarization and dendrite arborization (Wang et al., 2011; Zou et al., 2015). Rab10 also regulates glutamate receptor recycling in a clathrin-independent endocytosis pathway in *C. elegans* (Glodowski et al., 2007). However, it remains to be elucidated whether and how Rab4 and Rab10 are involved in synaptic plasticity.

1.5 Specific aims of this dissertation

Synaptic plasticity, or change of synaptic strength, underlies the brain's ability to encode and store information. One compelling and intensively studied example is LTP in hippocampus, which is the dominant cellular model for learning and memory. LTP induction stimuli trigger rapid Ca^{2+} influx and downstream protein cascades through NMDARs activation, which leads to the increase of synaptic efficacy and alternations of dendritic spine morphology (Lamprecht and LeDoux, 2004; Lang et al., 2004; Matsuzaki et al., 2004). It is a generous consensus that regulated AMPA receptors (AMPARs) trafficking contributes to synaptic plasticity (Huganir and Nicoll, 2013; Malinow and Malenka, 2002; Sheng and Kim, 2002). However, the molecular regulators that relay the upstream NMDARs activation to the synaptic AMPARs trafficking are only beginning to emerge.

In this dissertation, I studied two novel Rab proteins, Rab4 and Rab10, in structural plasticity and AMPARs trafficking. There are three specific aims as follows.

1.6.1 Examine the roles of Rab4 and Rab10 in structural LTP

Previous studies have indicated that Rab8 and Rab11 regulate the synaptic delivery of GluA1-containing AMPARs during LTP (Brown et al., 2007; Correia et al., 2008), whereas Rab5 drives the removal of AMPARs during LTD (Brown et al., 2005). However, little is known about the involvement and functions of other Rab proteins in AMPARs trafficking and synaptic plasticity. To examine the roles of Rab4 and Rab10 in structural LTP, I measured the spine volume change after inhibiting Rab4 and Rab10 signaling, respectively.

1.6.2 Measure the spatiotemporal dynamics of Rab4 and Rab10 in structural LTP

Traditional loss-of-function studies, such as electrophysiological recordings in acute slices, could only report whether a protein of interest is involved in LTP, with the spatiotemporal information missing. I overcame this by directly visualizing the spatiotemporal dynamics of Rab4 and Rab10 in single dendritic spines during sLTP, which is a proxy for functional LTP. Taking advantage of highly-sensitive FRET sensors, two-photon FLIM imaging and two-photon glutamate uncaging, I firstly measured the spatiotemporal activities of Rab4 and Rab10 in single dendritic spines during sLTP. Secondly, I probed into the signaling pathways that Rab4 and Rab10 are involved in, by applying pharmacological inhibitors targeting putative upstream components. Finally, I

also measured the activities of Rab4 and Rab10 at a near physiological temperature during sLTP.

1.6.3 Elucidate the functions of Rab4 and Rab10 in AMPARs endocytosis and activity-dependent AMPARs exocytosis

Tightly regulated AMPARs trafficking in and out of synapses is one major mechanism that regulates the synaptic plasticity. During LTP, more AMPARs are inserted to the postsynaptic membrane. During LTD, the rate of AMPARs endocytosis outweighs the rate of AMPARs exocytosis, which results in reduced postsynaptic AMPARs (Barry and Ziff, 2002; Bredt and Nicoll, 2003; Malinow and Malenka, 2002; Sheng and Lee, 2001; Song and Huganir, 2002). Considering that Rab GTPases are the major regulators in intracellular membrane trafficking, including AMPARs trafficking, I firstly studied the functions of Rab4 and Rab10 in AMPARs exocytosis in the stimulated spines during sLTP. Combining FRAP, two-photon glutamate uncaging and iRNA interference techniques, I measured the SEP-GluA1 recover in the stimulated spines after disrupting the Rab4 and Rab10 signaling, respectively. Secondly, I investigated the functions of Rab4 and Rab10 in constitutive GluA1 endocytosis by a live cell antibody feeding assay.

Chapter 2. Experimental procedure

2.1 DNA constructs and antibodies

DNA constructs

Rat full length Rab4a, Rab10, Rabenosyn5 [439-503] and Rim1 [20-227] cDNA were amplified by PCR from rat brain cDNA library (Dharmacon) and cloned into pEGFP-C1 (Clontech), pCAG-mEGFP (Murakoshi et al., 2008), pCAG-mTurquoise2, pCAG-mCherry-mCherry and pCAG-mVenus-mVenus constructs. All fluorescence proteins were tagged at the N-terminal of Rab4 and Rab10. Rab4a [S27N], Rab4a [Q72L], shRNA resistant Rab4a, Rab10 [T23N], Rab10 [Q68L], shRNA resistant Rab10 and Rab5a [S34N] were generated from wild type Rab GTPases by site-directed mutagenesis, and subcloned into pCAG-mEGFP, pCAG-3Flag and pCAG-mCherry constructs. PIK3R1 was amplified from rat brain cDNA library and cloned into pCAG-3HA construct. Full length Dennd4c, Evi5 and Rab3gap1 were amplified by PCR from MGC mouse cDNA (Dharmacon) and subcloned into pCAG-3HA construct. Tetanus toxin light chain (Eisel et al., 1993) was subcloned into pCAG-3Flag construct. pGW1-HA/T-GluA1 and pGW1-HA/T-GluA2 were gifts from Dr. Michael Ehlers (Pfizer). SEP-GluA1 was a gift from Dr. Scott Soderling (Duke University). Rat full length Rab4b was amplified by PCR from rat brain cDNA library and cloned into pCAG plasmid. piRFP670-N1 was a gift from Vladislav Verkhusha (Addgene plasmid # 45457). psiCHECK-2-Rab GTPases were generated by inserting Rab GTPases into psiCHECK-2-Sal4-wt_3'UTR, which was a gift

from Robert Blelloch (Addgene plasmid # 31862). mTurquoise2-pBAD and mVenus-pBAD were gifts from Michael Davidson (Addgene plasmid # 54844 and # 54845). The human codon-optimized S. pyogenes Cas9 (SpCas9) and single guide RNA (sgRNA) expression plasmid pX330 was a gift from F. Zhang (Addgene plasmid # 42230). pPB-CAG-mEGFP construct was a gift from Dr. Jun Nishiyama and Dr. Takayasu Mikuni. pCAG-Cre, pCAG-ERT2CreERT2 and AAV-pCAG-FLEX-CyRFP constructs were gifts from Dr. Tal Laviv. AAV-pCAG-FLEX-*rev*-mEGFP-Rab10 DN and AAV-pCAG-FLEX-*rev*-mEGFP-Rab10 CA were generated by reversely ligating mEGFP-Rab10 T23N and mEGFP-Rab10 Q68L into AAV-pCAG-FLEX-CyRFP with AscI and NheI sites.

Antibodies

Antibodies used in this project include HA.11 clone 16B12 monoclonal antibody (BioLegend), Alexa Fluor 488 goat anti-mouse IgG (H+L) antibody (Life technologies), Alexa Fluor 568 goat anti-mouse IgG (H+L) antibody (Life technologies), goat anti mouse IgG (H+L) antibody (Novex), rabbit anti-Rab10 antibody (D36C4, Cell Signaling Technology), mouse anti-Rab4a antibody (4E11) (ThermoFisher Scientific), mouse-anti Rab4b antibody (ThermoFisher Scientific), mouse anti-β-actin antibody (Sigma), and HRP-conjugated goat anti-rabbit and rabbit anti-mouse secondary antibodies (Bio-Rad).

2.2 Organotypic slices preparation, cell culture, electroporation and transfection

Organotypic rat hippocampal slices were prepared at postnatal day 6 or 7, as previously described (Stoppini et al., 1991), in accordance with the animal care and use guidelines of Duke University Medical Center and Max Planck Florida Institute for Neuroscience. After 9-13 days in culture, CA1 pyramidal neurons were transfected ballistically with gene gun (McAllister, 2000) using gold beads (Bio-rad, 1.6 μm, 10 mg) coated with plasmids, and imaged 3-5 days after transfection. For Rab4 FRET sensor, I used pEGFP-Rab4a and pCAG-mCherry-Rabenosyn-5 [439-503]-mCherry at 1 to 1 ratio. For Rab10 FRET sensor, I used pCAG-mTurquoise2-Rab10 and pCAG-mVenus-Rim1 [20-227]-mVenus at a 1 to 3 ratio.

HEK 293T cells were grown in DMEM (Giboco) supplemented with 10% fetal bovine serum and 1% penicillin. Imaging in HEK 293T cells were performed 24-48 h after transfection with Lipofectamine 2000 (Invitrogen), in a solution containing 20 mM HEPES (pH 7.3), 130 mM NaCl, 2.5 mM KCl, 2 mM $CaCl_2$, 2mM $MgCl_2$, 2 mM $NaHCO_3$, 1.25 mM NaH_2PO_4 and 25 mM D-glucose.

Murine Neuro-2a cells were cultured in DMEM medium supplemented with 10% fetal bovine serum. The cells (> 6 passage) were harvested with 0.25% trypsin. Prior to electroporation, cells were washed with Opti-MEM medium three times and reconstituted in Opti-MEM medium with a density of 1×10^7 cells/mL. Plasmids PX330-Rab4 sgRNA or PX330-Rab10 sgRNA, pPB-CAG-mEGFP and the ssODNs were prepared at a final concentration of 1 μg/μL, 1 μg/μL and 2 μM, respectively. 100 μL of

the reconstituted cells were gently mixed with 5 μL of the plasmid mixture, and then 100 μL were transferred into the electroporation cuvette. The electroporation was performed on NEPA21 electroporator by following the manufacture protocol. The electroporated cells were transferred into a 24-well culture plate containing 500 μL of pre-warmed DMEM medium and incubated at 37 °C for 72 h.

Dissociated hippocampal neuron cultures were prepared from E17-E18 rat embryos and maintained in vitro as described previously (Beaudoin III et al., 2012; Seibenhener and Wooten, 2012). Cultured hippocampal neurons were transfected with Lipofectamine 2000 (Invitrogen).

2.3 Two-photon fluorescence lifetime imaging and two-photon glutamate uncaging

I used a custom-built two-photon fluorescence lifetime imaging microscope (2pFLIM) with two Ti:Sapphire lasers (Chameleon, Coherent) as previously described (Murakoshi et al., 2008; Yasuda et al., 2006). One laser was tuned to 920 nm to excite both donor for lifetime measurement and acceptor for morphology. The second laser was tuned to 720 nm for glutamate uncaging. The imaging power for two lasers was controlled independently by electro-optical modulators (Conoptics). The fluorescence was collected by an objective (60X, 1.0 numerical aperture, Olympus), separated by a dichroic mirror (Chroma, 565 nm for mEGFP/mCherry and 505 nm for mTurquoise2/mVenus), filtered by wavelength filters (Chroma, ET520/60M-2p for mEGFP, ET620/60M-2p for mCherry, ET480/40M-2p for mTurquoise2, ET535/50M-2p for

mVenus), and finally detected by two independent photoelectron multiplier tubes (PMTs). I used 1.2-1.5 mW imaging power for mEGFP/mCherry sensor, and 1.6-1.8 mW for mTurquoise2/mVenus sensor.

Two-photon glutamate uncaging was performed in the Mg^{2+}-free artificial cerebrospinal fluid (ACSF; 127 mM NaCl, 2.5 mM KCl, 1.25 mM NaH_2PO_4, 25 mM $NaHCO_3$, 25 mM D-glucose, aerated with 95% O_2 and 5% CO_2) with 4 mM $CaCl_2$, 4 mM MNI-caged glutamate (Tocris) and 1 μM tetrodotoxin (TTX). Uncaging pulses (30 times at 0.5 Hz, 6 ms, 3.5-3.8 mW) were delivered to the back focal aperture of the objective, which was around 0.5 μm from the tip of the spine head. I used a heater controller (Warner Instruments TC-344B) to monitor the temperature at 25-27°C or 33-35°C. Images were analyzed by MATLAB (MathWorks) and ImageJ.

2.4 2pFLIM data analysis

As described previously (Harvey et al., 2008), to measure the donor fluorescence lifetime, I imaged a neuron expressing the donor, summed all pixels in the image, and fitted the fluorescence lifetime curve with a single exponential function convolved with the Gaussian pulse response function:

$$F(t) = F_0 H(t, t_0, \tau_D, \tau_G)$$

in which F_0 is the constant, and

$$H(t, t_0, \tau_D, \tau_G) = \frac{1}{2} exp\left(\frac{{\tau_G}^2}{2\tau_D} - \frac{t-t_0}{\tau_D}\right) erf\left(\frac{\tau_G^2 - \tau_D(t-t_0)}{\sqrt{2}\tau_D\tau_G}\right)$$

in which F_0 is the peak fluorescence before convolution, t_0 is the time offset, τ_D is the fluorescence lifetime of the free donor, τ_G is the width of the Gaussian pulse response function, and *erf* is the error function. I measured τ_D as 2.46 ns, 2.60 ns and 4.15 ns for the free mEGFP–Rab4, mEGFP-Rab10 and mTurquoise2-Rab10 donors, respectively.

To measure the binding fraction of donor bound to its acceptor, I summed all pixels over a whole image and fitted the fluorescence lifetime curve with a double exponential function convolved with the Gaussian pulse response function:

$$F(t) = F_0[P_D H(t, t_0, \tau_D, \tau_G) + P_{AD} H(t, t_0, \tau_{AD}, \tau_G)]$$

in which P_D and P_{AD} are the fractions of free donor and donor bound with its acceptor, respectively, and τ_{AD} is the fluorescence lifetime of donor bound with its acceptor (1.10 ns for mEGFP/mCherry pair and 1.60 ns for mTurquoise2/mVenus pair).

For small regions of interest in an image, such as spines and dendrites, the binding fraction P_{AD} is calculated as follows:

$$P_{AD} = \frac{\tau_D(\tau_D - \tau_m)}{(\tau_D - \tau_{AD})(\tau_D + \tau_{AD} - \tau_m)}$$

In which τ_m is the mean fluorescence lifetime, τ_D and τ_{AD} are fixed values.

2.5 iRNA interference

For shRNA-mediated knockdown of Rab4 and Rab10, I used SHCLND-NM_009003 plasmid for Rab4a (Sigma-Aldrich, TRCN0000088975), SHCLND-NM_016154 palsmid for Rab4b (Sigma-Aldrich, TRCN0000380038), and TRC-Mm1.0 plasmid for Rab10 (Dharmacon, TRCN0000100838). The respective sequences of shRNA

(according to manufacture and sequencing confirmation) are CCGGAGATGACTCAAATCATACCATCTCGAGATGGTATGATTTGAGTCATCTTTTTG for Rab4a, GTACCGGGGTCATCCTCTGTGGCAACAACTCGAGTTGTTGCCACAGAGGATGACCTTTTTTG for Rab4b, and TTGCCTTTCGGTACAACTCTC (mature antisense) for Rab10. For the control of shRNA, a scramble shRNA was used (Addgene plasmid # 1864). The sequence is CCTAAGGTTAAGTCGCCCTCGCTCGAGCGAGGGCGACTTAACCTTAGG. To visualize the transfected neurons, mEGFP was inserted into scramble shRNA, Rab4a and Rab10 shRNA by KpnI/BamHI, and into Rab4b shRNA by BamHI/BstEII. The mEGFP expression was driven by a separate hPGK promotor. For the rescue experiments, silent mutations of three amino acids were induced at the targeted region for Rab4a and Rab10 (For Rab4a, AAAGATGACTCCAACCACACCATA; for Rab10, GAGAGTTGTGCCCAA GGGCAA). Lentivirus was produced by Duke University Viral Vector Core.

2.6 Dual-luciferase reporter assay

I inserted rat Rab4a, Rab4b, Rab10, shRNA-resistant Rab4a, and shRNA-resistant Rab10 cDNA into psiCHECK-2-Sal4-wt_3'UTR plasmid using XhoI/NotI sites. As a positive control, the shRNA against hRluc was used. The shRNA sequence for hRluc is TCATAGTAGTTGATGAAGGAG (mature antisense). HEK 293T cells were plated in 24-well plates and cotransfected with psiCHECK-2-Rab GTPases and the respective shRNA at a 1 to 3 ratio. After 48 h transfection, luciferase activity was measured using the Dual-

Luciferase Reporter Assay System (Promega). After aspirating media, cells were rinsed in pre-warmed 0.1M phosphate-buffered saline once, and lysed with 100μL of 1X passive lysis buffer in the luciferase assay kit. After gently shaking for 15 min at room temperature, samples were prepared in 96-well plates for luminescence measurement according to the manufacturer's protocol using GloMax-Multi Detection System (Promega). For data analysis, the hRluc (firefly luciferase) luminescence was normalized by the hluc+ (renilla luciferase) luminescence in each well to control for transfection efficiency. All experiments were paired with the same day controls from the same batch of HEK 293T cells.

2.7 NMDA application

Rat organotypic hippocampal slices (DIV 9-DIV 13) were ballistically transfected with mEGFP-Rab4 and mCherry-RBD-mCherry (1:1), or mTurquoise2-Rab10 and mVenus-RBD-mVenus (1:3). After 4 days expression, CA1 pyramidal neurons were imaged in the basal solution (ACSF with 2 mM $CaCl_2$, 2 mM $MgCl_2$ and 1 μM TTX) for 6 min. NMDA (Tocris) was bath-applied in the zero Mg^{2+} solution (ACSF with 4 mM $CaCl_2$, 15 μM NMDA and 1 μM TTX) for 2 min, and replaced by the washout solution (ACSF with 2 mM $CaCl_2$, 2 mM $MgCl_2$, 1 μM TTX and 50 μM AP5) for 32 min.

2.8 Antibody feeding assay for GluA1 internalization

Dissociated hippocampal neurons from E18 were transfected at DIV 13-14 with indicated constructs (Figure 28) for 2-3 days in dominant negative experiments and for

4-5 days in shRNA experiments. The DNA ratio was 1:2 for piRFP670-N1, pGW1-HA/T-GluA1 (Ctrl); 1:2:2 for piRFP670-N1, pGW1-HA/T-GluA1 and pCAG-3Flag-Rab DN (Rab GTPase DN); 1:2:2 for piRFP670-N1, pGW1-HA/T-GluA1 and scramble shRNA (Ctrl shRNA); 1:2:1:1 for piRFP670-N1, pGW1-HA/T-GluA1, Rab4a shRNA and Rab4b shRNA (Rab4a/4b shRNA); 1:2:2 for piRFP670-N1, pGW1-HA/T-GluA1 and Rab10 shRNA (Rab10 shRNA); 1:2:2:3 for piRFP670-N1, pGW1-HA/T-GluA1, Rab10 shRNA and pCAG-3Flag-shRNA resistant Rab10 (Rab10 rescue). All experiments were paired with the same day controls from the same batch of neurons. Neurons were pre-incubated at 37°C for 10 min with 1 μM TTX to decrease the basal neuronal activity, and 100 μM Leupeptin (Roche) to inhibit protein degradation. Pitstop2 (200 μM, Abcam) and its vehicle control DMSO were applied 30 min before HA-GluA1 internalization. Surface HA-GluA1 was labelled with mouse anti-HA antibody (1:100) and internalized for 20 min at 37°C. After washing with 0.1 M phosphate-buffered saline (PBS, pH 7.4, Invitrogen), neurons were fixed with 4% paraformaldehyde/4% sucrose in 0.1 M PBS for 20 min at room temperature (RT). Neurons were then washed with 0.1 M PBS and incubated in Triton X negative solution (0.1 M PBS containing 2% BSA and 2% goat serum, Sigma) for 30 min at RT. To visualize the surface HA-GluA1, neurons were incubated in Alexa Fluor 568 goat anti-mouse antibody (1:1500 in Triton X negative solution) for 90 min at RT. After thorough washing with 0.1 M PBS, the surface-remaining HA-GluA1 was blocked by non-fluorescence goat anti-mouse secondary

antibody (1:100 in Triton X negative solution) for 30 min at RT. After washing, re-fixation and washing, neurons were permeabilized by Triton X positive solution (0.1 M PBS containing 2% BSA, 2% goat serum and 0.4% Triton X-100) and incubated with Alexa Fluor 488 goat anti-mouse antibody (1:1500 in Triton X positive solution) for 90 min at RT. After thorough washing with 0.1 M PBS, coverslips (Fisher, 12 mm) were mounted onto microscope slides (Fisher, 75 mm X 25 mm) for imaging with a confocal laser-scanning microscope (LSM780, Zeiss). The acquired images were processed with the Zen (Zeiss) and analyzed with the ImageJ.

2.9 Activity-dependent SEP-GluA1 exocytosis

Rat organotypic hippocampal slices were ballistically transfected with indicated constructs at DIV 9-DIV 13. The DNA constructs for each condition were: pCAG-mCherry, SEP-GluA1 and scramble shRNA (1:2:2); pCAG-mCherry, SEP-GluA1 and pCAG-3Flag-TeTxLC (1:2:2); pCAG-mCherry, SEP-GluA1, Rab4a shRNA and Rab4b shRNA (1:2:1.5:1.5); pCAG-mCherry, SEP-GluA1 and Rab10 shRNA (1:2:3); pCAG-mCherry, SEP-GluA1, Rab4a shRNA, Rab4b shRNA and pCAG-3Flag-shRNA resistant Rab4a (1:2:1.5:1.5:3); pCAG-mCherry, SEP-GluA1, Rab10 shRNA and pCAG-3Flag-shRNA resistant Rab10 (1:2:3:3). After 4 days expression, CA1 pyramidal neurons were imaged in ACSF with 4 mM $CaCl_2$, 4 mM MNI-caged glutamate and 1 μM TTX at 25-27°C. After taking five baseline images (1 min interval) with 1.2-1.5 mW imaging power, I bleached the whole imaging field by increasing the imaging power to 4.0-4.5 mW for 2

min. I further delivered two-photon glutamate uncaging (0.5 Hz, 30 pulses, 6 ms, 3.5-3.8 mW) at a single spine and continued to take eight images (1 min interval).

2.10 Spine volume measurement

To estimate the spine volume, I measured the integrated fluorescence intensity of mCherry-RBD-mCherry or mVenus-RBD-mCherry in the spine, which is proportional to the spine volume (Holtmaat et al., 2005), and normalized it by the fluorescence intensity in the thick apical dendrite from the same neuron. I further multiplied this normalized value by the volume of the point spread function, which gives the spine volume in fL (Harvey et al., 2008; Nimchinsky et al., 2004).

2.11 Measurement of sensor concentration in neurons

I measured the mean fluorescence intensity of mEGFP-Rab4a and mCherry-Rabenosyn-5 [439-503]-mCherry in the thick primary dendrites, and compared it to the mean fluorescence intensity of purified mEGFP (BioVision) and mCherry (BioVision) with known concentrations, respectively. For Rab10 FLIM sensor, I measured the mean fluorescence intensity of mTurquoise2-Rab10 and mVenus-Rim1 [20-227]-mVenus in the thick primary dendrites, and compared it to the mean fluorescence intensity of purified mTurquoise2 and mVenus with known concentrations, respectively. mTurquoise2-pBAD and mVenus-pBAD were transformed into TOP10 Chemically Competent E. coli (Invitrogen). Protein expression was induced by adding 0.002% L-arabinose when OD_{600} arrived 0.6, purified by a Ni^{+}-nitrilotriacetate column (HisTrap HP, GE Healthcare), and

desalted with a desalting column (PD10, GE Healthcare). The protein concentration was measured by the absorbance of the fluorophore (mTurquoise2, A_{434nm} = 30,000 $cm^{-1}M^{-1}$, mVenus, A_{515nm} = 92,200 $cm^{-1}M^{-1}$) (Goedhart et al., 2012; Nagai et al., 2002).

2.12 Lentivirus infection in dissociated culture neurons

Dissociate postnatal cortical cultures were prepared as previously published (Mikuni et al., 2016). Briefly, cortices dissected from 3 P0 rats were triturated and plated into 5 cm dishes coated with 50 μg/ml PDL (Sigma) in culture medium consisting of basal medium Eagle (BME) supplemented with 10% heat-inactivated fetal bovine serum (Invitrogen), 35 mM glucose (Sigma), 1 mM l-glutamine (Sigma), 100 U/ml penicillin (Sigma), and 0.1 mg/ml streptomycin (Sigma). Proliferation of non-neuronal cells was inhibited by adding Cytosine arabinoside (2.5 μM) at DIV2. At DIV6 cultures were infected with EGFP-shRNA against Rab4a (Rab4a shRNA), Rab4b (Rab4b shRNA), Rab10 (Rab10 shRNA) or the scrambled control shRNA (Ctrl shRNA) containing lentiviral particles. At DIV17 cells were washed with ice-cold PBS and immediately extracted with ice-cold T-PER lysis buffer (Pierce) supplemented with inhibitors for proteases and phosphatases (Roche). The lysates were centrifuged at 15000 g for 15 minutes at 4°C and the supernatant was used for further analysis.

2.13 SDS-PAGE and immunoblotting

Samples were prepared for standard SDS-PAGE and separated on 12% acrylamide gel (Mini-PROTEAN TGX precast gels, Bio-Rad), then transferred onto 0.2

μm pore size PVDF membranes (Millipore) using semi-dry immunoblotting (transfer buffer containing 25 mM Tris, 200 mM glycine and 20% methanol). Membranes were blocked with 5% nonfat milk (Great Value) in TBS-T (Tris Buffered Saline with 0.1% Tween-20) for 1 hour at room temperature, and incubated overnight at 4°C with primary antibodies diluted in 5% BSA in TBS-T. We used the following commercially available antibodies: rabbit anti-Rab10 (1:500; D36C4; Cell Signaling Technology); rabbit anti-Rab4b (1:500; ThermoFisher Scientific); mouse anti-Rab4a (1:500; ThermoFisher Scientific) and mouse anti-β-actin (1:2000; Sigma). Membranes were washed 3 times for 15 minutes in TBS-T, followed by incubation for 2 hours at room temperature with HRP-conjugated goat anti-rabbit or rabbit anti-mouse secondary antibodies (Bio-Rad), diluted 1:5000 in 5% nonfat milk in TBS-T. Membranes were washed 3 times for 15 minutes in TBS-T, and incubated with Pierce ECL Plus western blotting substrate (for Rab10, Rab4a and Rab4b) or Pierce ECL western blotting substrate (for β-actin) for detection of western blotted proteins. We used the Image Quant LAS4000 Imaging System (GE Healthcare) to visualize protein bands.

2.14 AMPA-induced GluA1 or GluA2 internalization

Dissociated hippocampal neurons from E18 were transfected at DIV 13-14 with piRFP670-N1 and pGW1-HA/T-GluA1 or pGW1-HA/T-GluA2 for 2-3 days. The DNA ratio was 1:2. All experiments were paired with the same day controls from the same batch of neurons. Neurons were pre-incubated at 37°C for 10 min with 1 μM TTX to

decrease the basal neuronal activity, and 100 μM Leupeptin (Roche) to inhibit protein degradation. Pitstop2 (200μM, Abcam) was applied 30 min before HA-GluA1 or HA-GluA2 internalization. Surface HA-GluA was labelled with mouse anti-HA antibody (1:100) and internalized for 20 min at 37°C. For AMPA application group, AMPA (100 μM, Tocris) was applied together with anti-HA antibody. After washing with 0.1 M phosphate-buffered saline (PBS, pH 7.4, Invitrogen), neurons were fixed with 4% paraformaldehyde/4% sucrose in 0.1 M PBS for 20 min at room temperature (RT). Neurons were then washed with 0.1 M PBS and incubated in Triton X negative solution (0.1 M PBS containing 2% BSA and 2% goat serum, Sigma) for 30 min at RT. To visualize the surface HA-GluA, neurons were incubated in Alexa Fluor 568 goat anti-mouse antibody (1:1500 in Triton X negative solution) for 90 min at RT. After thorough washing with 0.1 M PBS, the surface-remaining HA-GluA was blocked by non-fluorescence goat anti-mouse secondary antibody (1:100 in Triton X negative solution) for 30 min at RT. After washing, re-fixation and washing, neurons were permeabilized by Triton X positive solution (0.1 M PBS containing 2% BSA, 2% goat serum and 0.4% Triton X-100) and incubated with Alexa Fluor 488 goat anti-mouse antibody (1:1500 in Triton X positive solution) for 90 min at RT. After thorough washing with 0.1 M PBS, coverslips (Fisher, 12 mm) were mounted onto microscope slides (Fisher, 75 mm X 25 mm) for imaging with a confocal laser-scanning microscope (LSM780, Zeiss). The acquired images were processed with the Zen (Zeiss) and analyzed with the ImageJ.

2.15 Oligonucleotides and plasmid-based donor templates

sgRNA target sequences (5′-3′)

Rab4a: GCGGAGCTGTGGCGGCAGAA

Rab10: GCCCGAGCCGCTCCTCCCAA

ssODNs sequence (5′-3′, upper case: HA tag sequence)

Rab4a:

tgggcccgttcccggctctccacgctcggttcctctcgctctgcggagactggaggacggaccccgcggagctgtggcggcag

aatgTACCCATACGATGTTCCAGATTACGCTgcgcagaccgccatgtccgagacttacggtaagacgcg

cgggtttgcgtacgtgtttagaggggcaggccttggggtcccggaa

Rab10:

aacgcccgggtgaggagttggttgtagtgagcagttccgatcccttggggctaccggcggcgagcgcccgagccgctcctccc

aatgTACCCATACGATGTTCCAGATTACGCTgcgaagaagacgtacgacctgcttttcaagctgctcctg

atcggggactcgggagtgggcaagacctgcgtccttttcgtttt

2.16 Genomic PCR and DNA sequencing

Genomic DNA from the electroporation-transduced Neuro 2a cells was isolated with DNeasy Blood & Tissue Kit (Qiagen) following the manufacturer's instruction. Genomic PCR was performed using extracted DNA as a template with corresponding primer set as indicated in Figure 32. The PCR product was purified by QiaQuick gel extraction kit (Qiagen) and then proceeded to DNA sequencing using corresponding reverse primer.

Rab4a primer set, recombination

HA-FW: CCCATACGATGTTCCAGATT

Rab4a-RV1: CTCAAGATTCCAGCCTAGCC

Rab4a primer set, control

Rab4a-FW: AGCCGGTGTCTAGAATATCG

Rab4a-RV2: GGAGGGAACTTGGTAGAATC

Rab10 primer set, recombination

HA-FW: CCCATACGATGTTCCAGATT

Rab10-RV1: TCCCACAGGTCTTACCTATGGTGG

Rab10 primer set, control

Rab10-FW: TTTCAAGCTGCTCCTGATCG

Rab10-RV2: AGAAACCGGATTCTGGAACG

2.17 Statistic analysis

Results are reported as mean ± SEM. Statistical analysis was performed with GraphPad Prism 6. Comparisons between two groups were performed using unpaired two-tailed Student's t tests (* $p<0.05$, ** $p<0.01$, *** $p<0.001$, **** $p<0.0001$). Comparisons for more than two groups were calculated using one-way ANOVA followed by Bonferroni's multiple comparison tests (* $p<0.05$, ** $p<0.01$, *** $p<0.001$, **** $p<0.0001$).

Chapter 3. Disruption of Rab4 inhibits transient phase of sLTP whereas disruption of Rab10 enhances sLTP

3.1 Introduction

Structural LTP can be induced at a single dendritic spine of hippocampal CA1 pyramidal neurons by combing two-photon imaging and two-photon glutamate uncaging. After a train of two-photon glutamate uncaging (0.5 Hz, 60 s) in zero extracellular Mg^{2+}, the spine volume increases rapidly in the first few minutes (transient phase) and decays to a plateau that sustained for hours (sustained phase). This structural change of the stimulated spine is associated with the electrophysiological LTP, and considered as a robust morphological correlate of synaptic plasticity (Harvey et al., 2008; Lee et al., 2009; Matsuzaki et al., 2004; Murakoshi et al., 2011; Nishiyama and Yasuda, 2015).

3.2 Results

3.2.1 Rab4 positively regulates the transient phase of sLTP while Rab10 negatively regulates sLTP

To study the roles of Rab4 and Rab10 in sLTP, I used a protocol to induce sLTP in single dendritic spines using two-photon glutamate uncaging (Matsuzaki et al., 2011). I ballistically transfected cultured organotypic hippocampal slices of rats with shRNA against Rab4 or Rab10 or scrambled shRNA together with monomeric enhanced green fluorescence protein (mEGFP), and imaged the secondary apical dendrites of CA1 pyramidal neurons with two-photon microscopy (Murakoshi et al., 2011).

Under control condition with scrambled shRNA, application of a train of glutamate uncaging (0.5 Hz, 60 s) in zero extracellular Mg^{2+} induced a rapid spine volume increase in a few minutes (transient phase), which decayed over ~5 min. This was followed by a sustained volume increase lasing more than 30 min (sustained phase)(Figures 10A and 10B), consistent with previous studies (Harvey et al., 2008; Lee et al., 2009; Matsuzaki et al., 2004; Murakoshi et al., 2011; Nishiyama and Yasuda, 2015). However, neurons transfected with shRNA against Rab4a and Rab4b significantly impaired the transient phase of sLTP while leaving the sustained phase intact. This phenotype was rescued by coexpression of the shRNA-resistant Rab4a (Figures 10A and 10E). In contrast, knockdown of Rab10 by shRNA enhanced spine enlargement both in the transient and sustained phase of sLTP, which was rescued by co-expressing the shRNA-resistant Rab10 (Figure 10B). Overall, these results suggest that Rab4 is required for the transient phase of sLTP, while Rab10 negatively regulates both transient and sustained phases.

As an alternative strategy to inhibit Rab4 and Rab10 function, I examined the effects of overexpression of dominant negative (DN) mutants of Rab proteins, Rab4a [S27N] or Rab10 [T23N], in spin structural plasticity. Consistent with shRNA results, DN-Rab4a selectively inhibited the transient phase of sLTP (Figures 10C and 10E), while DN-Rab10 enhanced both transient and sustained phases (Figures 10D and 10E).

Finally, I studied the effects of overexpressing constitutively active (CA) Rab4 or Rab10 mutants (Rab4 [Q72L] or Rab10 [Q68L]) in sLTP. I found that this manipulation in general caused opposite results from DN proteins: CA-Rab4 slightly increased the transient phase of sLTP (but not statistically significant), while CA-Rab10 decreased both transient and sustained phases of sLTP (Figures 10C and 10D).

Overall, these results demonstrate that Rab4 positively regulates the transient phase of sLTP while Rab10 negatively regulates both the transient and sustained phases of sLTP.

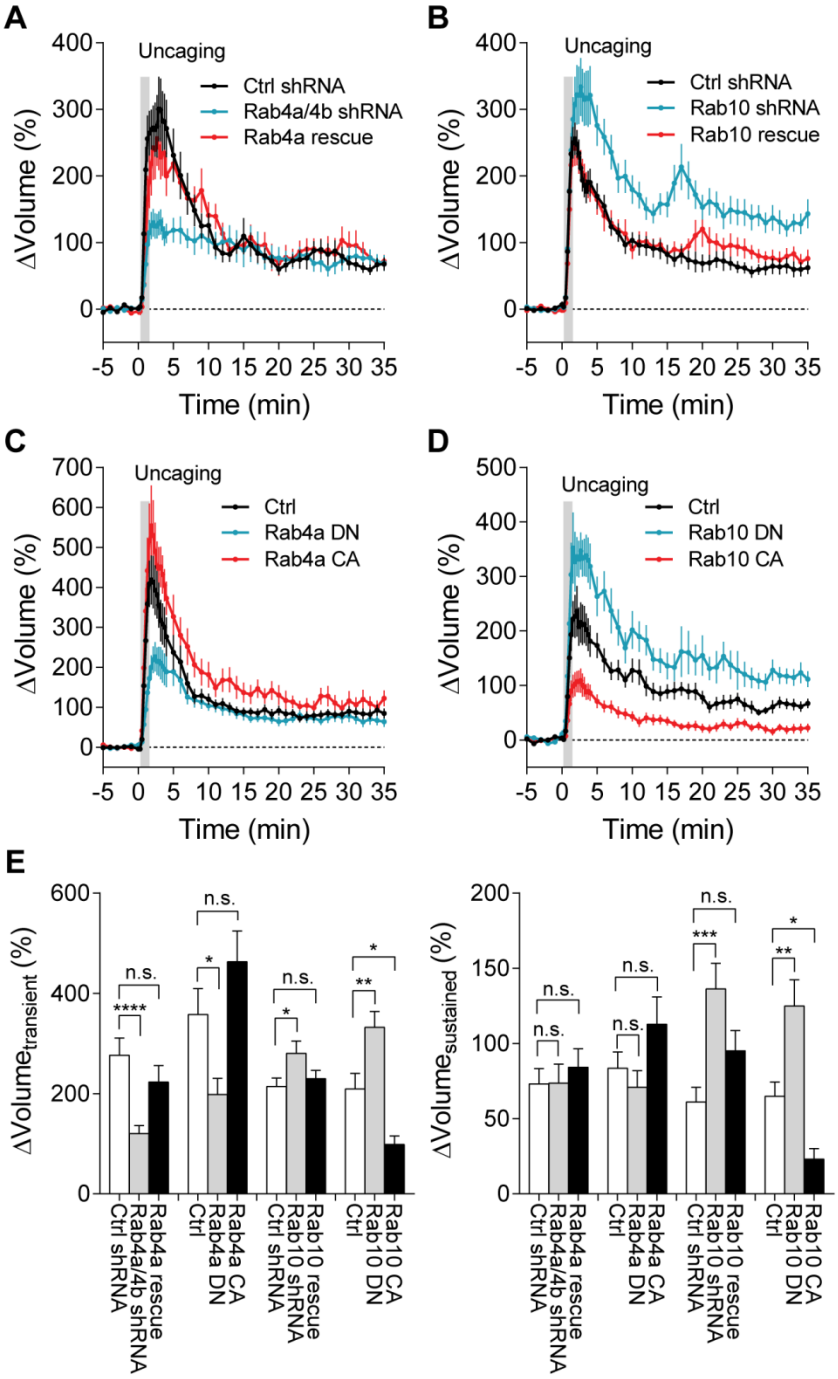

Figure 10 The Effect of Rab4 and Rab10 inhibition on structural LTP of spine head enlargement

(A-D) Averaged time courses of spine volume change in the stimulated spines after manipulations of Rab4 and Rab10 signaling. Fluorescence intensity of mEGFP was used to measure the spine volume change. Data represent means ± SEM. All experiments were paired with controls from the same batch of slices.
(A) CA1 pyramidal neurons were transfected with mEGFP and scramble shRNA (Ctrl shRNA, black); mEGFP and shRNA against Rab4a and Rab4b (Rab4a/4b shRNA, blue); mEGFP, shRNA against Rab4a and Rab4b and mCherry-shRNA resistant Rab4a (Rab4a rescue, red). N=16/16, 24/20 and 10/8 (spine/neuron) for Ctrl shRNA, Rab4a/4b shRNA and Rab4a rescue, respectively.
(B) CA1 pyramidal neurons were transfected with mEGFP (Ctrl, black); mEGFP and mCherry-Rab4a [S27N] (Rab4a DN, blue); mEGFP and mCherry-Rab4a [Q72L] (Rab4a CA, red). N=21/15, 19/18 and 16/11 (spine/neuron) for Ctrl, Rab4a DN and Rab4a CA, respectively.
(C) CA1 pyramidal neurons were transfected with mEGFP and scramble shRNA (Ctrl shRNA, black); mEGFP and shRNA against Rab10 (Rab10 shRNA, blue); mEGFP, shRNA against Rab10 and mCherry-shRNA resistant Rab10 (Rab10 rescue, red). N=22/20, 22/20 and 16/13 (spine/neuron) for Ctrl shRNA, Rab10 shRNA and Rab10 rescue, respectively.
(D) CA1 pyramidal neurons were transfected with mEGFP (Ctrl, black); mEGFP and mCherry-Rab10 [T23N] (Rab10 DN, blue); mEGFP and mCherry-Rab10 [Q68L] (Rab10 CA, red). N=22/18, 17/15 and 19/14 (spine/neuron) for Ctrl, Rab10 DN and Rab10 CA, respectively.
(E) Quantitative analysis of the transient volume change (volume change averaged over 1.3–4 min, left) and the sustained volume change (volume change averaged over 20–35 min, right) for (A-D). Data represent means ± SEM. Bonferroni's multiple comparison tests were performed (n.s., not significant, * $p<0.05$, ** $p<0.01$, *** $p<0.001$).

3.2.2 Verification of Rab shRNA and shRNA resistant Rab by dual-luciferase reporter assay

To verify the effect of shRNA, I tested the shRNA constructs in HEK 293T cells by a dual luciferase reporter assay as described in Chapter 2.6. hRluc (firefly luciferase) was used as the reporter gene, and Rab gene was cloned downstream of the hRluc translational stop codon. Once shRNA targets to the Rab sequence region, the fusion mRNA is cleaved and degraded, resulting in no luminescence from hRluc (Figure 11A).

Using this method, I demonstrated that Rab4a, Rab4b and Rab10 shRNAs are effective in targeting their respective Rab DNA sequence (Figure 11B). Furthermore, I also tested the Rab rescue constructs and found that Rab shRNAs could not target the respective Rab rescue construct, suggesting that the rescue constructs are working (Figures 11C and 11D).

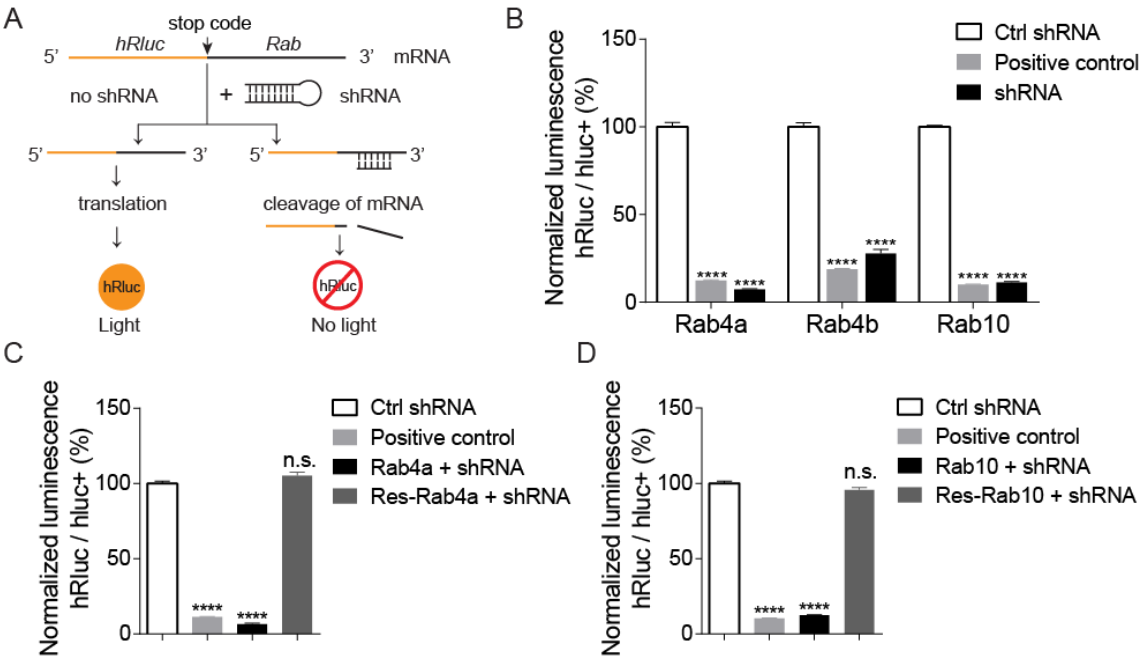

Figure 11 Verification of Rab GTPase shRNA and shRNA Resistant Rab GTPases

(A) Schematic of dual-luciferase reporter assay.
(B) Verification of Rab4a, Rab4b and Rab10 shRNA by dual-luciferase reporter assay. Individual psiCHECK-2-Rab GTPase was cotransfected into HEK 293T cells with scramble shRNA (Ctrl shRNA), hRluc shRNA (Positive control) or individual Rab GTPase shRNA. Data represent mean ± SEM. Bonferroni's multiple comparison tests were performed (**** $p<0.0001$). N=8, 8, 8, 8, 8, 8, 10, 10, 10 wells from left to right.
(C) Verification of shRNA resistant Rab4a. HEK 293T cells were transfected with psiCHECK-2-shRNA resistant Rab4a and scramble shRNA (Ctrl shRNA), psiCHECK-2-shRNA resistant Rab4a and hRluc shRNA (Positive control), psiCHECK-2 Rab4a and Rab4a shRNA (Rab4a+shRNA), or psiCHECK-2-shRNA resistant Rab4a and Rab4a shRNA (Res-Rab4a+shRNA). Data represent mean ± SEM. Bonferroni's multiple

comparison tests were performed (n.s., not significant, **** p<0.0001). N=4, 4, 4, 4 wells from left to right.
(D) Verification of shRNA resistant Rab10. HEK 293T cells were transfected with psiCHECK-2-shRNA resistant Rab10 and scramble shRNA (Ctrl shRNA), psiCHECK-2-shRNA resistant Rab10 and hRluc shRNA (Positive control), psiCHECK-2 Rab10 and Rab10 shRNA (Rab10+shRNA), or psiCHECK-2-shRNA resistant Rab10 and Rab10 shRNA (Res-Rab10+shRNA). Data represent mean ± SEM. Bonferroni's multiple comparison tests were performed (n.s., not significant, **** p<0.0001). N=5, 5, 5, 5 wells from left to right.

3.2.3 Verification of Rab shRNA by western blot

We also validated the knockdown effect of individual shRNA in dissociated cortical neurons by western blot as described in Chapter 2.12 and 2.13. Dissociated cortical neurons were infected with lentivirus of scramble shRNA, Rab4a shRNA, Rab4b shRNA or Rab10 shRNA for 11 days, and lysed for western blot analysis. Our results showed that Rab shRNAs can efficiently knock down the respective Rab protein in cortical neurons (Figures 12).

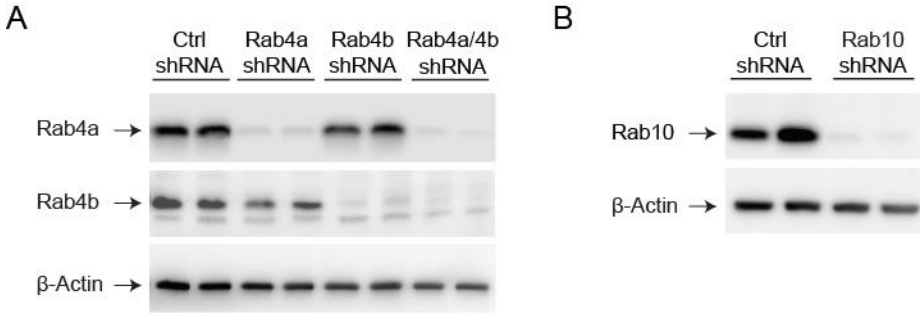

Figure 12 Validation of shRNA-mediated knockdown of Rab GTPases by western blot

(A) Western blot analysis of Rab4a and Rab4b shRNA in dissociated cortical neurons. Neurons were infected with the lentivirus of scramble control shRNA (Ctrl shRNA), Rab4a shRNA (Rab4a shRNA), Rab4b shRNA (Rab4b shRNA) or Rab4a and Rab4b shRNA (Rab4a/4b shRNA), and lysed for western blot analysis. N=2 for each group.

(B) Western blot analysis of Rab10 shRNA in dissociated cortical neurons. Neurons were infected with the lentivirus of scramble control shRNA (Ctrl shRNA) or Rab10 shRNA (Rab10 shRNA), and lysed for western blot analysis. N=2 for each group.

Chapter 4. Highly sensitive and selective FRET sensors for Rab4 and Rab10

4.1 Characterization of Rab4 and Rab10 FRET sensors in HEK 293T cells

Next, I aimed to image the activities of Rab4 and Rab10 in single dendritic spines during sLTP. To do so, I developed FRET sensors using a design similar to the previous HRas and Rho GTPase sensors (Harvey et al., 2008; Murakoshi et al., 2011). The Rab sensors consist of Rab fused with FRET donor (mEGFP or mTurquise2) and the Rab binding domain (RBD) of an effector molecule fused with the FRET acceptors (mCherry or mVenus) as an accepter (mCherry-RBD-mCherry or mVenus-RBD-mVenus). When the donor-Rab is activated, RBD would bind to Rab, increasing FRET between the donor and acceptor (Figures 15A and 20A). The fraction of Rab bound to the RBD (binding fraction) can be calculated by measuring the fluorescence lifetime change of donor.

For Rab4 sensor, I used mEGFP-Rab4 and mCherry-Rabenosyn5 [439-503]-mCherry (Eathiraj et al., 2005). To verify the sensitivity and selectivity of Rab4 FRET sensor, I transfected wild type (WT) Rab4, DN-Rab4 and CA-Rab4 sensors in HEK 293T cells. DN-Rab4 and CA-Rab4 displayed low and high binding (20.7 ± 1.1%, 30.8 ± 1.4%) compared to WT-Rab4 (26.6 ± 1.7%), suggesting that the sensor reports Rab4 signaling as expected (Figures 13A and 13B). Furthermore, when I coexpressed Rab4 sensor together with PIK3R1, a specific GAP for Rab4 (Chamberlain et al., 2004). The binding fraction of Rab4 sensor decreased as PIK3R1 expression increased, further demonstrating that the

Rab4 sensor specifically reports Rab4 signaling (Figures 13C and 13D). There is no known GEF for Rab4, thus I could not test if the Rab4 sensor could respond to the activation of GEF.

For Rab10, I used mTurquoise2-Rab10 paired with mVenus-Rim1 [20-277]-mVenus (Fukuda, 2003). I used the mTurqouise2-mVenus pair instead of the mEGFP-mCherry pair, since it provided higher signal to noise ratio in HEK 293T cells (Figure 13F) (Goedhart et al., 2012; Takahashi et al., 2015).

To verify the sensitivity and specificity of Rab10 FRET sensor, I transfected sensors using WT-Rab10, DN-Rab10 and CA-Rab10 in HEK 293T cells. The binding fractions were lower for DN-Rab10 (7.2 ± 0.8%) and higher for CA-Rab10 (46.0 ± 1.3%) compared to that of WT-Rab10 (27.2 ± 1.0%), consistent with their biochemical states (Figures 13A and 13B). Furthermore, GAPs and guanine nucleotide exchange factor (GEF) specific to Rab10 (Fukuda et al., 2008; Itoh et al., 2006; Yoshimura et al., 2010), decreased and increased the binding fraction of Rab10 sensor, respectively (Figures 13C and 13D). Altogether, these results suggest that Rab10 FRET sensor specifically reports Rab10 activation.

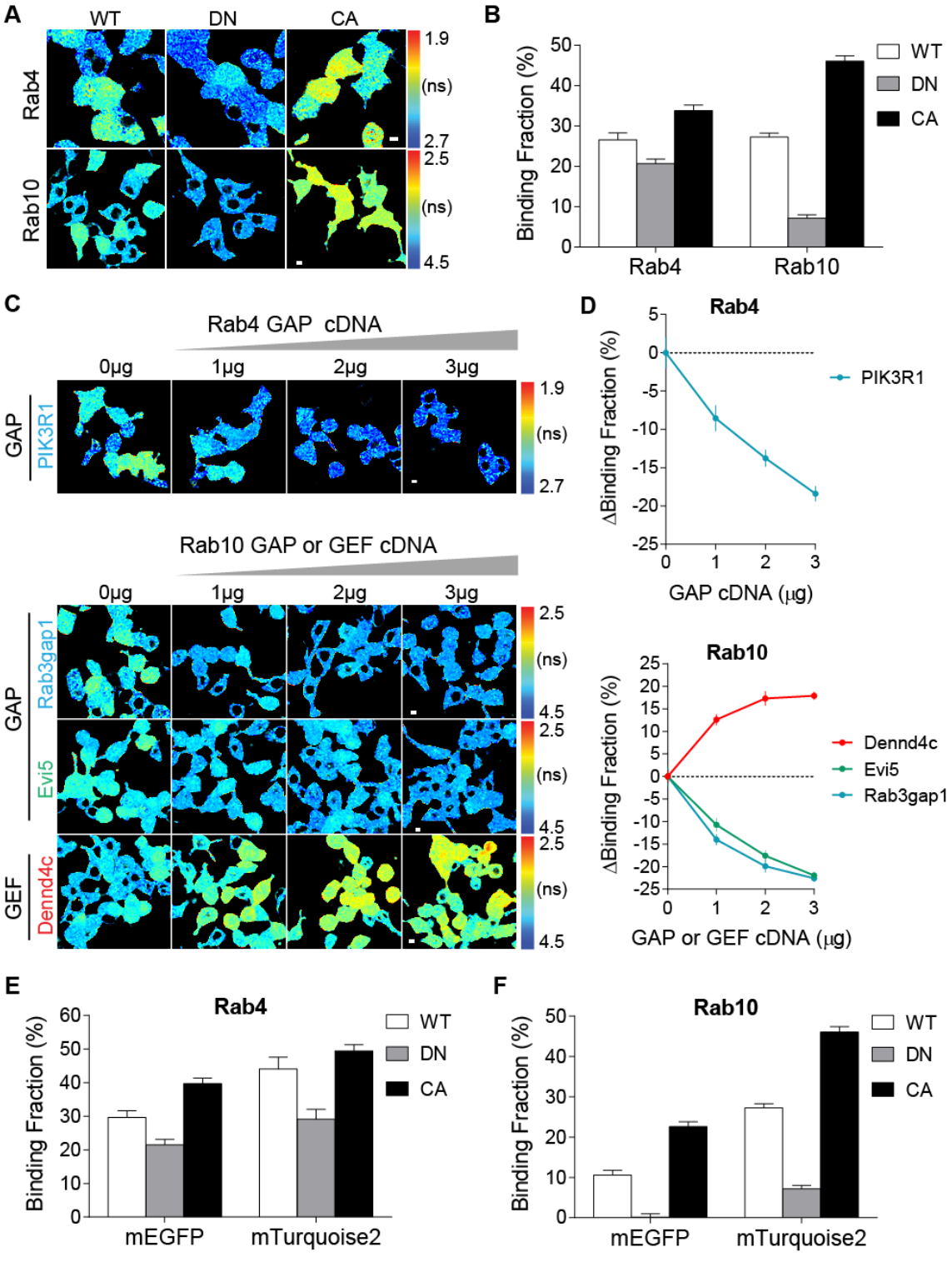

Figure 13 Characterization of Rab4 and Rab10 FRET sensors in HEK 293T cells

(A) Representative FLIM images of HEK 293T cells transfected with mEGFP-Rab4a (upper lane) and mTurquoise2-Rab10 (lower lane) wild type, dominant negative (Rab4a [S27N], Rab10 [T23N]) and constitutively active (Rab4a [Q72L] and Rab10 [Q68L]) sensors. Warmer color indicates shorter lifetime and higher activity. Colder color indicates longer lifetime and lower activity. Scale bars represent 5 μm.
(B) Quantification of binding fractions for mEGFP-Rab4 bound to mCherry-Rabenosyn5 [439-503]-mCherry, and mTurquoise2-Rab10 bound to mVenus-Rim1 [20-227]-mVenus. Data represent mean ± SEM. N=33, 29, 29, 32, 32, 32 fields from left to right.
(C) Upper: representative FLIM images of Rab4 mEGFP wild type sensor cotransfected with its specific GAP (PIK3R1) cDNA. Lower: representative FLIM images of Rab10 mTurqupose2 wild type sensor cotransfected with its specific GAP (Rab3gap1 and Evi5) or GEF (Dennd4c) cDNA. Scale bars represent 5 μm.
(D) Upper: binding fraction change of Rab4 mEGFP sensor in response to the increase of PIK3R1 cDNA. N=30, 35, 35, 40 fields. Lower: binding fraction change of Rab10 mTurquoise2 sensor in response to the increase of GAP or GEF cDNA. N=16, 16, 16, 16 fields for Rab3gap1, 16, 16, 16, 16 fields for Evi5, and 16, 16, 16, 16 fields for Dennd4c. Data represent mean ± SEM.
(E) Comparison of mEGFP-Rab4 and mTurquoise2-Rab4 sensors in HEK 293T cells.
(F) Comparison of mEGFP-Rab10 and mTurquoise2-Rab10 sensors in HEK 293T cells.

4.2 NMDARs-mediated Rab4 and Rab10 activation in neurons

To examine the activity of Rab4 in neurons, I ballistically transfected cultured organotypic hippocampal slices of rats with Rab4 mEGFP sensor, and imaged the proximal apical dendrites of CA1 pyramidal neurons by 2pFLIM. Bath application of N-Methyl-D-aspartic acid (NMDA)(15 μM, 2 min) in zero extracellular Mg^{2+} (Murakoshi et al., 2011) triggered a rapid activation of Rab4 FRET sensor both in the spines and dendrites, which peaked within 3 min and decayed with washout (Figures 14A and 14C). This fast activation further suggests that Rab4 FRET sensor could report neuronal Rab4 activity.

To test Rab10 FRET sensor in neurons, I ballistically transfected cultured rat organotypic hippocampal slices with Rab10 mTurquoise2 FRET sensor, and imaged the proximal apical dendrites of CA1 pyramidal neurons by 2pFLIM. Bath application of NMDA (15 μM, 2 min) in zero extracellular Mg^{2+} induced a slow but significant activation of Rab10 broadly, which peaked at 10 min and gradually decreased with washout (Figures 14B and 14D). This accumulated activation further confirms that Rab10 FRET sensor can report neuronal Rab10 activation.

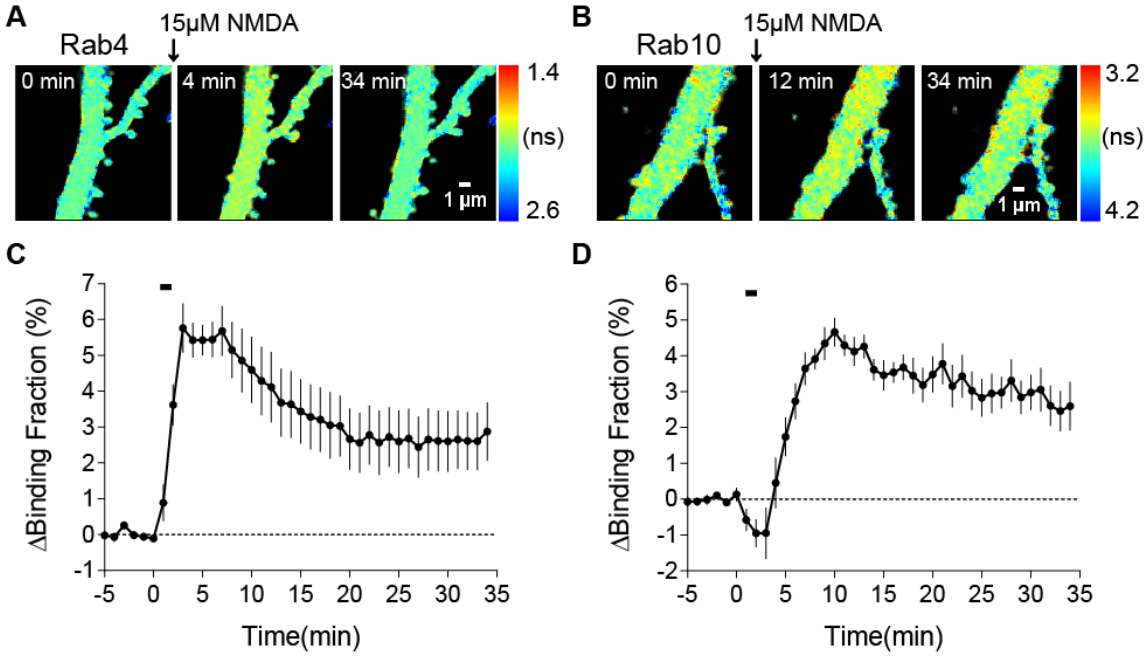

Figure 14 NMDARs-mediated Rab4 and Rab10 activation

(A and B) Representative FLIM images of mEGFP-Rab4 (A) and mTurquoise2-Rab10 (B) sensors in the primary dendrites of CA1 pyramidal neurons upon NMDA stimulation. 15 μM NMDA was bath-applied for 2 min and washed out. Warmer color indicates shorter lifetime and higher activity. Colder color indicates longer lifetime and lower activity. Scale bar represents 1 μm.

(C and D) Averaged time courses of Rab4 (C) and Rab10 (D) activity change in the same experiments as (A) and (B). Data represent mean ± SEM. N=11 and 9 neurons for Rab4 and Rab10, respectively.

Chapter 5. Rab4 is transiently activated in the stimulated spines during structural LTP

5.1 Spatiotemporal dynamics of Rab4 activation during structural LTP induced in single spines

To characterize the spatiotemporal dynamics of Rab4 in single dendritic spines during sLTP, I imaged the secondary apical dendrites of CA1 pyramidal neurons at 25-27°C by combining two-photon glutamate uncaging and 2pFLIM. Upon glutamate uncaging (0.5 Hz, 60 s) in zero extracellular Mg2+, a single spine underwent a rapid volume enlargement by 341.0 ± 29.4% in the transient phase, and decreased to an elevated 77.6 ± 8.0% in the sustained phase (Figures 15B and 15F-15H), both of which were independent of the initial spine volume (Figure 16A and 16B). Concomitant with the spine enlargement, Rab4 activity was transiently elevated in the stimulated spine and decayed, with no activity change in the adjacent spines or dendrites (Figures 15B-15E). Additionally, there was no correlation between the initial spine volume and the basal binding fraction (BBF) or binding fraction change of Rab4 sensor (Figures 16C-16E). In summary, my results demonstrate that Rab4 is transiently activated in the stimulated spines during sLTP, and this activation is compartmentalized in the stimulated spines.

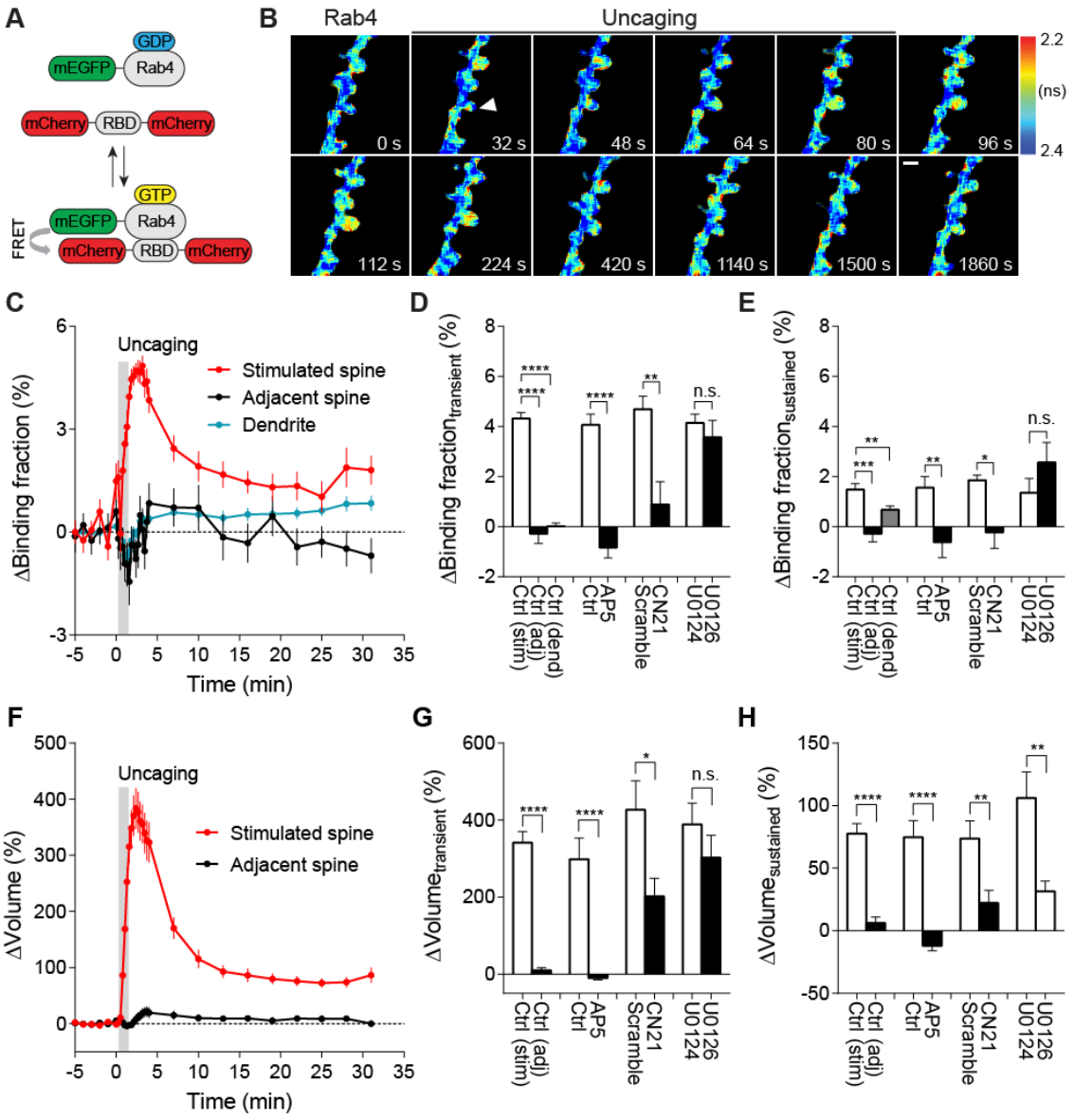

Figure 15 Spatiotemporal dynamics of Rab4 activation during structural LTP induced in single spines

(A) Schematic diagram illustrating the Rab4 FRET sensor design.
(B) Representative fluorescence lifetime images of Rab4 activation during sLTP induced by two-photon glutamate uncaging. Arrowhead indicates the stimulated spine. The warmer color indicates the shorter lifetime and higher Rab4 activity. Scale bar represents 1 μm.

(C) Averaged time courses of Rab4 activation measured as binding fraction change between mEGFP-Rab4 and mCherry-RBD-mCherry in the stimulated spine (red), adjacent spine (black) and dendrite (blue). Grey rectangle bar indicates glutamate uncaging (0.5 Hz, 60 s). Data are presented in mean ± SEM. N=42/34 (spine/neuron), 42/34 (spine/neuron) and 42/34 (dendrite/neuron) for the stimulated spine, adjacent spine and dendrite, respectively.
(D and E) Quantification of Rab4 binding fraction change in the transient phase (D, averaged over 1.3-4 min) and sustained phase (E, averaged over 19-31 min) in the stimulated spine (stim), adjacent spine (adj) and dendrite (dend) for the same experiments as (C). Data represent mean ± SEM. Bonferroni's multiple comparison tests were used for the adjacent spine and dendrite (** $p<0.01$, *** $p<0.001$, **** $p<0.0001$). Effects of pharmacological agents on Rab4 activation in the stimulated spines are also presented. All pharmacological inhibition experiments were paired with controls from the same batch of slices. Data represent mean ± SEM. Student's t-tests were performed (n.s., not significant, * $p<0.05$, ** $p<0.01$, **** $p<0.0001$). N=14/11, 12/9, 9/8, 13/11, 10/8 and 9/8 (spine/neuron) for Ctrl, AP5, scramble, CN21, U0124 and U0126, respectively.
(F) Averaged time courses of spine volume change in the same experiments as (C). Data represent mean ± SEM.
(G and H) Quantification of spine volume change in the transient phase (G, averaged over 1.3-4 min) and sustained phase (H, averaged over 19-31 min) for the same experiments as (D) and (E). Data represent mean ± SEM. Bonferroni's multiple comparison tests were used for the adjacent spine and dendrite (**** $p<0.0001$). Student's t-tests were performed for the pharmacological inhibitors (n.s., not significant, * $p<0.05$, ** $p<0.01$, **** $p<0.0001$).

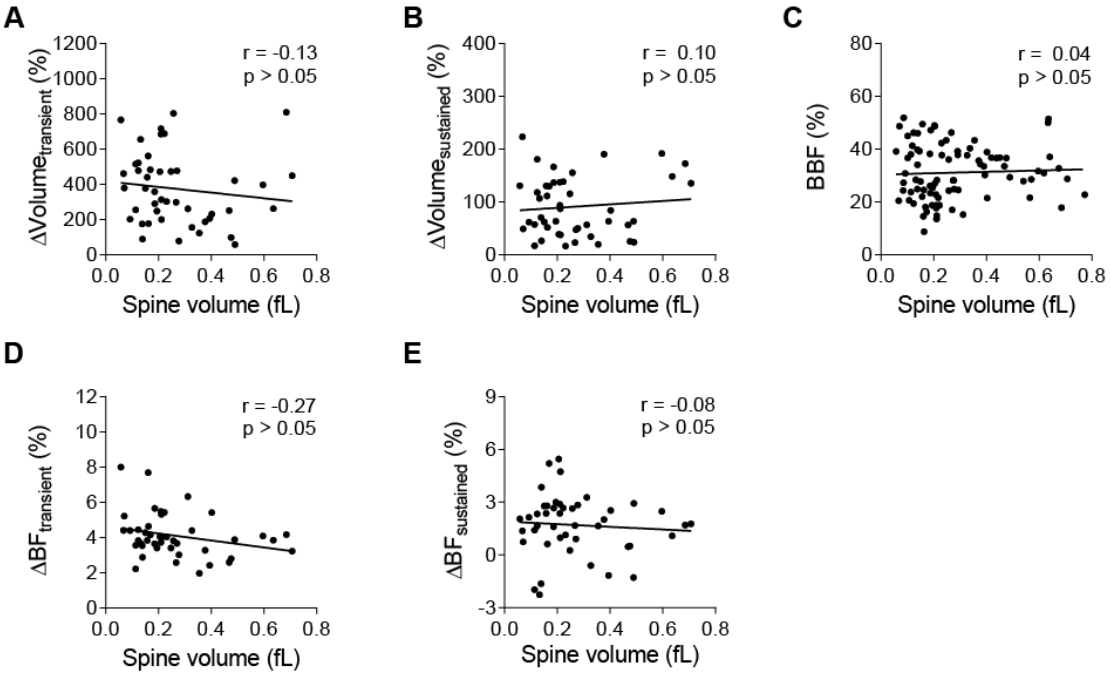

Figure 16 Relationships between initial spine volume and basal Rab4 activity, spine volume change or activity change during structural LTP

(A and B) Relationships between the initial spine volume and spine volume change in the transient (A, averaged over 1.3-4 min) and sustained phase (B, averaged over 19-31 min) in Rab4 sensor-expressing neurons. N=45/39 (spine/neuron). No significant correlation ($p > 0.05$) was found.
(C) Relationship between the spine volume and basal binding fraction (BBF) of Rab4 sensor. N=90/39 (spine/neuron). No significant correlation ($p > 0.05$) was found.
(D and E) Relationships between the initial spine volume and Rab4 activity change in the transient (D, averaged over 1.3-4 min) and sustained phase (E, averaged over 19-31 min) of sLTP in the stimulated spines. N=45/39 (spine/neuron). No significant correlation ($p > 0.05$) was found.

5.2 Rab4 activation under manipulations of putative upstream signaling pathways

To identify the signaling pathways that activate Rab4 during sLTP, I applied pharmacological inhibitors targeting putative upstream components (Patterson and

Yasuda, 2011). Inhibition of NMDA receptors by 2-amino-5-phosphonopentanoic acid (AP5, 50 μM) completely abolished Rab4 activation and the spine enlargement (Figures 15D, 15E, 15G, 15H, 17A and 17B). Application of CN21 (10 μM), a CaMKII inhibitory peptide, decreased Rab4 activity and volume change both in the transient phase and sustained phase (Figures 15D, 15E, 15G, 15H, 17C and 17D). In contrast, mitogen-activated protein kinase kinase (MEK) inhibitor U0126 (20 μM) had no effect on Rab4 activation although it impaired sLTP in the sustained phase (Figures 15D, 15E, 15G, 15H, 17E and 17F). Altogether, these results reveal that Rab4 is transiently activated during sLTP and this activation is dependent on NMDA receptors, CaMKII, but not on MAPK/ERK signaling pathway.

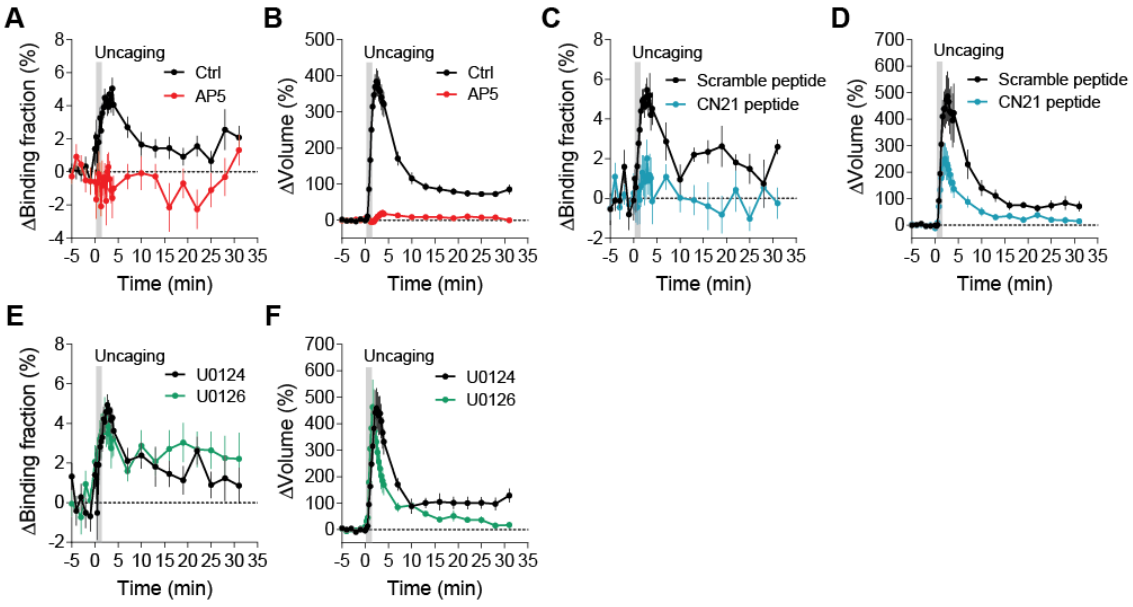

Figure 17 Rab4 activation under manipulations of putative upstream signaling pathways

(A and B) Averaged time courses of Rab4 activity change (A) and spine volume change (B) in the stimulated spines during sLTP. Black and red curves represent control (Ctrl) and AP5 (50 μM), respectively. Data represent mean ± SEM. N=14/11 and 12/9 (spine/neuron) for Ctrl and AP5, respectively.
(C and D) Averaged time courses of Rab4 activity change (C) and spine volume change (D) in the stimulated spines during sLTP. Black and blue curves represent scramble peptide control (10 μM) and CN21 peptide (10 μM), respectively. Data represent mean ± SEM. N=9/8 and 13/11 (spine/neuron) for scramble peptide and CN21 peptide, respectively.
(E and F) Averaged time courses of Rab4 activity change (E) and spine volume change (F) in the stimulated spines during sLTP. Black and green curves represent U0124 control (20 μM) and U0126 (20 μM), respectively. Data represent mean ± SEM. N=10/8 and 9/8 (spine/neuron) for U0124 and U0126, respectively.
For all pharmacological inhibition experiments, hippocampal slices were incubated in the indicated drugs for 30 min before experiments. All experiments were paired with controls from the same batch of neurons.

5.3 Binding fraction change of mEGFP-Rab4 paired with false acceptor during structural LTP

To verify the specificity of Rab4 FRET sensor response, I paired mEGFP-Rab4 with mCherry-Rim1 [20-227]-mCherry, the acceptor for Rab10 (false acceptor). Despite the similar spine enlargement (Figures 18C and 18D), there was no significant activity increase in the stimulated spines (Figures 18A and 18B). I also plotted the average binding fraction change versus different sensor concentrations in both the control and false acceptor groups (Figures 18E-18H). In general, the false acceptor group showed a lower binding fraction change at different sensor concentrations. In summary, my results prove that the Rab4 FRET sensor activity change in Figure 15 is specific and reflects Rab4 activation.

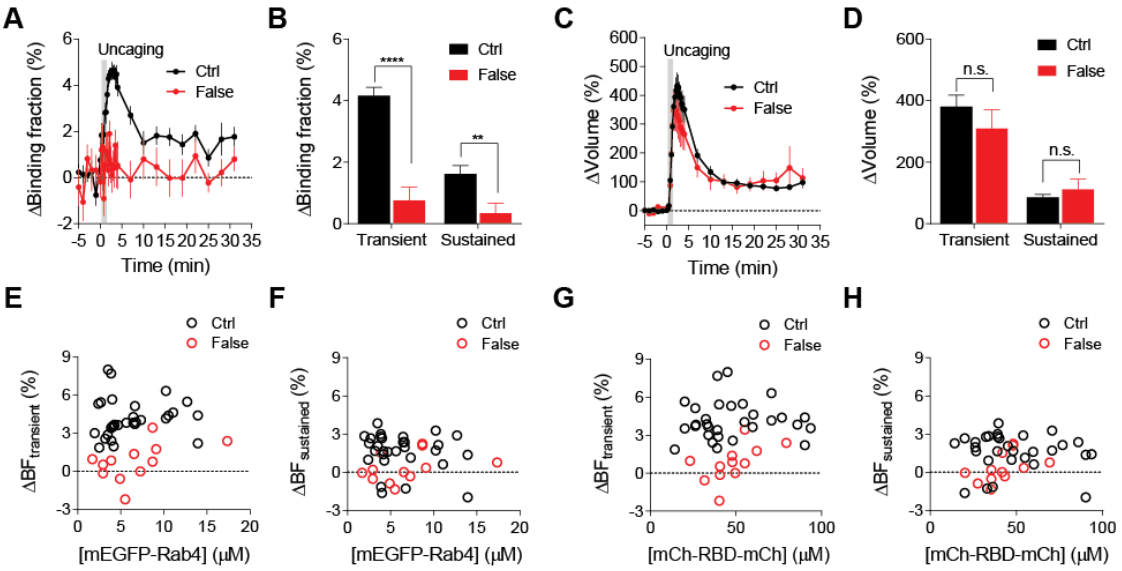

Figure 18 Binding fraction change of mEGFP-Rab4 paired with false acceptor during structural LTP

(A) Averaged time course of mEGFP-Rab4 sensor (Ctrl, black) activity change in the stimulated spines during sLTP. When mEGFP-Rab4 was paired with a false acceptor (False, red), mCherry-Rim1 [20-227]-mCherry, little activity change was observed. Data represent mean ± SEM. N=30/25 (spine/neuron) for Ctrl, and 12/9 for False.
(B) Quantification of binding fraction change in the transient phase (1.3-4 min) and sustained phase (19-31 min) for the same experiment as in (A). Data represent mean ± SEM. Student's t-tests were performed (** $p<0.01$, **** $p<0.0001$).
(C) Averaged time courses of spine volume change for the same experiments as (A). Data represent mean ± SEM. N=30/25, 12/9 (spine/neuron) for Ctrl and False, respectively.
(D) Quantification of spine volume change in the transient phase (1.3-4 min) and sustained phase (19-31 min) for the same experiments as in (A). Data represent mean ± SEM. Student's t-tests were performed (n.s., not significant).
(E and F) Relationships between mEGFP-Rab4 concentration and binding fraction change in the transient (E, 1.3-4 min) and sustained phase (F, 19-31 min) of sLTP. N=30/25, 12/9 (spine/neuron) for Ctrl (black) and False (red), respectively.
(G and H) Relationships between mCherry-RBD-mCherry concentration and binding fraction change in the transient (G, 1.3-4 min) and sustained phase (H, 19-31 min) of sLTP. N=30/25, 12/9 (spine/neuron) for Ctrl (black) and False (red), respectively.

5.4 Rab4 activation at a near physiological temperature during structural LTP

To investigate whether Rab4 displays a similar spatiotemporal profile at the physiological temperature, I performed the similar experiments as Figure 5 while clamping the temperature at 33-35°C. My results demonstrated that Rab4 showed a similar activation pattern and spine enlargement at the near physiological temperature (Figures 19A-19D). Moreover, I examined the relationships between the binding fraction change and sensor concentration, which showed no correlation and further confirmed that the activity change of Rab4 is independent of sensor overexpression level (Figures 19E-19H). In summary, my results demonstrate that Rab4 is transiently activated and restricted in the stimulated spines during sLTP, both at the room temperature and the physiological temperature.

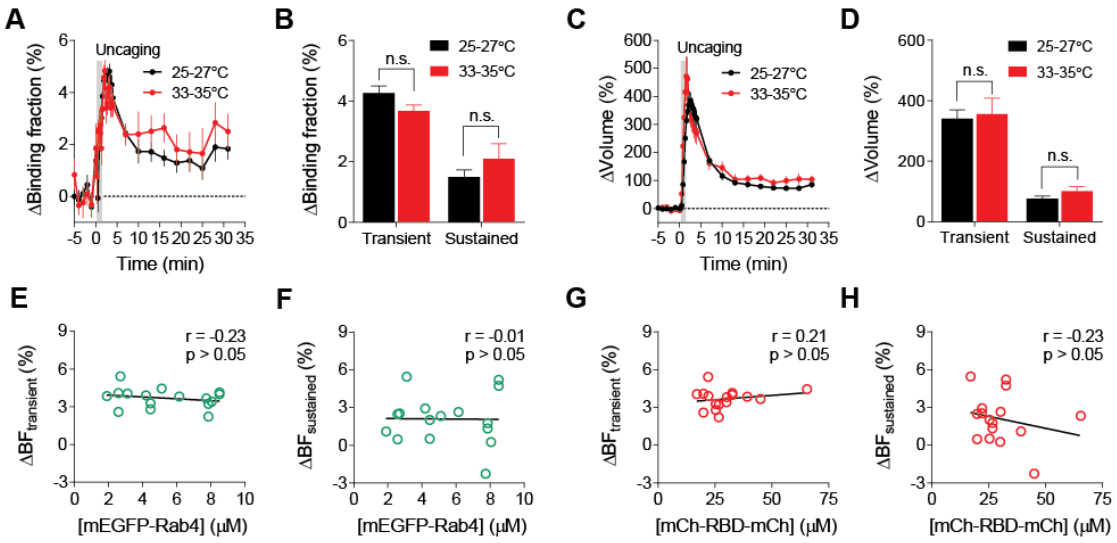

Figure 19 Rab4 activation at the near physiological temperature during structural LTP

(A) Averaged time courses of Rab4 activity change in the stimulated spines during sLTP at 25-27°C (black) and 33-35°C (red). Data represent mean ± SEM. N=42/34 and 16/13 (spine/neuron) for 25-27°C and 33-35°C, respectively.
(B) Quantification of binding fraction change in the transient phase (1.3-4 min) and sustained phase (19-31 min) for the same experiment as in (A). Data represent mean ± SEM. Student's t-tests were performed (n.s., not significant).
(C) Averaged time courses of spine volume change for the same experiments as (A). Data represent mean ± SEM.
(D) Quantification of spine volume change in the transient phase (1.3-4 min) and sustained phase (19-31 min) for the same experiments as in (A). Data represent mean ± SEM. Student's t-tests were performed (n.s., not significant).
(E and F) Correlation between mEGFP-Rab4 concentration and binding fraction change in the transient (E, 1.3-4 min) and sustained phase (F, 19-31 min) of sLTP at 33-35°C. No significant correlation ($p > 0.05$) was found. N=16/13 (spine/neuron).
(G and H) Correlation between mCherry-RBD-mCherry concentration and binding fraction change in the transient (G, 1.3-4 min) and sustained phase (H, 19-31 min) of sLTP at 33-35°C. No significant correlation ($p > 0.05$) was found. N=16/13 (spine/neuron).

Chapter 6. Rab10 is persistently inactivated in the stimulated spines during structural LTP

6.1 Spatiotemporal dynamics of Rab10 inactivation during structural LTP in single spines

I also measured the spatiotemporal profiles of Rab10 in single dendritic spines during sLTP. After a train of two-photon glutamate uncaging pulses (0.5 Hz, 60 s) in zero extracellular Mg^{2+} , a single spine underwent a rapid volume enlargement by 275.8 ± 24.5% in the transient phase, and decreased to an elevated 78.8 ± 6.6% in the sustained phase (Figures 20B and 20F-20H). Unexpectedly, Rab10 was rapidly inactivated in the stimulated spines, which lasted for more than 30 min, with no activity change in the adjacent spines or dendrites (Figures 20B-20E). The spine volume change, Rab10 BBF and binding fraction change were not correlated with the initial spine size (Figures 21A-21E). In summary, my results demonstrate that Rab10 is persistently inactivated in the stimulated spines during sLTP, and this inactivation is compartmentalized in the stimulated spines.

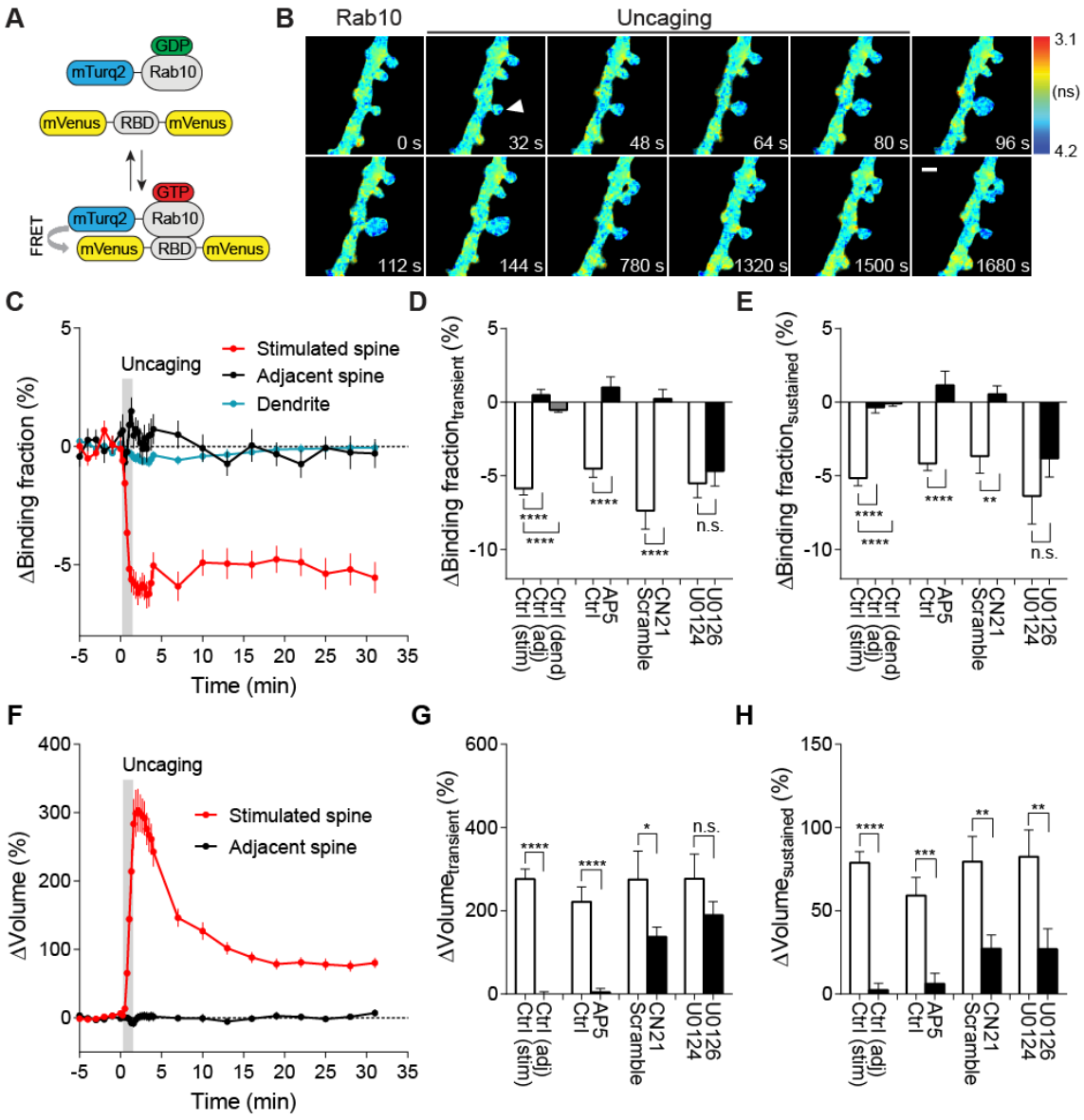

Figure 20 Spatiotemporal dynamics of Rab10 inactivation during structural LTP in single spines

(A) Schematic diagram illustrating the Rab10 FRET sensor design.
(B) Representative fluorescence lifetime images of Rab10 inactivation during sLTP induced by two-photon glutamate uncaging. Arrowhead indicates the stimulated spine. The colder color indicates the longer lifetime and lower Rab10 activity. Scale bar represents 1 μm.

(C) Averaged time courses of Rab10 inactivation measured as binding fraction change between mTurquoise2-Rab10 and mVenus-RBD-mVenus in the stimulated spine (red), adjacent spine (black) and dendrite (blue). Grey rectangle bar indicates glutamate uncaging (0.5 Hz, 60 s). Data are presented in mean ± SEM. N=50/44 (spine/neuron), 50/44 (spine/neuron) and 50/44 (dendrite/neuron) for the stimulated spine, adjacent spine and dendrite, respectively.
(D and E) Quantification of Rab10 binding fraction change in the transient phase (D, averaged over 1.3-4 min) and sustained phase (E, averaged over 19-31 min) in the stimulated spine (stim), adjacent spine (adj) and dendrite (dend) for the same experiments as (C). Data represent mean ± SEM. Bonferroni's multiple comparison tests were performed for the adjacent spine and dendrite (**** $p<0.0001$). Effects of pharmacological agents on Rab10 inactivation in the stimulated spines are also presented. All pharmacological inhibition experiments were paired with controls from the same batch of slices. Data represent mean ± SEM. Student's t-tests were performed (n.s., not significant, ** $p<0.01$, **** $p<0.0001$). N=15/14, 13/11, 9/8, 15/12, 9/8 and 11/8 (spine/neuron) for Ctrl, AP5, scramble, CN21, U0124 and U0126, respectively.
(F) Averaged time courses of spine volume change in the same experiment as (C). Data represent mean ± SEM.
(G and H) Quantification of spine volume change in the transient phase (G, averaged over 1.3-4 min) and sustained phase (H, averaged over 19-31 min) for the same experiments as (D) and (E). Data represent mean ± SEM. Bonferroni's multiple comparison tests were used for the adjacent spine and dendrite (**** $p<0.0001$). Student's t-tests were performed for the pharmacological inhibitors (n.s., not significant, * $p<0.05$, ** $p<0.01$, *** $p<0.001$, **** $p<0.0001$).

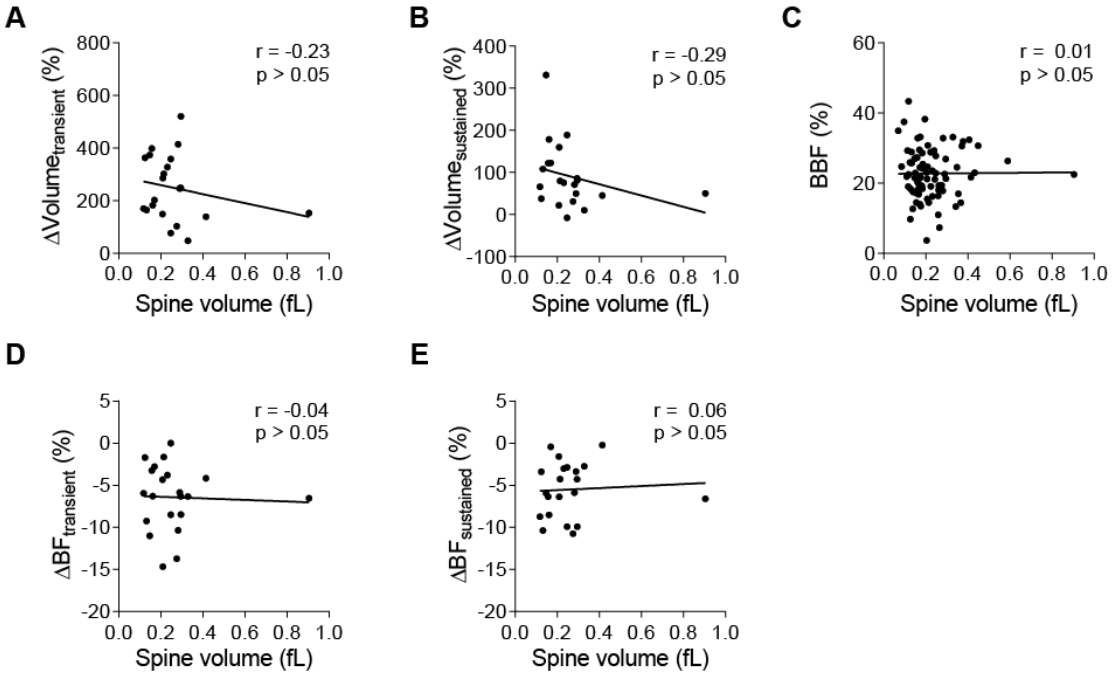

Figure 21 Relationships between initial spine volume and basal Rab4 activity, spine volume change or activity change during structural LTP

(A and B) Relationships between the initial spine volume and spine volume change in the transient (F, averaged over 1.3-4 min) and sustained phase (G, averaged over 19-31 min) in Rab10 sensor-expressing neurons. N=21/20 (spine/neuron). No significant correlation ($p > 0.05$) was found.
(C) Relationship between the spine volume and basal binding fraction (BBF) of Rab10 sensor. N=81/20 (spine/neuron). No significant correlation ($p > 0.05$) was found.
(D and E) Relationships between the initial spine volume and Rab10 activity change in the transient (I, averaged over 1.3-4 min) and sustained phase (J, averaged over 19-31 min) of sLTP in the stimulated spines. N=21/20 (spine/neuron). No significant correlation ($p > 0.05$) was found.

6.2 Rab10 inactivation under manipulations of putative upstream signaling pathways

To further identify the signaling pathways that inactivate Rab10 during sLTP, I applied pharmacological inhibitors targeting potential upstream components. Inhibition of NMDA receptors by AP5 (50 μM) completely abolished Rab10 inactivation and the

spine enlargement (Figures 20D, 20E, 20G, 20H, 22A and 22B). Application of CN21 (10 μM) decreased Rab10 inactivation and volume change both in the transient phase and sustained phase (Figures 20D, 20E, 20G, 20H, 22C and 22D). In contrast, MEK inhibitor U0126 (20 μM) had no effect on Rab10 inactivation although it impaired sLTP in the sustained phase (Figures 20D, 20E, 20G, 20H, 22E and 22F). Taken together, these results demonstrate that Rab10 is persistently inactivated in the stimulated spines during sLTP, and this inactivation is dependent on NMDA receptors, CaMKII, but not on MAPK/ERK signaling pathway.

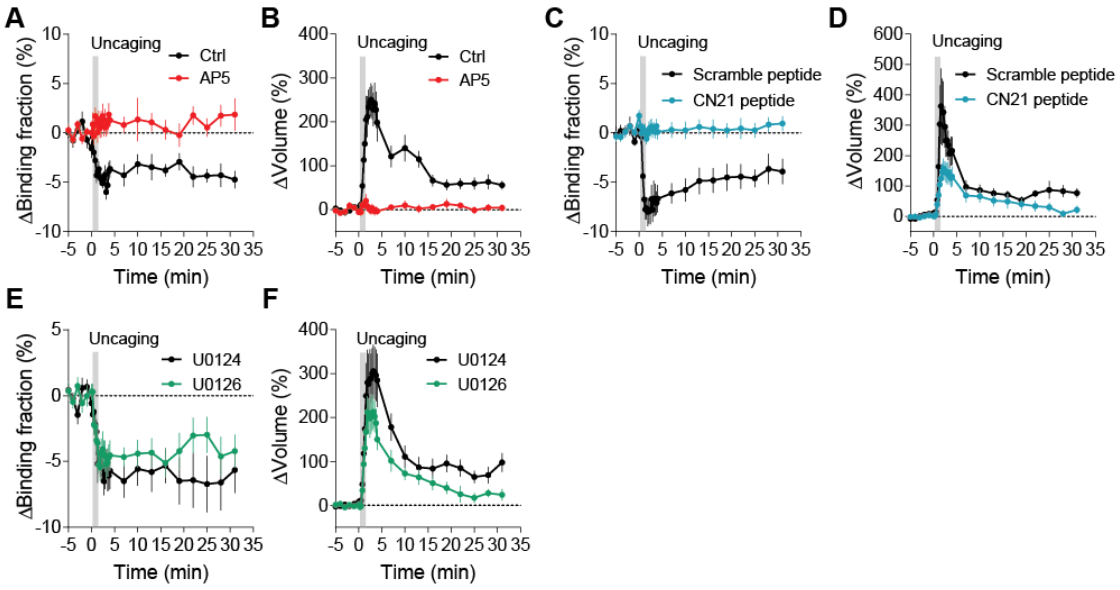

Figure 22 Rab10 inactivation under manipulations of putative upstream signaling pathways

(A and B) Averaged time courses of Rab10 activity change (A) and spine volume change (B) in the stimulated spines during sLTP. Black and red curves represent control (Ctrl) and AP5 (50 μM), respectively. Data represent mean ± SEM. N=15/14 and 13/11 (spine/neuron) for Ctrl and AP5, respectively.

(C and D) Averaged time courses of Rab10 activity change (C) and spine volume change (D) in the stimulated spines during sLTP. Black and blue curves represent scramble peptide control (10 μM) and CN21 peptide (10 μM), respectively. Data represent mean ± SEM. N=9/8 and 15/12 (spine/neuron) for scramble peptide and CN21 peptide, respectively.
(E and F) Averaged time courses of Rab10 activity change (E) and spine volume change (F) in the stimulated spines during sLTP. Black and green curves represent U0124 control (20 μM) and U0126 (20 μM), respectively. Data represent mean ± SEM. N=9/8 and 11/8 (spine/neuron) for U0124 and U0126, respectively.
For all pharmacological inhibition experiments, hippocampal slices were incubated in the indicated drugs for 30 min before experiments. All experiments were paired with controls from the same batch of neurons.

6.3 Binding fraction change of mTurquoise2-Rab10 paired with false acceptor during structural LTP

To test whether the Rab10 sensor response is specific, I paired mTurquoise-Rab10 with mVenus-Rabenosyn-5 [439-503]-mVenus, the binding domain for Rab4 (false acceptor). The false acceptor sensor showed no activity change in the stimulated spines during sLTP, indicating the specificity of sensor response (Figures 23A-23D). In addition, I plotted the binding fraction change versus sensor concentration in both control and false acceptor groups. Compared with control, the false acceptor showed almost no activity change at different sensor concentrations (Figures 23E-23H). Overall, my results demonstrate that Rab10 inactivation in Figure 20 is specific and reports Rab10 activity change.

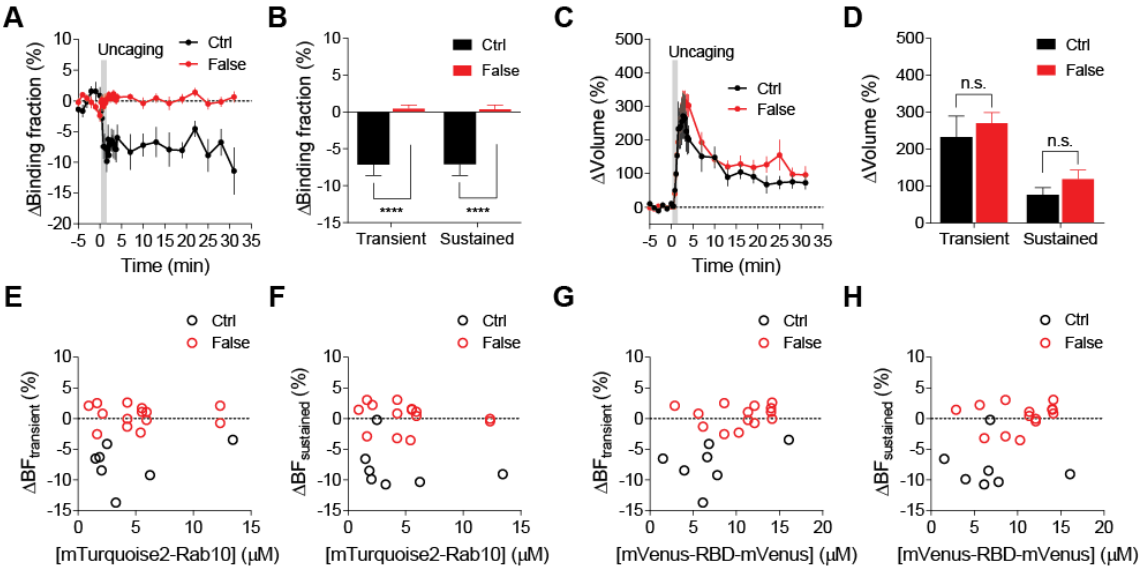

Figure 23 Binding fraction change of mTurquoise2-Rab10 paired with false acceptor during structural LTP

(A) Averaged time course of mTurquoise2-Rab10 sensor (Ctrl, black) activity change in the stimulated spines during sLTP. When mTurquoise2-Rab10 was paired with a false acceptor (False, red), mVenus-Rabenosyn-5 [439-503]-mVenus, little activity change was observed. Data represent mean ± SEM. N=7/7 and 14/9 (spine/neuron) for Ctrl and False, respectively.
(B) Quantification of binding fraction change in the transient phase (1.3-4 min) and sustained phase (19-31 min) for the same experiment as in (A). Data represent mean ± SEM. Student's t-tests were performed (**** $p<0.0001$).
(C) Averaged time courses of spine volume change for the same experiments as (A). Data represent mean ± SEM.
(D) Quantification of spine volume change in the transient phase (1.3-4 min) and sustained phase (19-31 min) for the same experiments as in (A). Data represent mean ± SEM. Student's t-tests were performed (n.s., not significant).
(E and F) Relationships between mTurquoise2-Rab10 concentration and binding fraction change in the transient (E, 1.3-4 min) and sustained phase (F, 19-31 min) of sLTP. N=7/7 and 14/9 (spine/neuron) for Ctrl (black) and False (red), respectively.
(G and H) Relationships between mVenus-RBD-mVenus concentration and binding fraction change in the transient (G, 1.3-4 min) and sustained phase (H, 19-31 min) of sLTP. N=7/7 and 14/9 (spine/neuron) for Ctrl (black) and False (red), respectively.

6.4 Rab10 inactivation at the near physiological temperature during structural LTP

To examine whether Rab10 demonstrates a similar inactivation pattern at the physiological temperature, I performed similar experiments to Figure 10 while monitoring the temperature at 33-35°C. Upon glutamate uncaging, Rab10 was rapidly inactivated and restricted in the stimulated spines, which lasted for more than 30 min (Figures 24A-24D). Moreover, there was no correlation between binding fraction change and sensor concentration (Figures 24E-24H), indicating that Rab10 activity change is independent of the sensor overexpression level. In summary, my results demonstrate that Rab10 is persistently inactivated and restricted in the stimulated spines at a near physiological temperature during sLTP.

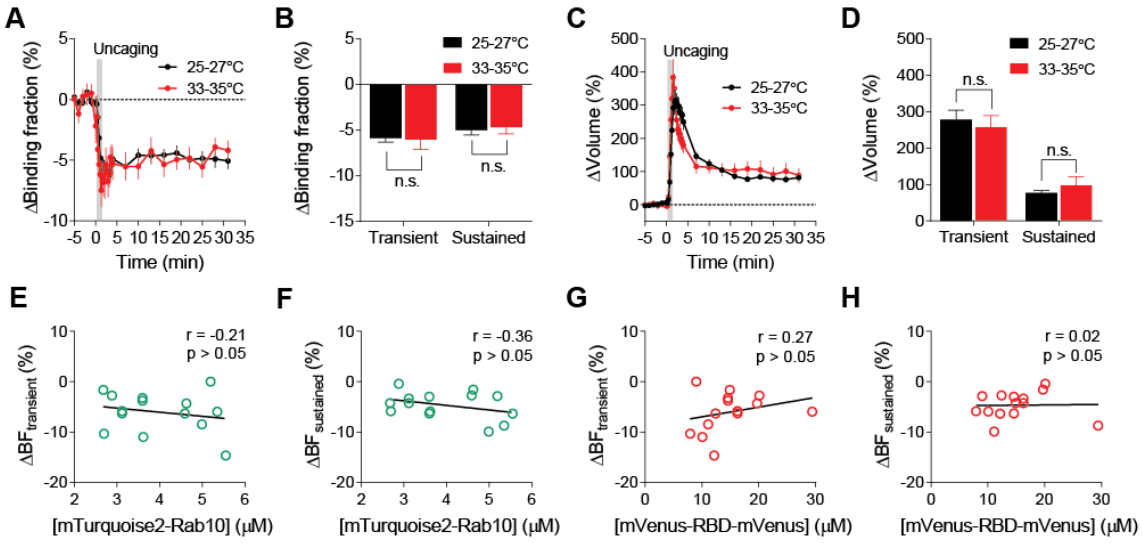

Figure 24 Rab10 inactivation at the near physiological temperature during structural LTP

(A) Averaged time courses of Rab10 activity change in the stimulated spines during sLTP at 25-27°C (black) and 33-35°C (red). Data represent mean ± SEM. N=50/44 and 14/12 (spine/neuron) for 25-27°C and 33-35°C, respectively.
(B) Quantification of binding fraction change in the transient phase (1.3-4 min) and sustained phase (19-31 min) for the same experiment as in (A). Data represent mean ± SEM. Student's t-tests were performed (n.s., not significant).
(C) Averaged time courses of spine volume change for the same experiments as (A). Data represent mean ± SEM.
(D) Quantification of spine volume change in the transient phase (1.3-4 min) and sustained phase (19-31 min) for the same experiments as in (A). Data represent mean ± SEM. Student's t-tests were performed (n.s., not significant).
(E and F) Correlation between mTurquoise2-Rab10 concentration and binding fraction change in the transient (E, 1.3-4 min) and sustained phase (F, 19-31 min) of sLTP at 33-35°C. N=14/12 (spine/neuron). No significant correlation ($p > 0.05$) was found.
(G and H) Correlation between mVenus-RBD-mVenus concentration and binding fraction change in the transient (G, 1.3-4 min) and sustained phase (H, 19-31 min) of sLTP at 33-35°C. N=14/12 (spine/neuron). No significant correlation ($p > 0.05$) was found.

Chapter 7. Rab4 and Rab10 in activity-dependent AMPARs exocytosis and constitutive AMPARs endocytosis

7.1 Rab4 and Rab10 positively and negatively regulate activity-dependent SEP-GluA1 exocytosis during structural LTP

To visualize the newly incorporated AMPARs from intracellular compartments during sLTP, I combined fluorescence recovery after photobleaching (FRAP) with two-photon glutamate uncaging. Hippocampal CA1 pyramidal neurons in rat organotypic slices were ballistically transfected with N-terminal superecliptic pHluorin (SEP)-tagged GluA1 (Patterson et al., 2010; Wang et al., 2008), mCherry and the scramble control shRNA. SEP-GluA1 is pH sensitive and only displays green fluorescence on the cell surface (Miesenböck et al., 1998), allowing us to distinguish between the surface and intracellular GluA1. mCherry is resistant to photobleaching, thus could serve as the volume marker.

I pre-bleached surface SEP-GluA1 in the whole dendrite at 0 min, and measured the FRAP after induction of sLTP at 1 min. Upon glutamate uncaging at a single spine, the volume of the stimulated spines increased by 352.8 ± 34.3% at 2 min (Figures 25A and 25B). Meanwhile, the fluorescence intensity of SEP-GluA1 was recovered from 15.4 ± 1.6% to 108.8 ± 10.8% in the stimulated spines, and retained till 8 min (115.2 ± 11.6%)(Figures 25A and 25B). However, in the non-stimulated adjacent spines and dendrites, SEP-GluA1 recovery was small and slow at 2 min (for adjacent spines, from 17.3 ± 1.3% to 28.9 ± 2.7%; for dendrites, from 27.8 ± 1.4% to 43.9 ± 1.9%), and failed to

achieve the original intensity at 8 min (for adjacent spines, 46.0 ± 4.1%; for dendrites, 57.1 ± 2.3%)(Figures 25A and 25B). As a positive control, overexpression of tetanus toxin light chain (TeTxLC)(Lin et al., 2009) decreased both the spine enlargement and SEP-GluA1 recover in the stimulated spines at 2 min (Figures 25C-25F and 26B). Overall, these results indicate that AMPARs are incorporated near the spines in an activity-dependent manner, which arrive at a plateau within 1 min after LTP induction and could be sustained for several minutes.

To investigate whether Rab4 and Rab10 are involved in the activity-dependent postsynaptic AMPA receptors exocytosis, I knocked down endogenous Rab4 and Rab10 by respective shRNA, and monitored SEP-GluA1 exocytosis in the stimulated spines during sLTP. Compared with the control shRNA, Rab4a and Rab4b shRNA expression impaired the spine enlargement at 2 min (Figures 25E, 25F and 26C). It also significantly attenuated SEP-GluA1 recover in the stimulated spines at 2 min (Figures 25C, 25D and 26C). In contrast, Rab10 shRNA knockdown enhanced the spine enlargement as well as SEP-GluA1 exocytosis at 2 min (Figures 25C-25F and 26E). These phenotypes were successfully rescued by co-expressing the shRNA-resistant Rab4a or Rab10 (Figures 25C-25F, 26D and 26F). To eliminate the passive SEP-GluA1 intensity increase due to the spine enlargement, I subtracted the SEP-GluA1 intensity by the spine surface area (volume $^{2/3}$), which also showed that Rab4 and Rab10 knockdown impaired and enhanced SEP-GluA1 recover in the stimulated spines, respectively (Figure 26I).

However, in the adjacent spines and dendrites, there was no significant variation in SEP-GluA1 recover and mCherry intensity change among all groups (Figure 27A-27H), implicating that Rab4 and Rab10 specifically regulate the activity-dependent GluA1 exocytosis in the stimulated spines. Taken together, my results demonstrate that Rab4 facilitates activity-dependent GluA1 exocytosis in the stimulated spines, whereas Rab10 inhibits this process.

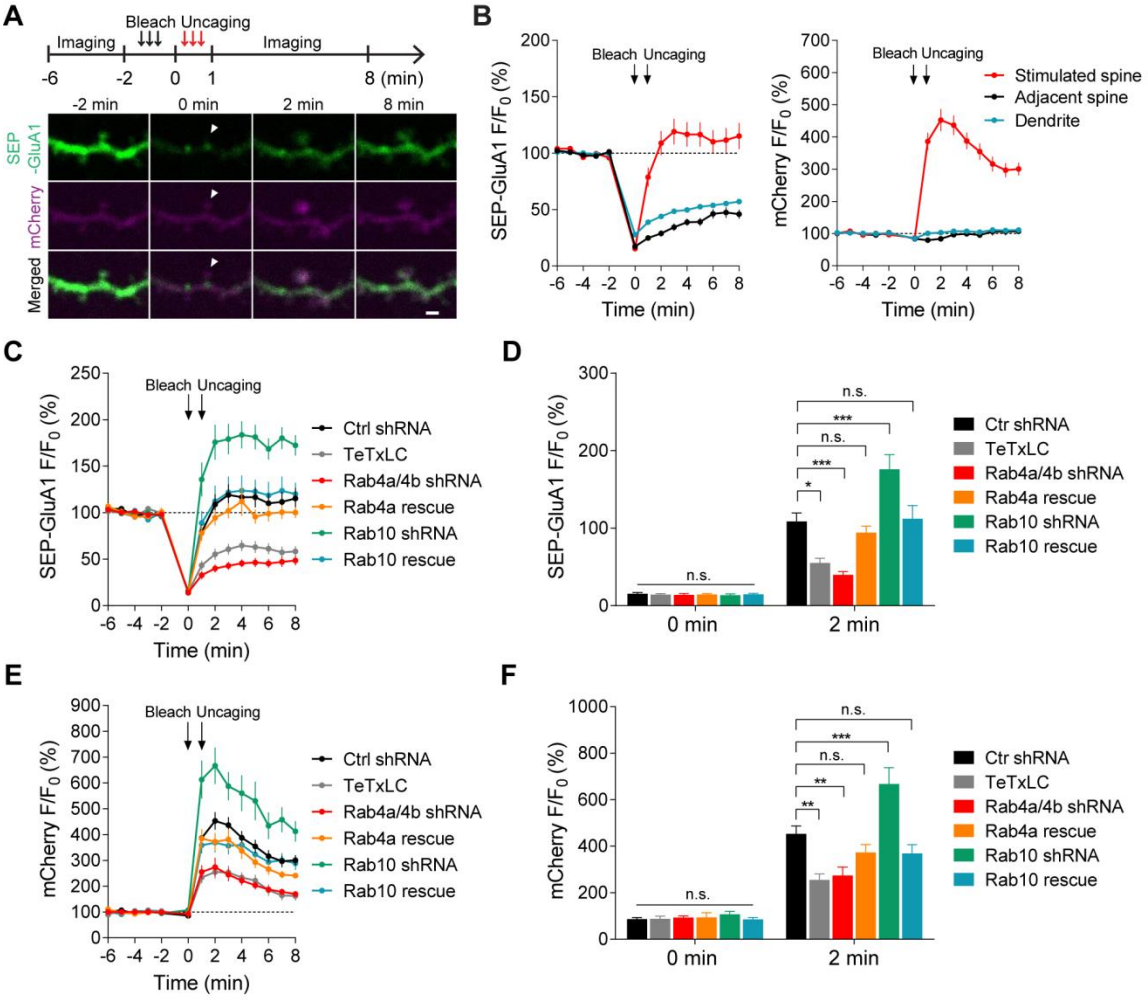

Figure 25 Rab4 and Rab10 oppositely regulate activity-dependent SEP-GluA1 exocytosis in the stimulated spines during structural LTP

(A) Upper lane: schematic for SEP-GluA1 FRAP and two-photon glutamate uncaging experiment. Whole vision bleach was performed from -2 min to 0 min, followed by the single spine glutamate uncaging from 0 min to 1 min (0.5 Hz, 30 pulses). Lower lane: representative pseudocolor images of SEP-GluA1 (green) FRAP after two-photon glutamate uncaging in a single spine of hippocampal CA1 pyramidal neurons coexpressing mCherry (magenta) and the scrambled shRNA. White arrowheads indicated the stimulated spine. Scale bar represents 1 μm.
(B) Averaged time courses of SEP-GluA1 (left) and mCherry (right) fluorescence intensity (F/F0) in the stimulated spine (red), adjacent spine (black) and dendrite (blue). Black arrows indicate the time points after bleaching and glutamate uncaging, respectively. Data represent mean ± SEM. N=43/35 (spine/neuron), 43/35 (spine/neuron) and 43/35 (dendrite/neuron) for the stimulated spine, adjacent spine and dendrite, respectively.
(C) Averaged time courses of SEP-GluA1 FRAP in the stimulated spines of neurons expressing SEP-GluA1, mCherry and the scrambled shRNA (Ctrl, black, n=43/35); SEP-GluA1, mCherry and TeTxLC (TeTxLC, grey, n=19/12); SEP-GluA1, mCherry and shRNAs against Rab4a and Rab4b (Rab4a/4b shRNA, red, n=26/16); SEP-GluA1, mCherry, shRNAs against Rab4a and Rab4b, and shRNA-resistant Rab4a (Rab4a rescue, orange, n=16/12); SEP-GluA1, mCherry and shRNA against Rab10 (Rab10 shRNA, green, n=23/15); SEP-GluA1, mCherry, shRNA against Rab10 and shRNA-resistant Rab10 (Rab10 rescue, blue, n=22/19). Data represent mean ± SEM. All experiments were paired with the same day controls from the same batch of slices.
(D) Quantification of SEP-GluA1 fluorescence intensity at 0 min and 2 min in the same experiments as (C). Data represent mean ± SEM. Bonferroni's multiple comparison tests were performed (n.s., not significant, * $p<0.05$, *** $p<0.001$).
(E) Averaged time courses of mCherry fluorescence intensity in the stimulated spines of the same neurons as (C). Data represent mean ± SEM.
(F) Quantification of mCherry fluorescence intensity at 0 min and 2 min in the same experiments as (C). Data represent mean ± SEM. Bonferroni's multiple comparison tests were performed (n.s., not significant, ** $p<0.01$, *** $p<0.001$).

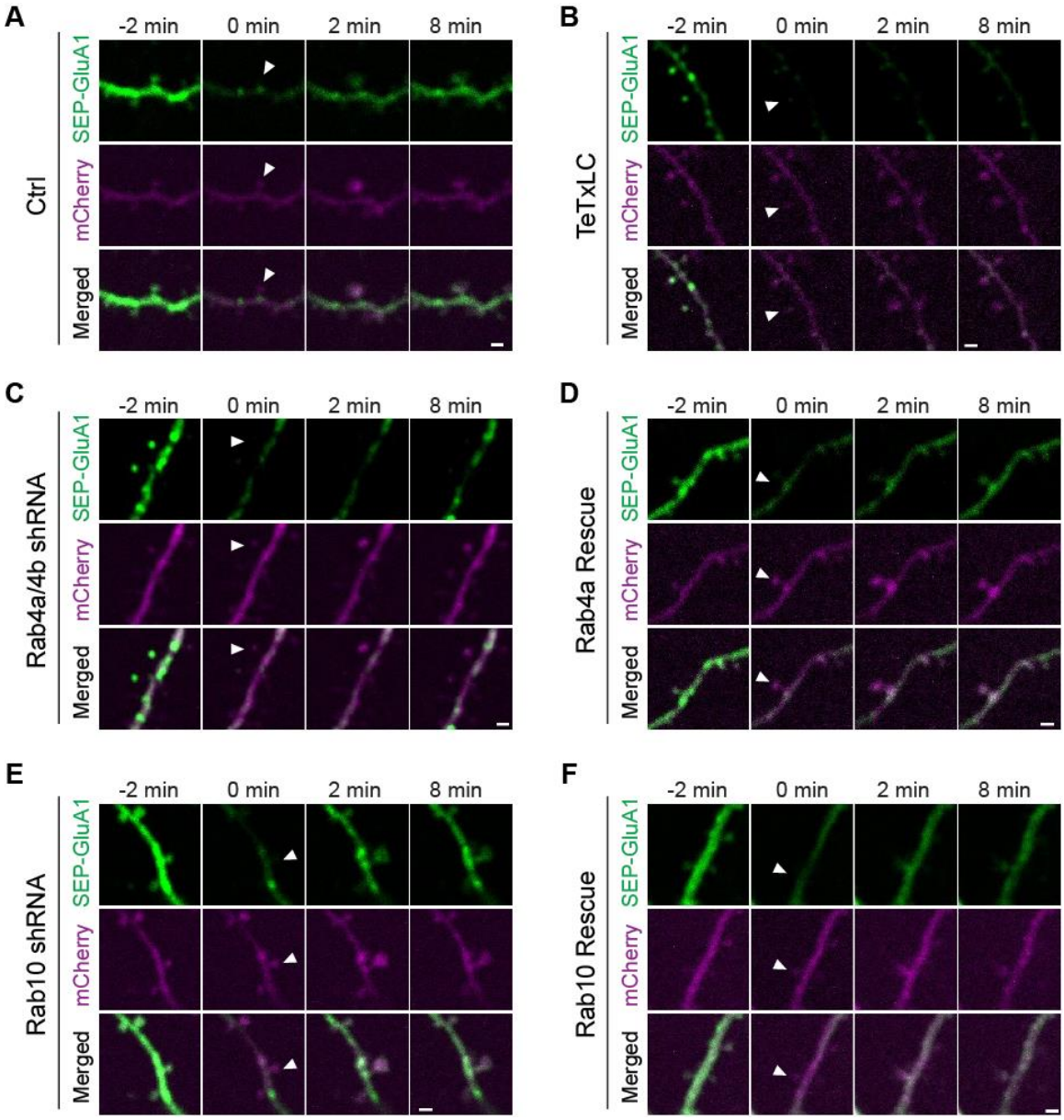

Figure 26 Representative images of SEP-GluA1 recover in all experimental groups

(A-F) Representative images of SEP-GluA1 (green) FRAP after two-photon glutamate uncaging in the stimulated spines of hippocampal neurons coexpressing mCherry (magenta) and the scramble shRNA (A); mCherry and TeTxLC (B); mCherry and Rab4a and Rab4b shRNA (C); mCherry, Rab4a and Rab4b shRNA and shRNA-resistant Rab4a (D); mCherry and Rab10 shRNA (E) or mCherry, Rab10 shRNA and shRNA-resistant Rab10 (F). White arrowheads indicated the stimulated spine. Scale bar represents 1 μm.

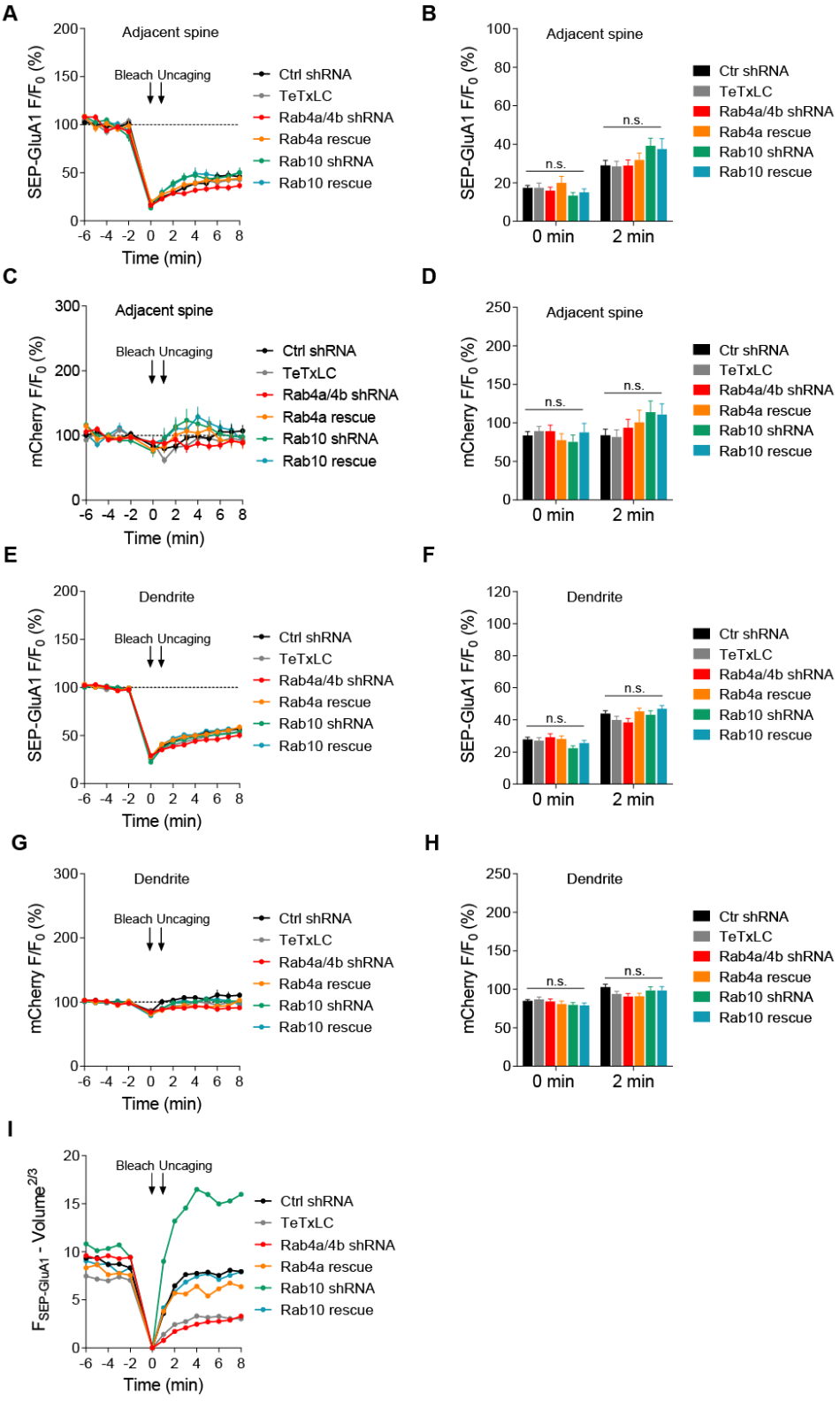
A
Adjacent spine
Bleach Uncaging
SEP-GluA1 F/F0 (%)
Time (min)
Ctrl shRNA
TeTxLC
Rab4a/4b shRNA
Rab4a rescue
Rab10 shRNA
Rab10 rescue
B
Adjacent spine
SEP-GluA1 F/F0 (%)
n.s.
0 min
2 min
Ctr shRNA
TeTxLC
Rab4a/4b shRNA
Rab4a rescue
Rab10 shRNA
Rab10 rescue
C
Adjacent spine
Bleach Uncaging
mCherry F/F0 (%)
Time (min)
Ctrl shRNA
TeTxLC
Rab4a/4b shRNA
Rab4a rescue
Rab10 shRNA
Rab10 rescue
D
Adjacent spine
mCherry F/F0 (%)
n.s.
0 min
2 min
Ctr shRNA
TeTxLC
Rab4a/4b shRNA
Rab4a rescue
Rab10 shRNA
Rab10 rescue
E
Dendrite
Bleach Uncaging
SEP-GluA1 F/F0 (%)
Time (min)
Ctrl shRNA
TeTxLC
Rab4a/4b shRNA
Rab4a rescue
Rab10 shRNA
Rab10 rescue
F
Dendrite
SEP-GluA1 F/F0 (%)
n.s.
0 min
2 min
Ctr shRNA
TeTxLC
Rab4a/4b shRNA
Rab4a rescue
Rab10 shRNA
Rab10 rescue
G
Dendrite
Bleach Uncaging
mCherry F/F0 (%)
Time (min)
Ctrl shRNA
TeTxLC
Rab4a/4b shRNA
Rab4a rescue
Rab10 shRNA
Rab10 rescue
H
Dendrite
mCherry F/F0 (%)
n.s.
0 min
2 min
Ctr shRNA
TeTxLC
Rab4a/4b shRNA
Rab4a rescue
Rab10 shRNA
Rab10 rescue
I
Bleach Uncaging
FSEP-GluA1 - Volume2/3
Time (min)
Ctrl shRNA
TeTxLC
Rab4a/4b shRNA
Rab4a rescue
Rab10 shRNA
Rab10 rescue

Figure 27 SEP-GluA1 intensity change in the adjacent spines and dendrites

(A and C) Averaged time courses of SEP-GluA1 (A) and mCherry (C) fluorescence intensity for the adjacent spines in the same experiments as Figure 25C. Data represent mean ± SEM. N=43/35, 19/12, 26/16, 16/12, 23/15 and 22/19 (spine/neuron) for Ctrl, TeTxLC, Rab4a/4b shRNA, Rab4a rescue, Rab10 shRNA and Rab10 rescue, respectively.
(B and D) Quantification of SEP-GluA1 (B) and mCherry (D) fluorescence intensity for the adjacent spines at 0 min and 2 min. Data represent mean ± SEM. Bonferroni's multiple comparison tests were performed (n.s., not significant). N=43/35, 19/12, 26/16, 16/12, 23/15 and 22/19 (spine/neuron) for Ctrl, TeTxLC, Rab4a/4b shRNA, Rab4a rescue, Rab10 shRNA and Rab10 rescue, respectively.
(E and G) Averaged time courses of SEP-GluA1 (E) and mCherry (G) fluorescence intensity for dendrites in the same experiments as Figure 25C. Data represent mean ± SEM. N=43/35, 19/12, 26/16, 16/12, 23/15 and 22/19 (spine/neuron) for Ctrl, TeTxLC, Rab4a/4b shRNA, Rab4a rescue, Rab10 shRNA and Rab10 rescue, respectively.
(F and H) Quantification of SEP-GluA1 (F) and mCherry (H) fluorescence intensity for the dendrites at 0 min and 2 min. Data represent mean ± SEM. Bonferroni's multiple comparison tests were performed (n.s., not significant). N=43/35, 19/12, 26/16, 16/12, 23/15 and 22/19 (spine/neuron) for Ctrl, TeTxLC, Rab4a/4b shRNA, Rab4a rescue, Rab10 shRNA and Rab10 rescue, respectively.
(I) SEP-GluA1 FRAP after subtraction of the surface area increase in the stimulated spines in Figure 25C. N=43/35, 19/12, 26/16, 16/12, 23/15 and 22/19 (spine/neuron) for Ctrl, TeTxLC, Rab4a/4b shRNA, Rab4a rescue, Rab10 shRNA and Rab10 rescue, respectively.

7.2 Disrupting Rab10 instead of Rab4 inhibits constitutive GluA1 endocytosis

To trace AMPA receptors endocytosis, I performed live-cell immunocytochemistry in hippocampal neurons using hemagglutinin (HA) antibody against N-terminal HA epitope of HA/T-GluA1 (Park et al., 2004; Passafaro et al., 2001). Surface GluA1 was pre-labelled with HA antibody, and internalize for 20 min at 37°C. With permeable and non-permeable secondary antibody staining, I quantified the internalized GluA1 and surface GluA1 intensity (Figure 28A), and used the ratio as an indicator for the constitutive GluA1 endocytosis at 20 min (internalized GluA1/surface GluA1). As expected, dominant negative Rab5a (Rab5a S34N) overexpression and pitstop2 application (200 μM)(von Kleist et al., 2011) blocked the constitutive GluA1 endocytosis at 20 min (Figures 28B and 28D). The staining was specific for internalized GluA1 since no visible staining was detected in nonpermeabilized neurons from Triton X (-) group (Figure 28D).

To test whether Rab4 and Rab10 are required for the constitutive GluA1 endocytosis, I monitored GluA1 internalization after suppression of Rab4 and Rab10. Overexpression of dominant negative Rab4a (Rab4a S22N) had no effect on the constitutive GluA1 endocytosis at 20 min (Figures 28B and 28D). In contrast, expression of dominant negative Rab10 (Rab10 T23N) significantly inhibited the constitutive GluA1 endocytosis at 20 min (Figures 28B and 28D). I further confirmed these phenotypes with shRNA knockdown. Similarly, Rab4a and Rab4b shRNA knockdown had no significant

effect on the constitutive GluA1 endocytosis at 20 min (Figures 28C and 28E). However, Rab10 shRNA knockdown significantly impaired the constitutive GluA1 endocytosis at 20 min, which was rescued by co-expressing the shRNA-resistant Rab10 (Figures 28C and 28E). As a negative control, application of pitstop2 (200 μM) abolished the constitutive GluA1 endocytosis at 20 min (Figures 28C and 28E). In summary, these results demonstrate that Rab10 contributes to the constitutive GluA1 endocytosis at 20 min, while Rab4 is not involved in this process.

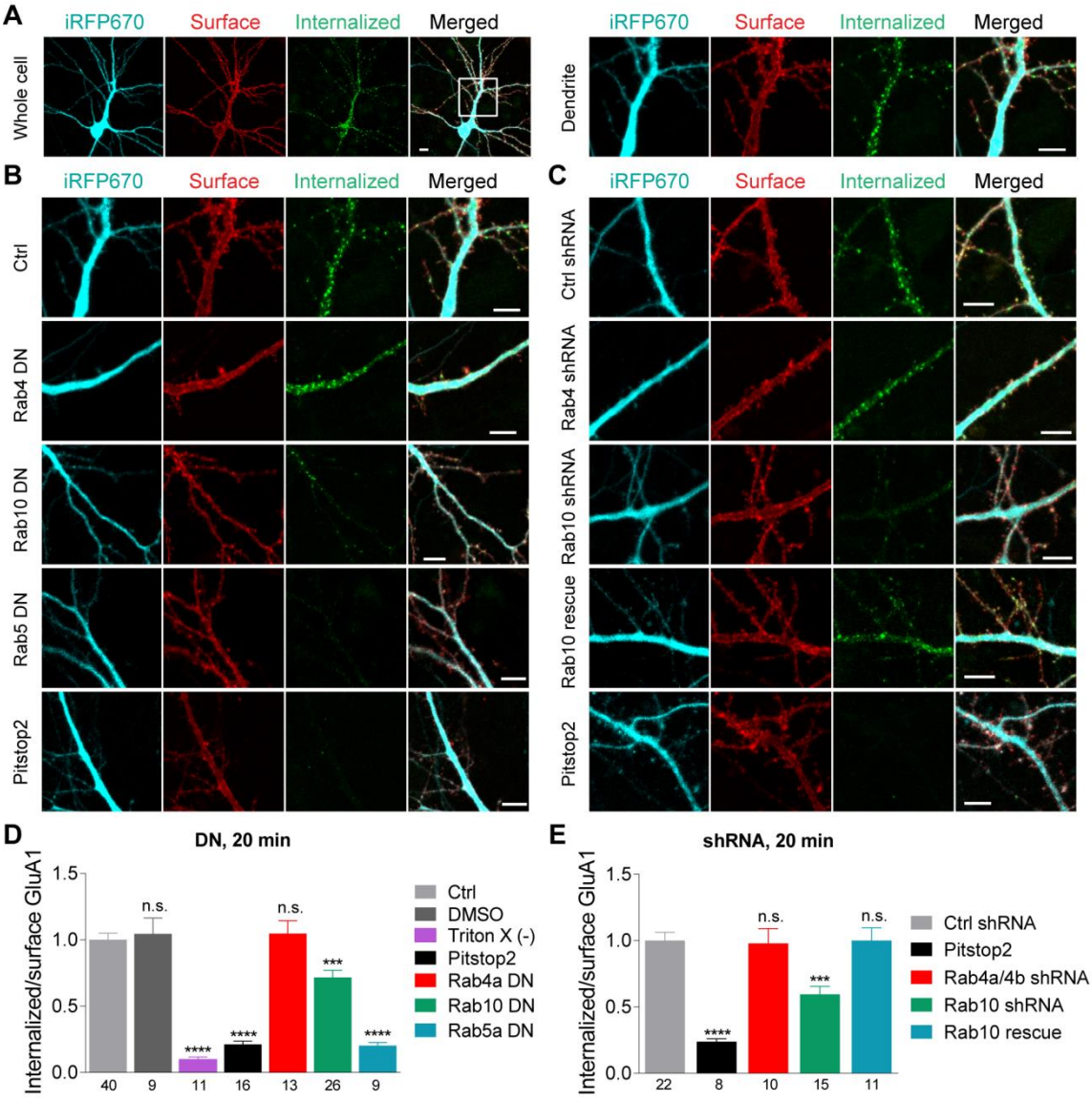

Figure 28 Downregulation of Rab10 results in decreased constitutive GluA1 endocytosis

(A) Left: representative images of surface HA/T-GluA1 (red) and internalized HA/T-GluA1 (green) in soma and dendrites of hippocampal neurons filled with iRFP670 (cyan) after 20 min HA/T-GluA1 internalization. Right: magnified images of the primary apical dendrite from the white rectangle at left. Scale bars represent 10 μm.
(B) Representative images of the primary apical dendrites from hippocampal neurons expressing iRFP670 and HA/T-GluA1 (Ctrl); iRFP670, HA/T-GluA1 and Rab4a [S27N] (Rab4a DN); iRFP670, HA/T-GluA1 and Rab10 [T23N] (Rab10 DN); iRFP670, HA/T-

GluA1 and Rab5a [S34N] (Rab5a DN). Pitstop2 (200 μM) was applied 30 min before experiment. Scale bars represent 10 μm.
(C) Representative images of the primary apical dendrites from hippocampal neurons expressing iRFP670, HA/T-GluA1 and scramble shRNA (Ctrl shRNA); iRFP670, HA/T-GluA1 and shRNAs against Rab4a and Rab4b (Rab4a/4b shRNA); iRFP670, HA/T-GluA1 and shRNA against Rab10 (Rab10 shRNA); iRFP670, HA/T-GluA1, shRNA against Rab10 and shRNA-resistant Rab10 (Rab10 rescue). Pitstop2 (200 μM) was applied 30 min before experiment. Scale bars represent 10 μm.
(D) Quantification of HA/T-GluA1 endocytosis at 20 min in the same experiments as (B). Dimethyl sulfoxide (DMSO) was the paired vehicle control for pitstop2 application. Immunostaining in Triton X (-) group was performed without cell surface permeabilization by Triton X-100. Data represent mean ± SEM. Bonferroni's multiple comparison tests were performed. N=40, 9, 11, 16, 13, 26, 9 neurons for each condition from left to right (n.s., not significant, *** $p<0.001$, **** $p<0.0001$).
(E) Quantification of HA/T-GluA1 endocytosis at 20 min in the same experiments as (C). Data represent mean ± SEM. Bonferroni's multiple comparison tests were performed (n.s., not significant, *** $p<0.001$, **** $p<0.0001$). N=22, 8, 10, 15, 11 neurons for each condition from left to right.

Chapter 8. Discussion

8.1 Proposed model

Combining novel live-cell imaging techniques, highly sensitive FRET sensors, pharmacological manipulations, dominant negative and iRNA interference approaches, as well as delicate dissections of AMPARs endocytosis and exocytosis, I provide a link between the Rab GTPases signaling pathways, AMPARs membrane trafficking and sLTP in single dendritic spines. In brief, NMDARs activation triggers Ca^{2+} influx and CaMKII activation that lead to the transient activation of Rab4 and persistent inactivation of Rab10, which further result in the potentiated AMPARs exocytosis and sLTP in single dendritic spines. In addition, Rab10 mediates the constitutive GluA1 endocytosis in the dendrites. In summary, my results reveal a new mechanism to establish the specificity and directionality of AMPARs trafficking and sLTP via distinct regulations of two Rab proteins, which is parallel to the previous identified Ras-ERK signaling pathway (Figure 29)(Patterson et al., 2010; Zhu et al., 2002).

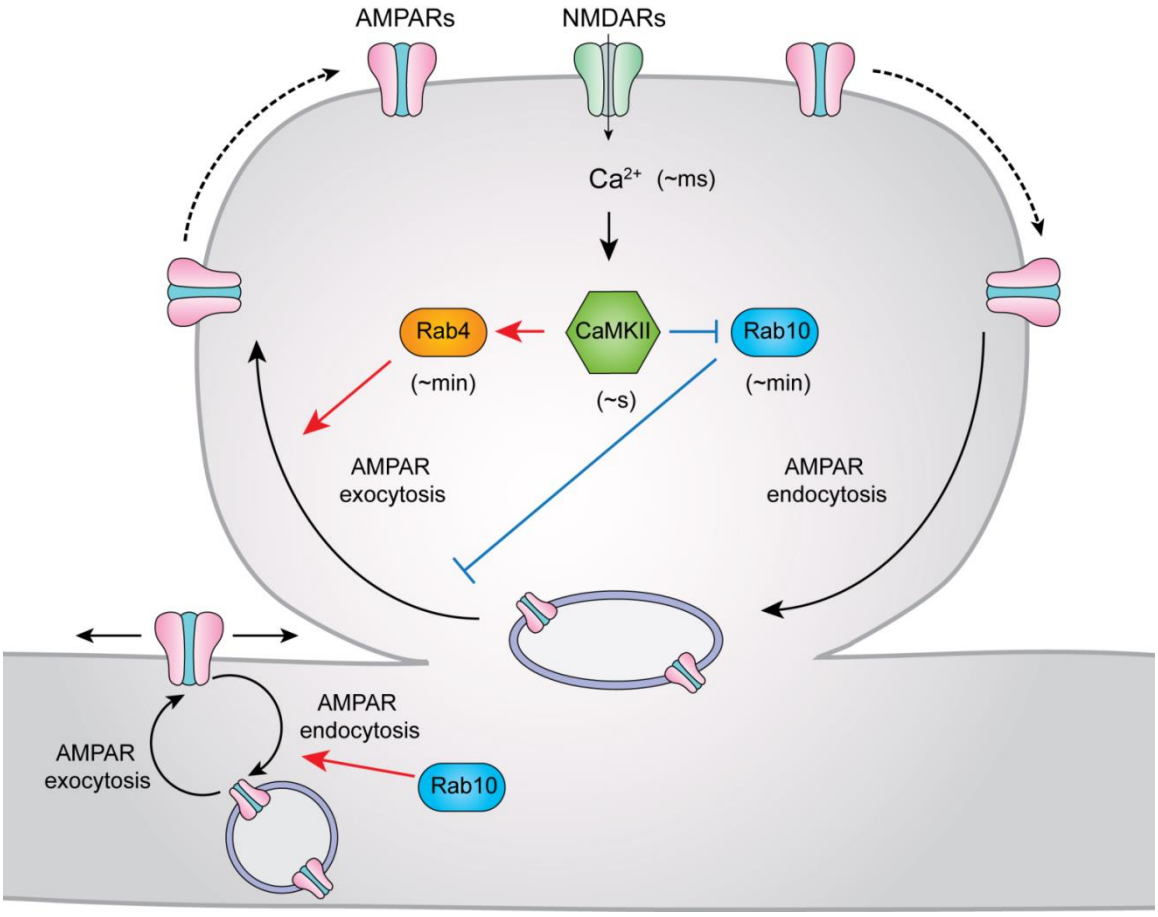

Figure 29 Proposed model for Rab4 and Rab10 mediated AMPARs trafficking and structural LTP

Activation of postsynaptic NMDARs triggers rapid Ca2+ influx (~ms) and CaMKII activation (~s), which is relayed by the transient activation of Rab4 (~min) and persistent inactivation of Rab10 (~min). Rab4 activation and Rab10 inactivation result in the potentiated AMPARs exocytosis to the postsynaptic membrane and sLTP in single dendritic spines, which is parallel to the CaMKII-Ras/ERK signaling pathway. In addition, Rab10 regulates the constitutive GluA1 endocytosis in the dendrites.

8.2 Discussion

8.2.1 Discussion of the results

Traditional loss-of-function studies, such as electrophysiological recordings in acute slices, could only report whether a protein of interest is involved in LTP, with the spatiotemporal information missing. In the present study, I overcame this by directly visualizing the spatiotemporal dynamics of Rab4 and Rab10 in single dendritic spines during sLTP, which is a proxy for functional LTP. Taking advantage of highly-sensitive FRET sensors, two-photon FLIM imaging and two-photon glutamate uncaging, I found that Rab4 and Rab10 display distinct activity profiles, with Rab4 transiently activated and Rab10 persistently inactivated in the stimulated spines during sLTP. These activity patterns coincide well with their respective role in different phases of sLTP.

Previous cellular studies have shown that, for some fluorescent lipid analogues, about half of the molecules directly return to the plasma membrane through the fast recycling pathway with a $t_{1/2}$ of 2 min, while the other half go through the slow recycling pathway with a $t_{1/2}$ of 12 min (Hao and Maxfield, 2000; Maxfield and McGraw, 2004). Rab4 has been identified as a regulator in the fast recycling of transferrin in cells (Sönnichsen et al., 2000). Interestingly, my Rab4 FRET sensor reports a similar time scale for Rab4 activation in the stimulated spines, which peaks around 1.9 min after sLTP induction and decays afterwards. In the transient phase of sLTP, the dramatic enlargement of spine head requires a fast supply of membrane proteins and

lipids to accomplish the membrane remodeling. Therefore, I speculate that Rab4 regulates the fast recycling to the plasma membrane in the transient phase of sLTP. Consistently, disruption of Rab4 impairs the activity-dependent GluA1 exocytosis within 1 min, as well as the transient enlargement of spine head during sLTP. Nevertheless, inhibition of Rab4 has no effect on the sustained phase of sLTP although Rab4 FRET sensor reports a little residual activity in the sustained phase (Figure 15). This indicates that Rab4 is not a major player in the sustained phase of sLTP. Other Rab proteins, such as Rab11 and Rab8, can compensate for the minor residual activity of Rab4 in the sustained phase of sLTP. Furthermore, Rab4 is not involved in the constitutive GluA1 endocytosis in dendrites, implicating its function in the recycling pathway. Overall, my data demonstrate that Rab4 is a positive regulator in AMPARs exocytosis and sLTP, and its transient activation pattern is a reminiscent of the fast recycling.

Surprisingly, Rab10 sensor shows a persistent inactivation pattern during sLTP, which is contradictory to a previous study claiming that Rab10 regulates glutamate receptor recycling in a clathrin-independent endocytosis pathway in *C. elegans* (Glodowski et al., 2007). However, their conclusion was based on the morphology analysis and indicative behavior tests of Rab10 mutants in *C. elegans*. Considering that Rab10 is important for axonal and dendritic development (Wang et al., 2011; Zou et al., 2015), it is entirely possible that the large accumulation of GLR-1 along the ventral cord

neurite bundle is merely a developmental phenotype instead of the GLR-1 transport defect. To better understand the functions of Rab10 in AMPARs trafficking, I directly monitored the dynamic GluA1 endocytosis and exocytosis after acute inhibition of Rab10 signaling. With live cell antibody feeding assay and activity-dependent SEP-GluA1 exocytosis assay, I demonstrated that Rab10 oppositely regulates the constitutive GluA1 endocytosis and activity-dependent GluA1 exocytosis. On basis of this, I propose that Rab10 inactivation drives the balance between AMPARs endocytosis and exocytosis to the exocytosis side, which results in more AMPARs insertion to the postsynaptic membrane and LTP expression.

What is the biological meaning of the persistent inactivation of a protein? One major concern is the dilution of sensor activity during the spine head enlargement. To test this possibility, I applied the actin polymerization inhibitor latrunculin A (LatA, 100 nM). LatA application strongly impairs spine enlargement, but has little effect on Rab10 inactivation (Figure 30). This result indicates that Rab10 inactivation is partially dependent on actin polymerization, and is not attributed to the dilution of sensor activity during spine enlargement. Another concern is whether the binding fraction decrease is due to the dissociation of acceptor instead of Rab10 inactivation. For example, after sLTP induction, Rab10 could bind to other effectors with higher affinity, which competes with the acceptor and leads to the binding fraction decrease. To test this

possibility, it would be helpful to use another Rab10 binding domain acceptor, which interacts with Rab10 at a different site.

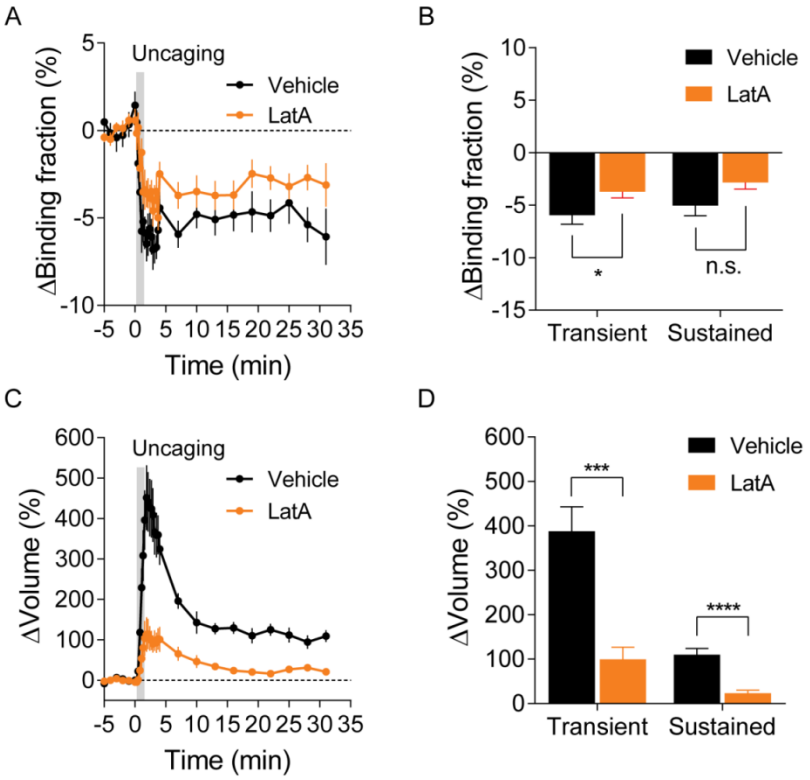

Figure 30 Actin polymerization inhibition on Rab10 signaling pathway

(A) Averaged time courses of Rab10 activity change in the stimulated spines during sLTP. Black and orange curves represent DMSO control (Vehicle) and LatA (100 nM), respectively. Data represent mean ± SEM. N=10/8 and 13/12 (spine/neuron) for Vehicle and LatA, respectively.
(B) Quantification of binding fraction change in the transient phase (1.3-4 min) and sustained phase (19-31 min) for the same experiment as in (A). Data represent mean ± SEM. Student's t-tests were performed (n.s., not significant, * $p<0.05$,).
(C) Averaged time courses of spine volume change in the stimulated spines for the same experiments as in (A). Data represent mean ± SEM.
(D) Quantification of spine volume change in the transient phase (1.3-4 min) and sustained phase (19-31 min) for the same experiment as in (A). Data represent mean ± SEM. Student's t-tests were performed (*** $p<0.001$, **** $p<0.0001$).

8.2.2 Future directions

8.2.2.1 Remaining questions in AMPARs trafficking

AMPARs mediate the majority of fast excitatory synaptic transmission in the mammalian brain. A simple way to modify synaptic strength is to change the function or number of postsynaptic AMPARs (Sheng and Kim, 2002). It has been shown that CaMKII plays a central role in regulating AMPARs-mediated transmission during LTP (Lisman et al., 2012). CaMKII can directly phosphorylate GluA1 at Ser^{831} and increase the single channel conductance of AMPARs (Derkach et al., 1999). In addition, the NMDARs-Ca^{2+}-CaMKII signaling can trigger downstream protein cascades that transduce the transient CaMKII activation into AMPARs incorporation and LTP expression (Colgan and Yasuda, 2014). However, the molecular mechanism by which CaMKII gives rise to LTP has remained a mystery. Here, I identified two small Rab GTPases that extend the CaMKII signaling from seconds to minutes, which further execute the AMPARs incorporation during sLTP.

However, the steps between CaMKII activation, Rab4 activation and Rab10 inactivation, and AMPARs exocytosis are still unclear. Firstly, it remains to be elucidated how CaMKII regulates the activities of Rab4 and Rab10. One possibility is through the regulations of specific Rab GAPs or GEFs. It has been shown that CaMKII can directly regulate the GEFs or GAPs of other small GTPases. For example, NMDA receptor activation causes CaMKII-dependent phosphorylation of the GEF kalirin-7 at residue threonine 95, which leads to the activation of small GTPase Rac1 and rapid

enlargement of existing spines (Herring and Nicoll, 2016; Xie et al., 2007). A recent study reported that SynGAP, a GAP for Rho GTPase, is rapidly dispersed from spines upon LTP induction in hippocampal neurons, and this dispersion is dependent on the phosphorylation of SynGAP by CaMKII (Araki et al., 2015). Based on these previous studies, it is interesting to study whether the GAPs or GEFs of Rab4 and Rab10 are the downstream of CaMKII activation during sLTP.

Secondly, the molecular mechanisms how Rab4 and Rab10 execute the AMPARs exocytosis is still not clear. One possibility is through the interaction with actin motor proteins such as Myosin V family. Previous studies have shown that Ca^{2+} influx through NMDARs activates Myosin Vb, an actin motor protein that travels along the actin filaments upon activation. Rab11 can interact with the activated Myosin Vb through its effector RABFIP2, and this interaction can promote the translocation of recycling endosome into the spine and facilitate the exocytosis of AMPARs (Figure 31). It has been shown that Rab10 can interact with Myosin Vb, which determines the formation of Rab10-containing post-Golgi carriers during axon development (Liu et al., 2013). It is interesting to examine whether this interaction also plays a role in regulating AMPARs trafficking. Besides, it remains to be elucidated whether other Rab effector proteins are involved in this process.

Finally, in the current work, I have shown that Rab10 instead of Rab4 regulates the constitutive GluA1 endocytosis in the dendrite. It might be interesting to examine

whether the same phenomenon also exists in the spines. Furthermore, we can study whether Rab4 and Rab10 are involved in the constitutive and activity-dependent GluA2 endocytosis. I did some preliminary tests on basal GluA2 endocytosis in the dendrites at 20 min (Figure 32). However, the internalized portion of GluA2 is much smaller than that of GluA1 at 20 min, which leads to the poor sensitivity of this assay. Interestingly, AMPA application (100 μM) greatly potentiated GluA2 endocytosis at 20 min. This potentiation is specific to GluA2, without any significant effect on GluA1 internalization (Figure 32). Using this AMPA-induced GluA2 endocytosis assay, we can further examine whether Rab4 and Rab10 contribute to AMPA-induced GluA2 endocytosis in the dendrites.

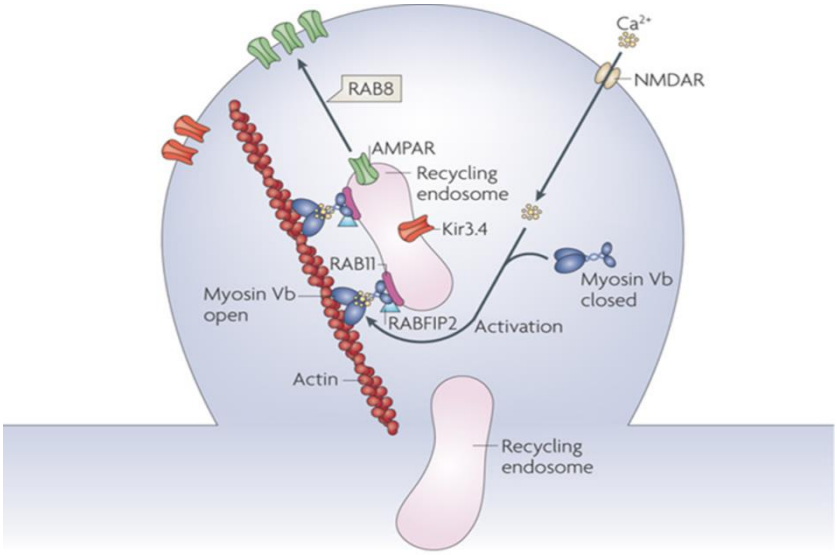

Figure 31 Rab11 and Myosin Vb in AMPARs trafficking and LTP

Adapted from (Grant and Donaldson, 2009)

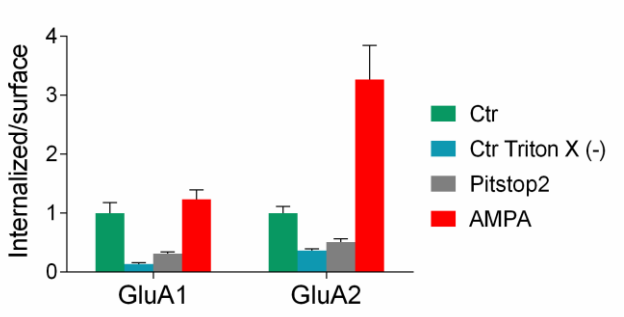

Figure 32 Constitutive and AMPA-induced GluA1 or GluA2 endocytosis assay

Quantification of constitutive (green) and AMPA-induced (red) GluA1 (left) and GluA2 (right) endocytosis assay at 20 min. Primary apical dendrites from dissociated hippocampal neurons expressing iRFP670 and HA/T-GluA1 or HA/T-GluA2 were analyzed. Immunostaining in Ctr Triton X (-) group was performed without cell surface permeabilization by Triton X-100. AMPA (100 μM) was applied for 20 min together with anti-HA antibody. Pitstop2 (200 μM in DMSO) was applied 30 min before experiment. Data represent mean ± SEM. N = 2, 3, 4, 4, 3, 3, 4, 4 neurons from left to right.

8.2.2.2 Localization of Rab4 and Rab10 in hippocampal CA1 pyramidal neurons

In the present work, I have shown that Rab4 is transiently activated while Rab10 is persistently inactivated in the stimulated spines during sLTP. However, the direct evidence showing their existence in the spines is still missing. Moreover, I have shown that Rab4 and Rab10 play distinct roles in AMPARs trafficking. However, the "zoomed in" localization of Rab4 and Rab10 on the recycling pathway is unclear, which is tightly related to their functions.

To answer these remaining questions, I will examine the localization of endogenous Rab4a and Rab10 with CRISPR-Cas9-mediated homology-directed repair (SLENDR) technique (Mikuni et al., 2016). To achieve the *in vivo* labeling of endogenous Rab4 and Rab10, I designed specific single-guide RNAs (sgRNAs) targeting the

upstream of the start codon of *Rab4a* and *Rab10*, and the single-strand oligodeoxynucleotides (ssODNs) as the repair template to integrate the HA tag sequence into the genome (Figures 33A and 33B). Theoretically, sgRNA can pair with the DNA target (red) and guide Cas9 nuclease to the genomic DNA. Cas9 nuclease then makes the double-stranded break at about ~3bp upstream of the protospacer adjacent motif (PAM) (blue). In the presence of the oligo donor template, homology-directed repair (HDR) can introduce the HA tag to the genome for future immunohistochemistry staining. Since HDR is generally active in the dividing cells, we are going to combine the HDR with *in utero* electroporation (IUE), and examine the endogenous localization of Rab4 and Rab10 with anti-HA antibody.

To test whether the genomic editing can occur at DNA level, we transfected Neuro-2a cells with pPB-CAG-mEGFP, sgRNA and ssODNs for Rab4 or Rab10 by electroporation, and amplified the targeted locus by genomic PCR. We found that the correct sgRNA-ssODNs pair showed successful integration of HA tag into the genome, which could be amplified by the HA-specific recombination primer set. In contrast, untransfected cells, sgRNA alone or incorrect sgRNA-ssODNs pair showed no PCR band at the corresponding size, indicating that the HA integration is specific to the correct sgRNA-ssODNs combination (Figures 33C and 33D). Moreover, DNA sequencing of the PCR product confirmed that HA tag was indeed inserted into the genome (Figures 33C and 33D). We are going to introduce these constructs to the neuro-

progenitor cells in mice by IUE, and target the hippocampal CA1 pyramidal neurons. Next, we can examine the localization of endogenous Rab4 and Rab10 by immunostaining the brain slices with anti-HA antibody. We can even examine the colocalization of Rab4 or Rab10 with endosome markers such as Rab5 for early endosome, and Rab11 for recycling endosome. The latter can provide a detailed localization picture of Rab4 and Rab10 in the recycling pathway, and deepen our understanding of their functions.

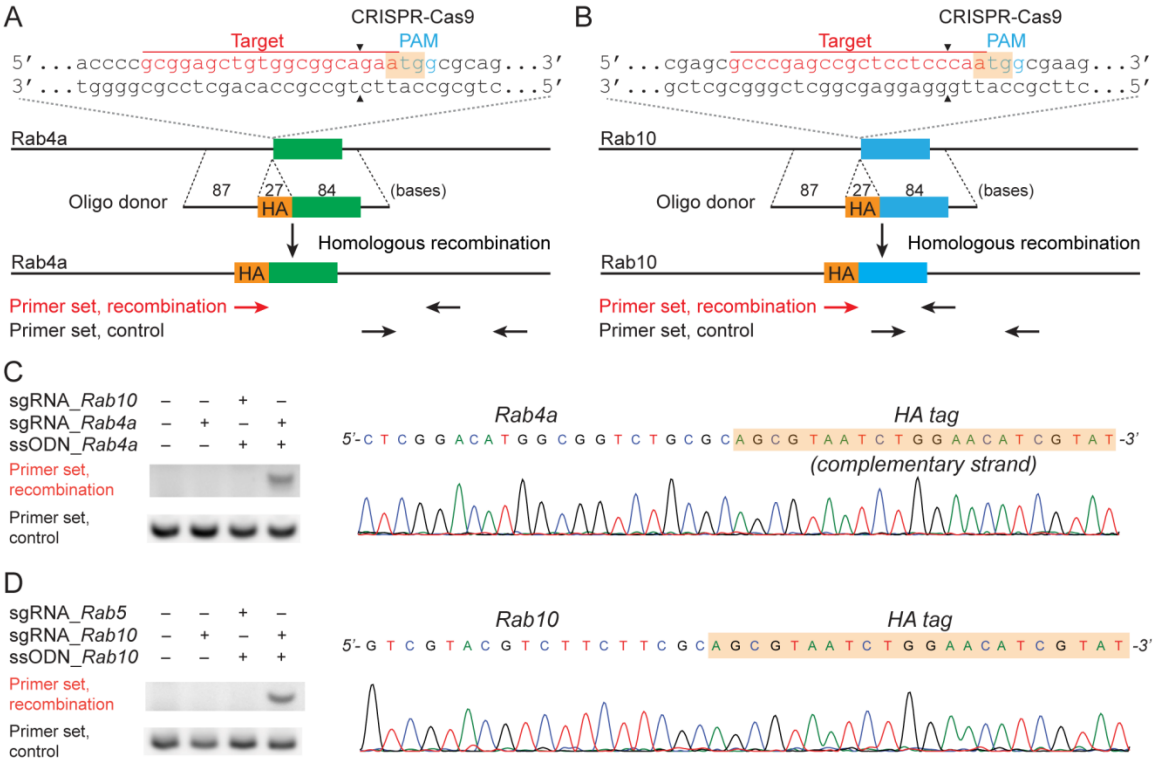

Figure 33 Design and verification of SLENDR constructs for Rab4 and Rab10

(A and B) Schematics of mouse genomic loci of Rab4a and Rab10 showing the target sites for Cas9, sgRNA and ssODNs. The sgRNA target regions and PAM sequences are labelled with red and blue, respectively. The start codons are marked with orange. The Cas9 cleavage sites are indicated by black arrowheads. PCR primer sets are indicated by

the arrows. For Rab4a, the recombination primer set is HA-FW and Rab4a-RV1, the control primer set is Rab4a-FW and Rab4a-RV2. For Rab10, the recombination primer set is HA-FW and Rab10-RV1, the control primer set is Rab10-FW and Rab10-RV2.
(C and D) Left: PCR genotyping using genomic DNA extracted from the electroporated Neuro-2a cells. The primer sets are the same as in (A) and (B). Right: DNA sequencing results of the PCR products from HA-Rab4a and HA-Rab10.

8.2.2.3 Rab4 and Rab10 in functional LTP and learning and memory

In the current study, I have shown that Rab4 positively regulates the transient phase of sLTP, while Rab10 negatively regulates both the transient and sustained phase of sLTP. However, I didn't examine their functions in electrophysiological LTP. A previous study has shown that overexpression of Rab4 dominant negative (Rab4 DN) mutant in organotypic slice cultures didn't significantly alter LTP in the CA1 pyramidal neurons (Brown et al., 2007). However, the initial phase of EPSCs in Rab4 DN group showed reduced amplitude, which is consistent with my finding that Rab4 is only involved in the transient phase of sLTP.

To examine the involvement of Rab10 in functional LTP, we will acutely express Rab10 dominant negative or constitutively active mutants in living mice, and examine the effects on LTP. I have generated the Cre-inducible AAV-pCAG-FLEX-rev-mEGFP-Rab10 DN/CA constructs and verified them in HEK 293T cells (Figure 34). We will introduce AAV-pCAG-FLEX-rev-mEGFP-Rab10 DN/CA, CyRFP and conditionally active Cre (ERT2CreERT2) into mice hippocampus by IUE. At P14-P21, we will apply tamoxifen to activate Cre and induce the acute expression of mEGFP-Rab10 CA/DN. Next, we will examine the effects on LTP in hippocampal CA3-CA1 pathway.

Finally, future *in vivo* behavioral studies are required to understand the functions of Rab4 and Rab10 in learning and memory. We are generating the conditional knockout mice of Rab10, which will reveal Rab10's functions in learning and memory.

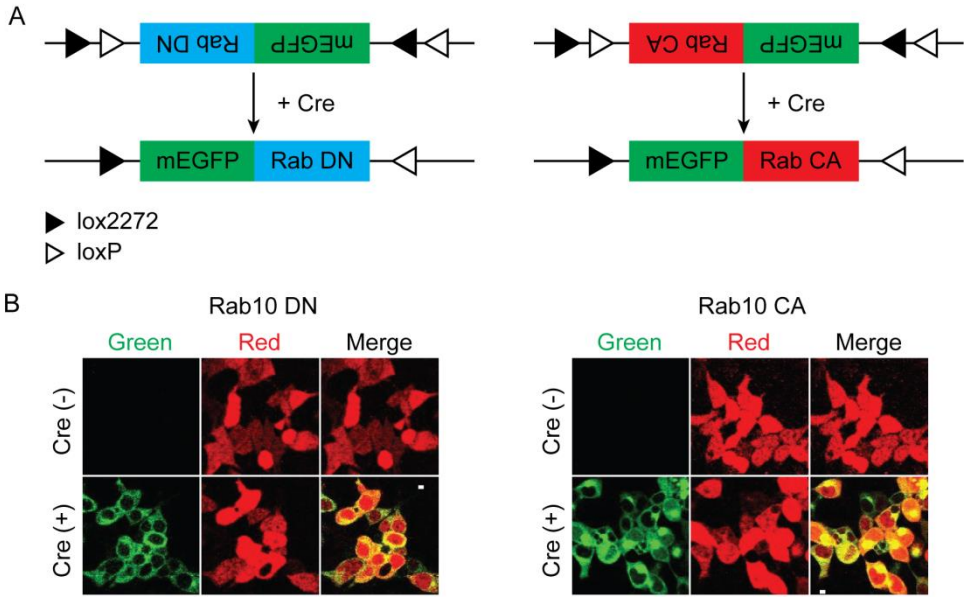

Figure 34 Design and verification of Cre-inducible DN/CA constructs for Rab4 and Rab10

(A) Schematics of Cre-inducible expression of mEGFP-Rab DN or mEGFP-Rab CA.
(B) Verification of Cre-induced Rab DN or Rab CA expression in HEK 293T cells. HEK 293T cells were transfected with mCherry (red) and AAV-pCAG-FLEX-*rev*-mEGFP-Rab10 DN or AAV-pCAG-FLEX-*rev*-mEGFP-Rab10 CA. In the presence of Cre, mEGFP-Rab10 DN (green) or mEGFP-Rab CA (green) were expressed. Scale bars represent 5 μm.

References

Abeliovich, A., Chen, C., Goda, Y., Silva, A.J., Stevens, C.F., and Tonegawa, S. (1993a). Modified hippocampal long-term potentiation in PKCγ-mutant mice. Cell *75*, 1253-1262.

Abeliovich, A., Paylor, R., Chen, C., Kim, J.J., Wehner, J.M., and Tonegawa, S. (1993b). PKCγ mutant mice exhibit mild deficits in spatial and contextual learning. Cell *75*, 1263-1271.

Andersen, P., Bliss, T., and Skrede, K.K. (1971). Lamellar organization of hippocampal excitatory pathways. Experimental Brain Research *13*, 222-238.

Andersen, P., Sundberg, S., and Sveen, O. (1977). Specific long-lasting potentiation of synaptic transmission in hippocampal slices. Nature *266*, 736-737.

Andres, D.A., Seabra, M.C., Brown, M.S., Armstrong, S.A., Smeland, T.E., Cremers, F.P., and Goldstein, J.L. (1993). cDNA cloning of component A of Rab geranylgeranyl transferase and demonstration of its role as a Rab escort protein. Cell *73*, 1091-1099.

Anggono, V., and Huganir, R.L. (2012). Regulation of AMPA receptor trafficking and synaptic plasticity. Current opinion in neurobiology *22*, 461-469.

Araki, Y., Zeng, M., Zhang, M., and Huganir, R.L. (2015). Rapid dispersion of SynGAP from synaptic spines triggers AMPA receptor insertion and spine enlargement during LTP. Neuron *85*, 173-189.

Armstrong, N., Sun, Y., Chen, G.-Q., and Gouaux, E. (1998). Structure of a glutamate-receptor ligand-binding core in complex with kainate. Nature *395*, 913-917.

Atkins, C.M., Selcher, J.C., Petraitis, J.J., Trzaskos, J.M., and Sweatt, J.D. (1998). The MAPK cascade is required for mammalian associative learning. Nature neuroscience *1*, 602-609.

Babbey, C.M., Ahktar, N., Wang, E., Chen, C.C.-H., Grant, B.D., and Dunn, K.W. (2006). Rab10 regulates membrane transport through early endosomes of polarized Madin-Darby canine kidney cells. Molecular biology of the cell *17*, 3156-3175.

Ballester, R., Marchuk, D., Boguski, M., Saulino, A., Letcher, R., Wigler, M., and Collins, F. (1990). The NF1 locus encodes a protein functionally related to mammalian GAP and yeast IRA proteins. Cell *63*, 851-859.

Barria, A., Muller, D., Derkach, V., Griffith, L.C., and Soderling, T.R. (1997). Regulatory phosphorylation of AMPA-type glutamate receptors by CaM-KII during long-term potentiation. Science *276*, 2042-2045.

Barry, M.F., and Ziff, E.B. (2002). Receptor trafficking and the plasticity of excitatory synapses. Current opinion in neurobiology *12*, 279-286.

Bayer, K.-U., De Koninck, P., Leonard, A.S., Hell, J.W., and Schulman, H. (2001). Interaction with the NMDA receptor locks CaMKII in an active conformation. Nature *411*, 801-805.

Beaudoin III, G.M., Lee, S.-H., Singh, D., Yuan, Y., Ng, Y.-G., Reichardt, L.F., and Arikkath, J. (2012). Culturing pyramidal neurons from the early postnatal mouse hippocampus and cortex. Nature protocols *7*, 1741-1754.

Benke, T.A., Lüthi, A., Isaac, J.T., and Collingridge, G.L. (1998). Modulation of AMPA receptor unitary conductance by synaptic activity. Nature *393*, 793-797.

Bliss, T.V., and Collingridge, G.L. (1993). A synaptic model of memory: long-term potentiation in the hippocampus. Nature *361*, 31-39.

Bliss, T.V., and Lømo, T. (1973). Long-lasting potentiation of synaptic transmission in the dentate area of the anaesthetized rabbit following stimulation of the perforant path. The Journal of physiology *232*, 331-356.

Bock, J.B., Matern, H.T., Peden, A.A., and Scheller, R.H. (2001). A genomic perspective on membrane compartment organization. Nature *409*, 839-841.

Bonhoeffer, T., and Yuste, R. (2002). Spine motility: phenomenology, mechanisms, and function. Neuron *35*, 1019-1027.

Bonifacino, J.S., and Glick, B.S. (2004). The mechanisms of vesicle budding and fusion. cell *116*, 153-166.

Borgdorff, A.J., and Choquet, D. (2002). Regulation of AMPA receptor lateral movements. Nature *417*, 649-653.

Borgesius, N.Z., van Woerden, G.M., Buitendijk, G.H., Keijzer, N., Jaarsma, D., Hoogenraad, C.C., and Elgersma, Y. (2011). βCaMKII plays a nonenzymatic role in hippocampal synaptic plasticity and learning by targeting αCaMKII to synapses. The Journal of Neuroscience *31*, 10141-10148.

Bosch, M., Castro, J., Saneyoshi, T., Matsuno, H., Sur, M., and Hayashi, Y. (2014). Structural and molecular remodeling of dendritic spine substructures during long-term potentiation. Neuron *82*, 444-459.

Bowie, D., Lange, G.D., and Mayer, M.L. (1998). Activity-dependent modulation of glutamate receptors by polyamines. The Journal of neuroscience *18*, 8175-8185.

Bredt, D.S., and Nicoll, R.A. (2003). AMPA receptor trafficking at excitatory synapses. Neuron *40*, 361-379.

Brown, T.C., Correia, S.S., Petrok, C.N., and Esteban, J.A. (2007). Functional compartmentalization of endosomal trafficking for the synaptic delivery of AMPA receptors during long-term potentiation. The Journal of Neuroscience *27*, 13311-13315.

Brown, T.C., Tran, I.C., Backos, D.S., and Esteban, J.A. (2005). NMDA receptor-dependent activation of the small GTPase Rab5 drives the removal of synaptic AMPA receptors during hippocampal LTD. Neuron *45*, 81-94.

Cajal, S.R.Y. (1894). The Croonian Lecture: La fine structure des centres nerveux. Proceedings of the Royal Society of London *55*, 444-468.

Callaghan, J., Simonsen, A., GAULLIER, J.-M., Ban-Hock, T., and STENMARK, H. (1999). The endosome fusion regulator early-endosomal autoantigen 1 (EEA1) is a dimer. Biochemical Journal *338*, 539-543.

Cantley, L.C. (2002). The phosphoinositide 3-kinase pathway. Science *296*, 1655-1657.

Carroll, K.S., Hanna, J., Simon, I., Krise, J., Barbero, P., and Pfeffer, S.R. (2001). Role of Rab9 GTPase in facilitating receptor recruitment by TIP47. Science *292*, 1373-1376.

Chamberlain, M.D., Berry, T.R., Pastor, M.C., and Anderson, D.H. (2004). The p85α subunit of phosphatidylinositol 3'-kinase binds to and stimulates the GTPase activity of Rab proteins. Journal of Biological Chemistry *279*, 48607-48614.

Chen, H.-J., Rojas-Soto, M., Oguni, A., and Kennedy, M.B. (1998). A synaptic Ras-GTPase activating protein (p135 SynGAP) inhibited by CaM kinase II. Neuron *20*, 895-904.

Chen, L., Chetkovich, D.M., Petralia, R.S., Sweeney, N.T., Kawasaki, Y., Wenthold, R.J., Bredt, D.S., and Nicoll, R.A. (2000). Stargazin regulates synaptic targeting of AMPA receptors by two distinct mechanisms. Nature *408*, 936-943.

Chen, X., Garelick, M.G., Wang, H., Li, V., Athos, J., and Storm, D.R. (2005). PI3 kinase signaling is required for retrieval and extinction of contextual memory. Nature neuroscience *8*, 925-931.

Christoforidis, S., Miaczynska, M., Ashman, K., Wilm, M., Zhao, L., Yip, S.-C., Waterfield, M.D., Backer, J.M., and Zerial, M. (1999). Phosphatidylinositol-3-OH kinases are Rab5 effectors. Nature cell biology *1*, 249-252.

Chung, H.J., Steinberg, J.P., Huganir, R.L., and Linden, D.J. (2003). Requirement of AMPA receptor GluR2 phosphorylation for cerebellar long-term depression. Science *300*, 1751-1755.

Clugnet, M.C., and LeDoux, J.E. (1990). Synaptic plasticity in fear conditioning circuits: induction of LTP in the lateral nucleus of the amygdala by stimulation of the medial geniculate body. The Journal of neuroscience *10*, 2818-2824.

Cohen, R.S., Chung, S.K., and Pfaff, D.W. (1985). Immunocytochemical localization of actin in dendritic spines of the cerebral cortex using colloidal gold as a probe. Cellular and molecular neurobiology *5*, 271-284.

Colgan, L.A., and Yasuda, R. (2014). Plasticity of dendritic spines: subcompartmentalization of signaling. Annual review of physiology *76*, 365.

Collingridge, G.L., Isaac, J.T., and Wang, Y.T. (2004). Receptor trafficking and synaptic plasticity. Nature Reviews Neuroscience *5*, 952-962.

Correia, S.S., Bassani, S., Brown, T.C., Lisé, M.-F., Backos, D.S., El-Husseini, A., Passafaro, M., and Esteban, J.A. (2008). Motor protein–dependent transport of AMPA receptors into spines during long-term potentiation. Nature neuroscience *11*, 457-466.

Costa, R.M., Federov, N.B., Kogan, J.H., Murphy, G.G., Stern, J., Ohno, M., Kucherlapati, R., Jacks, T., and Silva, A.J. (2002). Mechanism for the learning deficits in a mouse model of neurofibromatosis type 1. nature *415*, 526-530.

Cullen, P.J., and Lockyer, P.J. (2002). Integration of calcium and Ras signalling. Nature Reviews Molecular Cell Biology *3*, 339-348.

Dailey, M.E., and Smith, S.J. (1996). The dynamics of dendritic structure in developing hippocampal slices. The Journal of neuroscience *16*, 2983-2994.

Derkach, V., Barria, A., and Soderling, T.R. (1999). Ca2+/calmodulin-kinase II enhances channel conductance of α-amino-3-hydroxy-5-methyl-4-isoxazolepropionate type glutamate receptors. Proceedings of the National Academy of Sciences *96*, 3269-3274.

Derkach, V.A., Oh, M.C., Guire, E.S., and Soderling, T.R. (2007). Regulatory mechanisms of AMPA receptors in synaptic plasticity. Nature Reviews Neuroscience *8*, 101-113.

Dingledine, R., Borges, K., Bowie, D., and Traynelis, S.F. (1999). The glutamate receptor ion channels. Pharmacological reviews *51*, 7-62.

Eathiraj, S., Pan, X., Ritacco, C., and Lambright, D.G. (2005). Structural basis of family-wide Rab GTPase recognition by rabenosyn-5. Nature *436*, 415-419.

Echard, A., Jollivet, F., Martinez, O., Lacapère, J.-J., Rousselet, A., Janoueix-Lerosey, I., and Goud, B. (1998). Interaction of a Golgi-associated kinesin-like protein with Rab6. Science *279*, 580-585.

Engert, F., and Bonhoeffer, T. (1997). Synapse specificity of long-term potentiation breaks down at short distances. Nature *388*, 279-284.

English, A.R., and Voeltz, G.K. (2013). Rab10 GTPase regulates ER dynamics and morphology. Nature cell biology *15*, 169-178.

English, J.D., and Sweatt, J.D. (1997). A requirement for the mitogen-activated protein kinase cascade in hippocampal long term potentiation. Journal of Biological Chemistry *272*, 19103-19106.

Erondu, N.E., and Kennedy, M.B. (1985). Regional distribution of type II Ca2+/calmodulin-dependent protein kinase in rat brain. The Journal of neuroscience *5*, 3270-3277.

Farnsworth, C.L., Freshney, N.W., Rosen, L.B., Ghosh, A., Greenberg, M.E., and Feig, L.A. (1995). Calcium activation of Ras mediated by neuronal exchange factor Ras-GRF.

Fischer, M., Kaech, S., Knutti, D., and Matus, A. (1998). Rapid actin-based plasticity in dendritic spines. Neuron *20*, 847-854.

Fontijn, R.D., Goud, B., Echard, A., Jollivet, F., van Marle, J., Pannekoek, H., and Horrevoets, A.J. (2001). The human kinesin-like protein RB6K is under tight cell cycle control and is essential for cytokinesis. Molecular and cellular biology *21*, 2944-2955.

Fox, C.A., and Barnard, J.W. (1957). A quantitative study of the Purkinje cell dendritic branchlets and their relationship to afferent fibres. Journal of Anatomy *91*, 299.

Fujii, H., Inoue, M., Okuno, H., Sano, Y., Takemoto-Kimura, S., Kitamura, K., Kano, M., and Bito, H. (2013). Nonlinear decoding and asymmetric representation of neuronal input information by CaMKIIα and calcineurin. Cell Reports *3*, 978-987.

Fukuda, M. (2003). Distinct Rab binding specificity of Rim1, Rim2, Rabphilin, and Noc2 identification of a critical determinant of Rab3A/Rab27A recognition by Rim2. Journal of Biological Chemistry *278*, 15373-15380.

Fukuda, M. (2008). Regulation of secretory vesicle traffic by Rab small GTPases. Cell Mol Life Sci *65*, 2801-2813.

Fukuda, M., Kanno, E., Ishibashi, K., and Itoh, T. (2008). Large scale screening for novel rab effectors reveals unexpected broad Rab binding specificity. Molecular & Cellular Proteomics *7*, 1031-1042.

Gabe Lee, M.T., Mishra, A., and Lambright, D.G. (2009). Structural mechanisms for regulation of membrane traffic by rab GTPases. Traffic *10*, 1377-1389.

Giese, K.P., Fedorov, N.B., Filipkowski, R.K., and Silva, A.J. (1998). Autophosphorylation at Thr286 of the α calcium-calmodulin kinase II in LTP and learning. Science *279*, 870-873.

Glodowski, D.R., Chen, C.C.-H., Schaefer, H., Grant, B.D., and Rongo, C. (2007). RAB-10 regulates glutamate receptor recycling in a cholesterol-dependent endocytosis pathway. Molecular biology of the cell *18*, 4387-4396.

Goedhart, J., von Stetten, D., Noirclerc-Savoye, M., Lelimousin, M., Joosen, L., Hink, M.A., van Weeren, L., Gadella Jr, T.W., and Royant, A. (2012). Structure-guided evolution of cyan fluorescent proteins towards a quantum yield of 93%. Nature communications *3*, 751.

Granger, A.J., Shi, Y., Lu, W., Cerpas, M., and Nicoll, R.A. (2013). LTP requires a reserve pool of glutamate receptors independent of subunit type. Nature *493*, 495-500.

Grant, B.D., and Donaldson, J.G. (2009). Pathways and mechanisms of endocytic recycling. Nature reviews Molecular cell biology *10*, 597-608.

Gray, E. (1959). Electron microscopy of synaptic contacts on dendrite spines of the cerebral cortex. Nature *183*, 1592-1593.

Grienberger, C., and Konnerth, A. (2012). Imaging calcium in neurons. Neuron *73*, 862-885.

Hales, C.M., Vaerman, J.-P., and Goldenring, J.R. (2002). Rab11 family interacting protein 2 associates with Myosin Vb and regulates plasma membrane recycling. Journal of Biological Chemistry *277*, 50415-50421.

Hao, M., and Maxfield, F.R. (2000). Characterization of rapid membrane internalization and recycling. Journal of Biological Chemistry *275*, 15279-15286.

Harvey, C.D., Yasuda, R., Zhong, H., and Svoboda, K. (2008). The spread of Ras activity triggered by activation of a single dendritic spine. Science *321*, 136-140.

Hayama, T., Noguchi, J., Watanabe, S., Takahashi, N., Hayashi-Takagi, A., Ellis-Davies, G.C., Matsuzaki, M., and Kasai, H. (2013). GABA promotes the competitive selection of dendritic spines by controlling local Ca2+ signaling. Nature neuroscience *16*, 1409-1416.

Hayashi, Y., Shi, S.-H., Esteban, J.A., Piccini, A., Poncer, J.-C., and Malinow, R. (2000). Driving AMPA receptors into synapses by LTP and CaMKII: requirement for GluR1 and PDZ domain interaction. Science *287*, 2262-2267.

Hebb, D.O. (2005). The organization of behavior: A neuropsychological theory (Psychology Press).

Helmchen, F., Svoboda, K., Denk, W., and Tank, D.W. (1999). In vivo dendritic calcium dynamics in deep-layer cortical pyramidal neurons. Nature neuroscience *2*, 989-996.

Herring, B.E., and Nicoll, R.A. (2016). Long-term potentiation: from CaMKII to AMPA receptor trafficking. Annual review of physiology *78*, 351-365.

Hollmann, M., Maron, C., and Heinemann, S. (1994). N-glycosylation site tagging suggests a three transmembrane domain topology for the glutamate receptor GluR1. Neuron *13*, 1331-1343.

Holtmaat, A.J., Trachtenberg, J.T., Wilbrecht, L., Shepherd, G.M., Zhang, X., Knott, G.W., and Svoboda, K. (2005). Transient and persistent dendritic spines in the neocortex in vivo. Neuron *45*, 279-291.

Höning, S., Ricotta, D., Krauss, M., Späte, K., Spolaore, B., Motley, A., Robinson, M., Robinson, C., Haucke, V., and Owen, D.J. (2005). Phosphatidylinositol-(4, 5)-bisphosphate regulates sorting signal recognition by the clathrin-associated adaptor complex AP2. Molecular cell *18*, 519-531.

Hoogenraad, C.C., Popa, I., Futai, K., Sanchez-Martinez, E., Wulf, P.S., van Vlijmen, T., Dortland, B.R., Oorschot, V., Govers, R., and Monti, M. (2010). Neuron specific Rab4 effector GRASP-1 coordinates membrane specialization and maturation of recycling endosomes. PLoS Biol *8*, e1000283.

Hu, G.-Y., Hvalby, Ø., Walaas, S., Albert, K., Skjeflo, P., Andersen, P., and Greengard, P. (1987). Protein kinase C injection into hippocampal pyramidal cells elicits features of long term potentiation.

Hu, H., Real, E., Takamiya, K., Kang, M.-G., Ledoux, J., Huganir, R.L., and Malinow, R. (2007). Emotion enhances learning via norepinephrine regulation of AMPA-receptor trafficking. Cell *131*, 160-173.

Huganir, R.L., and Nicoll, R.A. (2013). AMPARs and synaptic plasticity: the last 25 years. Neuron *80*, 704-717.

Husi, H., Ward, M.A., Choudhary, J.S., Blackstock, W.P., and Grant, S.G. (2000). Proteomic analysis of NMDA receptor–adhesion protein signaling complexes. Nature neuroscience *3*, 661-669.

Hutagalung, A.H., and Novick, P.J. (2011). Role of Rab GTPases in membrane traffic and cell physiology. Physiological reviews *91*, 119-149.

Ito, I., Hidaka, H., and Sugiyama, H. (1991). Effects of KN-62, a specific inhibitor of calcium/calmodulin-dependent protein kinase II, on long-term potentiation in the rat hippocampus. Neuroscience letters *121*, 119-121.

Itoh, T., Satoh, M., Kanno, E., and Fukuda, M. (2006). Screening for target Rabs of TBC (Tre-2/Bub2/Cdc16) domain-containing proteins based on their Rab-binding activity. Genes to Cells *11*, 1023-1037.

Jackson, A.C., and Nicoll, R.A. (2011). The expanding social network of ionotropic glutamate receptors: TARPs and other transmembrane auxiliary subunits. Neuron *70*, 178-199.

Jackson, A.P., Flett, A., Smythe, C., Hufton, L., Wettey, F.R., and Smythe, E. (2003). Clathrin promotes incorporation of cargo into coated pits by activation of the AP2 adaptor μ2 kinase. The Journal of cell biology *163*, 231-236.

Jaffe, D.B., Fisher, S.A., and Brown, T.H. (1994). Confocal laser scanning microscopy reveals voltage-gated calcium signals within hippocampal dendritic spines. Journal of neurobiology *25*, 220-233.

Jonas, P., and Burnashev, N. (1995). Molecular mechanisms controlling calcium entry through AMPA-type glutamate receptor channels. Neuron *15*, 987-990.

Jordens, I., Fernandez-Borja, M., Marsman, M., Dusseljee, S., Janssen, L., Calafat, J., Janssen, H., Wubbolts, R., and Neefjes, J. (2001). The Rab7 effector protein RILP controls lysosomal transport by inducing the recruitment of dynein-dynactin motors. Current Biology *11*, 1680-1685.

Kalashnikova, E., Lorca, R.A., Kaur, I., Barisone, G.A., Li, B., Ishimaru, T., Trimmer, J.S., Mohapatra, D.P., and Díaz, E. (2010). SynDIG1: an activity-regulated, AMPA-receptor-interacting transmembrane protein that regulates excitatory synapse development. Neuron *65*, 80-93.

Kameyama, K., Lee, H.-K., Bear, M.F., and Huganir, R.L. (1998). Involvement of a postsynaptic protein kinase A substrate in the expression of homosynaptic long-term depression. Neuron *21*, 1163-1175.

Kask, K., Zamanillo, D., Rozov, A., Burnashev, N., Sprengel, R., and Seeburg, P.H. (1998). The AMPA receptor subunit GluR-B in its Q/R site-unedited form is not essential for brain development and function. Proceedings of the National Academy of Sciences *95*, 13777-13782.

Kato, A.S., Gill, M.B., Yu, H., Nisenbaum, E.S., and Bredt, D.S. (2010). TARPs differentially decorate AMPA receptors to specify neuropharmacology. Trends in neurosciences *33*, 241-248.

Kennedy, M.J., Davison, I.G., Robinson, C.G., and Ehlers, M.D. (2010). Syntaxin-4 defines a domain for activity-dependent exocytosis in dendritic spines. Cell *141*, 524-535.

Kessels, H.W., and Malinow, R. (2009). Synaptic AMPA receptor plasticity and behavior. Neuron *61*, 340-350.

Kim, E., and Sheng, M. (2004). PDZ domain proteins of synapses. Nature Reviews Neuroscience *5*, 771-781.

Kim, J.H., Liao, D., Lau, L.-F., and Huganir, R.L. (1998). SynGAP: a synaptic RasGAP that associates with the PSD-95/SAP90 protein family. Neuron *20*, 683-691.

Korkotian, E., and Segal, M. (1999). Release of calcium from stores alters the morphology of dendritic spines in cultured hippocampal neurons. Proceedings of the National Academy of Sciences *96*, 12068-12072.

Kott, S., Werner, M., Körber, C., and Hollmann, M. (2007). Electrophysiological properties of AMPA receptors are differentially modulated depending on the associated member of the TARP family. The Journal of neuroscience *27*, 3780-3789.

Krapivinsky, G., Medina, I., Krapivinsky, L., Gapon, S., and Clapham, D.E. (2004). SynGAP-MUPP1-CaMKII synaptic complexes regulate p38 MAP kinase activity and NMDA receptor-dependent synaptic AMPA receptor potentiation. Neuron *43*, 563-574.

Kristensen, A.S., Jenkins, M.A., Banke, T.G., Schousboe, A., Makino, Y., Johnson, R.C., Huganir, R., and Traynelis, S.F. (2011). Mechanism of Ca2+/calmodulin-dependent kinase II regulation of AMPA receptor gating. Nature neuroscience *14*, 727-735.

Kumar, A. (2011). Long-term potentiation at CA3–CA1 hippocampal synapses with special emphasis on aging, disease, and stress. Frontiers in aging neuroscience *3*, 7.

Lamprecht, R., and LeDoux, J. (2004). Structural plasticity and memory. Nature Reviews Neuroscience *5*, 45-54.

Lang, C., Barco, A., Zablow, L., Kandel, E.R., Siegelbaum, S.A., and Zakharenko, S.S. (2004). Transient expansion of synaptically connected dendritic spines upon induction of hippocampal long-term potentiation. Proceedings of the National Academy of Sciences of the United States of America *101*, 16665-16670.

Laroche, S., Jay, T.M., and Thierry, A.-M. (1990). Long-term potentiation in the prefrontal cortex following stimulation of the hippocampal CA1/subicular region. Neuroscience letters *114*, 184-190.

Lee, H.-K., Kameyama, K., Huganir, R.L., and Bear, M.F. (1998). NMDA induces long-term synaptic depression and dephosphorylation of the GluR1 subunit of AMPA receptors in hippocampus. Neuron *21*, 1151-1162.

Lee, H.-K., Takamiya, K., Han, J.-S., Man, H., Kim, C.-H., Rumbaugh, G., Yu, S., Ding, L., He, C., and Petralia, R.S. (2003). Phosphorylation of the AMPA receptor GluR1 subunit is required for synaptic plasticity and retention of spatial memory. Cell *112*, 631-643.

Lee, S.-J.R., Escobedo-Lozoya, Y., Szatmari, E.M., and Yasuda, R. (2009). Activation of CaMKII in single dendritic spines during long-term potentiation. Nature *458*, 299-304.

Lendvai, B., Stern, E.A., Chen, B., and Svoboda, K. (2000). Experience-dependent plasticity of dendritic spines in the developing rat barrel cortex in vivo. Nature *404*, 876-881.

Levy, W.B., and Steward, O. (1979). Synapses as associative memory elements in the hippocampal formation. Brain research *175*, 233-245.

Lin, C.-H., Yeh, S.-H., Lin, C.-H., Lu, K.-T., Leu, T.-H., Chang, W.-C., and Gean, P.-W. (2001). A role for the PI-3 kinase signaling pathway in fear conditioning and synaptic plasticity in the amygdala. Neuron *31*, 841-851.

Lin, D.-T., Makino, Y., Sharma, K., Hayashi, T., Neve, R., Takamiya, K., and Huganir, R.L. (2009). Regulation of AMPA receptor extrasynaptic insertion by 4.1 N, phosphorylation and palmitoylation. Nature neuroscience *12*, 879-887.

Ling, D.S., Benardo, L.S., Serrano, P.A., Blace, N., Kelly, M.T., Crary, J.F., and Sacktor, T.C. (2002). Protein kinase Mζ is necessary and sufficient for LTP maintenance. Nature neuroscience *5*, 295-296.

Lisman, J., Schulman, H., and Cline, H. (2002). The molecular basis of CaMKII function in synaptic and behavioural memory. Nature Reviews Neuroscience *3*, 175-190.

Lisman, J., Yasuda, R., and Raghavachari, S. (2012). Mechanisms of CaMKII action in long-term potentiation. Nature Reviews Neuroscience *13*, 169-182.

Liu, Y., Xu, X.-H., Chen, Q., Wang, T., Deng, C.-Y., Song, B.-L., Du, J.-L., and Luo, Z.-G. (2013). Myosin Vb controls biogenesis of post-Golgi Rab10 carriers during axon development. Nature communications *4*.

Lledo, P.-M., Hjelmstad, G.O., Mukherji, S., Soderling, T.R., Malenka, R.C., and Nicoll, R.A. (1995). Calcium/calmodulin-dependent kinase II and long-term potentiation

enhance synaptic transmission by the same mechanism. Proceedings of the National Academy of Sciences *92*, 11175-11179.

Lømo, T. (2003). The discovery of long-term potentiation. Philosophical Transactions of the Royal Society of London B: Biological Sciences *358*, 617-620.

Lovinger, D.M., Wong, K.L., Murakami, K., and Routtenberg, A. (1987). Protein kinase C inhibitors eliminate hippocampal long-term potentiation. Brain research *436*, 177-183.

Lu, W., Shi, Y., Jackson, A.C., Bjorgan, K., During, M.J., Sprengel, R., Seeburg, P.H., and Nicoll, R.A. (2009). Subunit composition of synaptic AMPA receptors revealed by a single-cell genetic approach. Neuron *62*, 254-268.

Lynch, G., Larson, J., Kelso, S., Barrionuevo, G., and Schottler, F. (1983). Intracellular injections of EGTA block induction of hippocampal long-term potentiation. Nature *305*, 719-721.

Makino, H., and Malinow, R. (2009). AMPA receptor incorporation into synapses during LTP: the role of lateral movement and exocytosis. Neuron *64*, 381-390.

Makino, Y., Johnson, R.C., Yu, Y., Takamiya, K., and Huganir, R.L. (2011). Enhanced synaptic plasticity in mice with phosphomimetic mutation of the GluA1 AMPA receptor. Proceedings of the National Academy of Sciences *108*, 8450-8455.

Malenka, R.C. (1988). Postsynaptic Calcium Is Suflicient for Potentiation of Hippocampal Synaptic Transmission.

Malenka, R.C. (2003). The long-term potential of LTP. Nature Reviews Neuroscience *4*, 923-926.

Malenka, R.C., Lancaster, B., and Zucker, R.S. (1992). Temporal limits on the rise in postsynaptic calcium required for the induction of long-term potentiation. Neuron *9*, 121-128.

Malenka, R.C., and Nicoll, R.A. (1999). Long-term potentiation--a decade of progress? Science *285*, 1870-1874.

Malinow, R., and Malenka, R.C. (2002). AMPA receptor trafficking and synaptic plasticity. Annual review of neuroscience *25*, 103-126.

Malinow, R., Schulman, H., and Tsien, R.W. (1989). Inhibition of postsynaptic PKC or CaMKII blocks induction but not expression of LTP. Science *245*, 862-866.

Man, H.-Y., Wang, Q., Lu, W.-Y., Ju, W., Ahmadian, G., Liu, L., D'Souza, S., Wong, T., Taghibiglou, C., and Lu, J. (2003). Activation of PI3-kinase is required for AMPA receptor insertion during LTP of mEPSCs in cultured hippocampal neurons. Neuron *38*, 611-624.

Manabe, T., Aiba, A., Yamada, A., Ichise, T., Sakagami, H., Kondo, H., and Katsuki, M. (2000). Regulation of long-term potentiation by H-Ras through NMDA receptor phosphorylation. The Journal of Neuroscience *20*, 2504-2511.

Matanis, T., Akhmanova, A., Wulf, P., Del Nery, E., Weide, T., Stepanova, T., Galjart, N., Grosveld, F., Goud, B., and De Zeeuw, C.I. (2002). Bicaudal-D regulates COPI-independent Golgi–ER transport by recruiting the dynein–dynactin motor complex. Nature Cell Biology *4*, 986-992.

Matsuzaki, M., Honkura, N., Ellis-Davies, G.C., and Kasai, H. (2004). Structural basis of long-term potentiation in single dendritic spines. Nature *429*, 761-766.

Matus, A. (2000). Actin-based plasticity in dendritic spines. Science *290*, 754-758.

Maxfield, F.R., and McGraw, T.E. (2004). Endocytic recycling. Nature reviews Molecular cell biology *5*, 121-132.

McAllister, A.K. (2000). Biolistic transfection of neurons. Science Signaling *2000*, pl1-pl1.

McLauchlan, H., Newell, J., Morrice, N., Osborne, A., West, M., and Smythe, E. (1998). A novel role for Rab5–GDI in ligand sequestration into clathrin-coated pits. Current Biology *8*, 34-45.

McNaughton, B.L., Douglas, R., and Goddard, G.V. (1978). Synaptic enhancement in fascia dentata: cooperativity among coactive afferents. Brain research *157*, 277-293.

MELLOR, H., and PARKER, P.J. (1998). The extended protein kinase C superfamily. Biochemical Journal *332*, 281-292.

Meng, Y., Zhang, Y., and Jia, Z. (2003). Synaptic transmission and plasticity in the absence of AMPA glutamate receptor GluR2 and GluR3. Neuron *39*, 163-176.

Miesenböck, G., De Angelis, D.A., and Rothman, J.E. (1998). Visualizing secretion and synaptic transmission with pH-sensitive green fluorescent proteins. Nature *394*, 192-195.

Mikuni, T., Nishiyama, J., Sun, Y., Kamasawa, N., and Yasuda, R. (2016). High-Throughput, High-Resolution Mapping of Protein Localization in Mammalian Brain by In Vivo Genome Editing. Cell.

Miller, S.G., and Kennedy, M.B. (1986). Regulation of brain Type II Ca2+ calmodulin-dependent protein kinase by autophosphorylation: A Ca 2+-triggered molecular switch. Cell *44*, 861-870.

Miyawaki, A. (2003). Visualization of the spatial and temporal dynamics of intracellular signaling. Developmental cell *4*, 295-305.

Mosbacher, J., Schöpfer, R., Monyer, H., Burnashev, N., Seeburg, P.H., and Ruppersberg, J.P. (1994). A molecular determinant for submillisecond desensitization in glutamate receptors. SCIENCE-NEW YORK THEN WASHINGTON-, 1059-1059.

Murakoshi, H., Lee, S.-J., and Yasuda, R. (2008). Highly sensitive and quantitative FRET–FLIM imaging in single dendritic spines using improved non-radiative YFP. Brain cell biology *36*, 31-42.

Murakoshi, H., Wang, H., and Yasuda, R. (2011). Local, persistent activation of Rho GTPases during plasticity of single dendritic spines. Nature *472*, 100-104.

Nicoll, R.A., and Malenka, R.C. (1995). Contrasting properties of two forms of long-term potentiation in the hippocampus.

Nicoll, R.A., and Roche, K.W. (2013). Long-term potentiation: peeling the onion. Neuropharmacology *74*, 18-22.

Nicoll, R.A., Tomita, S., and Bredt, D.S. (2006). Auxiliary subunits assist AMPA-type glutamate receptors. Science *311*, 1253-1256.

Nielsen, E., Christoforidis, S., Uttenweiler-Joseph, S., Miaczynska, M., Dewitte, F., Wilm, M., Hoflack, B., and Zerial, M. (2000). Rabenosyn-5, a novel Rab5 effector, is complexed with hVPS45 and recruited to endosomes through a FYVE finger domain. The Journal of cell biology *151*, 601-612.

Nikandrova, Y.A., Jiao, Y., Baucum, A.J., Tavalin, S.J., and Colbran, R.J. (2010). Ca2+/calmodulin-dependent protein kinase II binds to and phosphorylates a specific SAP97 splice variant to disrupt association with AKAP79/150 and modulate α-amino-3-hydroxy-5-methyl-4-isoxazolepropionic acid-type glutamate receptor (AMPAR) activity. Journal of Biological Chemistry *285*, 923-934.

Nimchinsky, E.A., Sabatini, B.L., and Svoboda, K. (2002). Structure and function of dendritic spines. Annual review of physiology *64*, 313-353.

Nimchinsky, E.A., Yasuda, R., Oertner, T.G., and Svoboda, K. (2004). The number of glutamate receptors opened by synaptic stimulation in single hippocampal spines. The Journal of neuroscience *24*, 2054-2064.

Nishiyama, J., and Yasuda, R. (2015). Biochemical computation for spine structural plasticity. Neuron *87*, 63-75.

Noebels, J., Qiao, X., Bronson, R., Spencer, C., and Davisson, M. (1990). Stargazer: a new neurological mutant on chromosome 15 in the mouse with prolonged cortical seizures. Epilepsy research *7*, 129-135.

Oh, W.C., Parajuli, L.K., and Zito, K. (2015). Heterosynaptic structural plasticity on local dendritic segments of hippocampal CA1 neurons. Cell reports *10*, 162-169.

Oliveira, A.F., and Yasuda, R. (2014). Neurofibromin is the major ras inactivator in dendritic spines. The Journal of Neuroscience *34*, 776-783.

Opazo, P., Sainlos, M., and Choquet, D. (2012). Regulation of AMPA receptor surface diffusion by PSD-95 slots. Current opinion in neurobiology *22*, 453-460.

Park, M., Penick, E.C., Edwards, J.G., Kauer, J.A., and Ehlers, M.D. (2004). Recycling endosomes supply AMPA receptors for LTP. Science *305*, 1972-1975.

Passafaro, M., Piëch, V., and Sheng, M. (2001). Subunit-specific temporal and spatial patterns of AMPA receptor exocytosis in hippocampal neurons. Nature neuroscience *4*, 917-926.

Pastalkova, E., Serrano, P., Pinkhasova, D., Wallace, E., Fenton, A.A., and Sacktor, T.C. (2006). Storage of spatial information by the maintenance mechanism of LTP. Science *313*, 1141-1144.

Patterson, M., and Yasuda, R. (2011). Signalling pathways underlying structural plasticity of dendritic spines. British journal of pharmacology *163*, 1626-1638.

Patterson, M.A., Szatmari, E.M., and Yasuda, R. (2010). AMPA receptors are exocytosed in stimulated spines and adjacent dendrites in a Ras-ERK–dependent manner during long-term potentiation. Proceedings of the National Academy of Sciences *107*, 15951-15956.

Pereira-Leal, J.B., and Seabra, M.C. (2001). Evolution of the Rab family of small GTP-binding proteins. Journal of molecular biology *313*, 889-901.

Peters, A., and Kaiserman-Abramof, I.R. (1969). The small pyramidal neuron of the rat cerebral cortex. Zeitschrift für Zellforschung und mikroskopische Anatomie *100*, 487-506.

Pettit, D., Perlman, S., and Malinow, R. (1994). Potentiated transmission and prevention of further LTP by increased CaMKII activity in postsynaptic hippocampal slice neurons. Science *266*, 1881.

Pfeffer, S., and Aivazian, D. (2004). Targeting Rab GTPases to distinct membrane compartments. Nature reviews Molecular cell biology *5*, 886-896.

Platt, S.R. (2007). The role of glutamate in central nervous system health and disease–a review. The Veterinary Journal *173*, 278-286.

Purves, D., Augustine, G.J., Fitzpatrick, D., Hall, W.C., LaMantia, A.-S., McNamara, J.O., and Williams, S. (2004). Neuroscience. Massachusetts. Publishers Sunderland.

Reymann, K.G., Frey, U., Jork, R., and Matthies, H. (1988). Polymyxin B, an inhibitor of protein kinase C, prevents the maintenance of synaptic long-term potentiation in hippocampal CA1 neurons. Brain research *440*, 305-314.

Roberts, T.F., Tschida, K.A., Klein, M.E., and Mooney, R. (2010). Rapid spine stabilization and synaptic enhancement at the onset of behavioural learning. Nature *463*, 948-952.

Salin, P.A., Malenka, R.C., and Nicoll, R.A. (1996). Cyclic AMP mediates a presynaptic form of LTP at cerebellar parallel fiber synapses. Neuron *16*, 797-803.

Sanhueza, M., Fernandez-Villalobos, G., Stein, I.S., Kasumova, G., Zhang, P., Bayer, K.U., Otmakhov, N., Hell, J.W., and Lisman, J. (2011). Role of the CaMKII/NMDA receptor complex in the maintenance of synaptic strength. The Journal of Neuroscience *31*, 9170-9178.

Sano, H., Eguez, L., Teruel, M.N., Fukuda, M., Chuang, T.D., Chavez, J.A., Lienhard, G.E., and McGraw, T.E. (2007). Rab10, a target of the AS160 Rab GAP, is required for

insulin-stimulated translocation of GLUT4 to the adipocyte plasma membrane. Cell metabolism *5*, 293-303.

Schuck, S., Gerl, M.J., Ang, A., Manninen, A., Keller, P., Mellman, I., and Simons, K. (2007). Rab10 is involved in basolateral transport in polarized Madin–Darby canine kidney cells. Traffic *8*, 47-60.

Schwenk, J., Harmel, N., Zolles, G., Bildl, W., Kulik, A., Heimrich, B., Chisaka, O., Jonas, P., Schulte, U., and Fakler, B. (2009). Functional proteomics identify cornichon proteins as auxiliary subunits of AMPA receptors. Science *323*, 1313-1319.

Seibenhener, M.L., and Wooten, M.W. (2012). Isolation and culture of hippocampal neurons from prenatal mice. JoVE (Journal of Visualized Experiments), e3634-e3634.

Selcher, J.C., Atkins, C.M., Trzaskos, J.M., Paylor, R., and Sweatt, J.D. (1999). A necessity for MAP kinase activation in mammalian spatial learning. Learning & Memory *6*, 478-490.

Selcher, J.C., Weeber, E.J., Christian, J., Nekrasova, T., Landreth, G.E., and Sweatt, J.D. (2003). A role for ERK MAP kinase in physiologic temporal integration in hippocampal area CA1. Learning & Memory *10*, 26-39.

Semerdjieva, S., Shortt, B., Maxwell, E., Singh, S., Fonarev, P., Hansen, J., Schiavo, G., Grant, B.D., and Smythe, E. (2008). Coordinated regulation of AP2 uncoating from clathrin-coated vesicles by rab5 and hRME-6. The Journal of cell biology *183*, 499-511.

Sheng, M., and Kim, M.J. (2002). Postsynaptic signaling and plasticity mechanisms. Science *298*, 776-780.

Sheng, M., and Lee, S.H. (2001). AMPA receptor trafficking and the control of synaptic transmission. Cell *105*, 825-828.

Shi, S.-H., Hayashi, Y., Esteban, J.A., and Malinow, R. (2001). Subunit-specific rules governing AMPA receptor trafficking to synapses in hippocampal pyramidal neurons. Cell *105*, 331-343.

Shi, S.-H., Hayashi, Y., Petralia, R.S., Zaman, S.H., Wenthold, R.J., Svoboda, K., and Malinow, R. (1999). Rapid spine delivery and redistribution of AMPA receptors after synaptic NMDA receptor activation. Science *284*, 1811-1816.

Shin, H.-W., Hayashi, M., Christoforidis, S., Lacas-Gervais, S., Hoepfner, S., Wenk, M.R., Modregger, J., Uttenweiler-Joseph, S., Wilm, M., and Nystuen, A. (2005). An enzymatic cascade of Rab5 effectors regulates phosphoinositide turnover in the endocytic pathway. The Journal of cell biology *170*, 607-618.

Sholl, D.A. (1956). The organization of the cerebral cortex.

Silva, A.J., Paylor, R., Wehner, J.M., and Tonegawa, S. (1992a). Impaired spatial learning in alpha-calcium-calmodulin kinase II mutant mice. Science *257*, 206-211.

Silva, A.J., Stevens, C.F., Tonegawa, S., and Wang, Y. (1992b). Deficient hippocampal long-term potentiation in alpha-calcium-calmodulin kinase II mutant mice. Science *257*, 201-206.

Simonsen, A., Lippe, R., Christoforidis, S., Gaullier, J.-M., Brech, A., Callaghan, J., Toh, B.-H., Murphy, C., Zerial, M., and Stenmark, H. (1998). EEA1 links PI (3) K function to Rab5 regulation of endosome fusion. Nature *394*, 494-498.

Sobolevsky, A.I., Rosconi, M.P., and Gouaux, E. (2009). X-ray structure, symmetry and mechanism of an AMPA-subtype glutamate receptor. Nature *462*, 745-756.

Sommer, B., Keinanen, K., Verdoorn, T.A., Wisden, W., Burnashev, N., Herb, A., Kohler, M., Takagi, T., Sakmann, B., and Seeburg, P.H. (1990). Flip and flop: a cell-specific functional switch in glutamate-operated channels of the CNS. Science *249*, 1580-1585.

Song, I., and Huganir, R.L. (2002). Regulation of AMPA receptors during synaptic plasticity. Trends in neurosciences *25*, 578-588.

Sönnichsen, B., De Renzis, S., Nielsen, E., Rietdorf, J., and Zerial, M. (2000). Distinct membrane domains on endosomes in the recycling pathway visualized by multicolor imaging of Rab4, Rab5, and Rab11. The Journal of cell biology *149*, 901-914.

Spruston, N. (2008). Pyramidal neurons: dendritic structure and synaptic integration. Nature Reviews Neuroscience *9*, 206-221.

Star, E.N., Kwiatkowski, D.J., and Murthy, V.N. (2002). Rapid turnover of actin in dendritic spines and its regulation by activity. Nature neuroscience *5*, 239-246.

Stenmark, H. (2009). Rab GTPases as coordinators of vesicle traffic. Nature reviews Molecular cell biology *10*, 513-525.

Stern-Bach, Y., Bettler, B., Hartley, M., Sheppard, P.O., O'Hara, P.J., and Heinemann, S.F. (1994). Agonist selectivity of glutamate receptors is specified by two domains structurally related to bacterial amino acid-binding proteins. Neuron *13*, 1345-1357.

Stoppini, L., Buchs, P.-A., and Muller, D. (1991). A simple method for organotypic cultures of nervous tissue. Journal of neuroscience methods *37*, 173-182.

Strack, S., Robison, A.J., Bass, M.A., and Colbran, R.J. (2000). Association of calcium/calmodulin-dependent kinase II with developmentally regulated splice variants of the postsynaptic density protein densin-180. Journal of Biological Chemistry *275*, 25061-25064.

Straub, C., and Tomita, S. (2012). The regulation of glutamate receptor trafficking and function by TARPs and other transmembrane auxiliary subunits. Current opinion in neurobiology *22*, 488-495.

Stripling, J.S., Patneau, D.K., and Gramlich, C.A. (1988). Selective long-term potentiation in the pyriform cortex. Brain research *441*, 281-291.

Svoboda, K., Denk, W., Kleinfeld, D., and Tank, D.W. (1997). In vivo dendritic calcium dynamics in neocortical pyramidal neurons. Nature *385*, 161-165.

Takahashi, N., Kitamura, K., Matsuo, N., Mayford, M., Kano, M., Matsuki, N., and Ikegaya, Y. (2012). Locally synchronized synaptic inputs. Science *335*, 353-356.

Takahashi, N., Sawada, W., Noguchi, J., Watanabe, S., Ucar, H., Hayashi-Takagi, A., Yagishita, S., Ohno, M., Tokumaru, H., and Kasai, H. (2015). Two-photon fluorescence lifetime imaging of primed SNARE complexes in presynaptic terminals and [beta] cells. Nature communications *6*.

Tomita, S., Chen, L., Kawasaki, Y., Petralia, R.S., Wenthold, R.J., Nicoll, R.A., and Bredt, D.S. (2003). Functional studies and distribution define a family of transmembrane AMPA receptor regulatory proteins. The Journal of cell biology *161*, 805-816.

Tomita, S., Stein, V., Stocker, T.J., Nicoll, R.A., and Bredt, D.S. (2005). Bidirectional synaptic plasticity regulated by phosphorylation of stargazin-like TARPs. Neuron *45*, 269-277.

Trachtenberg, J.T., Chen, B.E., Knott, G.W., Feng, G., Sanes, J.R., Welker, E., and Svoboda, K. (2002). Long-term in vivo imaging of experience-dependent synaptic plasticity in adult cortex. Nature *420*, 788-794.

Traynelis, S.F., Wollmuth, L.P., McBain, C.J., Menniti, F.S., Vance, K.M., Ogden, K.K., Hansen, K.B., Yuan, H., Myers, S.J., and Dingledine, R. (2010). Glutamate receptor ion channels: structure, regulation, and function. Pharmacological reviews *62*, 405-496.

van der Sluijs, P., Hull, M., Webster, P., Mâle, P., Goud, B., and Mellman, I. (1992). The small GTP-binding protein rab4 controls an early sorting event on the endocytic pathway. Cell *70*, 729-740.

Von Engelhardt, J., Mack, V., Sprengel, R., Kavenstock, N., Li, K.W., Stern-Bach, Y., Smit, A.B., Seeburg, P.H., and Monyer, H. (2010). CKAMP44: a brain-specific protein attenuating short-term synaptic plasticity in the dentate gyrus. Science *327*, 1518-1522.

von Kleist, L., Stahlschmidt, W., Bulut, H., Gromova, K., Puchkov, D., Robertson, M.J., MacGregor, K.A., Tomilin, N., Pechstein, A., and Chau, N. (2011). Role of the clathrin terminal domain in regulating coated pit dynamics revealed by small molecule inhibition. Cell *146*, 471-484.

Walikonis, R.S., Oguni, A., Khorosheva, E.M., Jeng, C.-J., Asuncion, F.J., and Kennedy, M.B. (2001). Densin-180 forms a ternary complex with the α-subunit of Ca2+/calmodulin-dependent protein kinase II and α-actinin. The Journal of Neuroscience *21*, 423-433.

Wang, J.-h., and Feng, D.-P. (1992). Postsynaptic protein kinase C essential to induction and maintenance of long-term potentiation in the hippocampal CA1 region. Proceedings of the National Academy of Sciences *89*, 2576-2580.

Wang, T., Liu, Y., Xu, X.-H., Deng, C.-Y., Wu, K.-Y., Zhu, J., Fu, X.-Q., He, M., and Luo, Z.-G. (2011). Lgl1 activation of rab10 promotes axonal membrane trafficking underlying neuronal polarization. Developmental cell *21*, 431-444.

Wang, Z., Edwards, J.G., Riley, N., Provance, D.W., Karcher, R., Li, X.-d., Davison, I.G., Ikebe, M., Mercer, J.A., and Kauer, J.A. (2008). Myosin Vb mobilizes recycling endosomes and AMPA receptors for postsynaptic plasticity. Cell *135*, 535-548.

Wenthold, R.J., Petralia, R.S., and Niedzielski, A. (1996). Evidence for multiple AMPA receptor complexes in hippocampal CA1/CA2 neurons. The Journal of neuroscience *16*, 1982-1989.

Wu, X.S., Rao, K., Zhang, H., Wang, F., Sellers, J.R., Matesic, L.E., Copeland, N.G., Jenkins, N.A., and Hammer, J.A. (2002). Identification of an organelle receptor for myosin-Va. Nature cell biology *4*, 271-278.

Wymann, M.P., and Pirola, L. (1998). Structure and function of phosphoinositide 3-kinases. Biochimica et Biophysica Acta (BBA)-Molecular and Cell Biology of Lipids *1436*, 127-150.

Xie, Z., Srivastava, D.P., Photowala, H., Kai, L., Cahill, M.E., Woolfrey, K.M., Shum, C.Y., Surmeier, D.J., and Penzes, P. (2007). Kalirin-7 controls activity-dependent structural and functional plasticity of dendritic spines. Neuron *56*, 640-656.

Xu, T., Yu, X., Perlik, A.J., Tobin, W.F., Zweig, J.A., Tennant, K., Jones, T., and Zuo, Y. (2009). Rapid formation and selective stabilization of synapses for enduring motor memories. Nature *462*, 915-919.

y Cajal, S.R. (1888). Estructura de los centros nerviosos de las aves.

y Cajal, S.R. (1934). Les preuves objetives de l´unité anatomique des cellules nerveuses.

Yasuda, R. (2006). Imaging spatiotemporal dynamics of neuronal signaling using fluorescence resonance energy transfer and fluorescence lifetime imaging microscopy. Current opinion in neurobiology *16*, 551-561.

Yasuda, R. (2012). Studying signal transduction in single dendritic spines. Cold Spring Harbor perspectives in biology *4*, a005611.

Yasuda, R., Harvey, C.D., Zhong, H., Sobczyk, A., Van Aelst, L., and Svoboda, K. (2006). Supersensitive Ras activation in dendrites and spines revealed by two-photon fluorescence lifetime imaging. Nature neuroscience *9*, 283-291.

Yoshihara, Y., De Roo, M., and Muller, D. (2009). Dendritic spine formation and stabilization. Current opinion in neurobiology *19*, 146-153.

Yoshimura, S.-i., Gerondopoulos, A., Linford, A., Rigden, D.J., and Barr, F.A. (2010). Family-wide characterization of the DENN domain Rab GDP-GTP exchange factors. The Journal of cell biology *191*, 367-381.

Zamanillo, D., Sprengel, R., Hvalby, Ø., Jensen, V., Burnashev, N., Rozov, A., Kaiser, K.M., Köster, H.J., Borchardt, T., and Worley, P. (1999). Importance of AMPA receptors for hippocampal synaptic plasticity but not for spatial learning. Science *284*, 1805-1811.

Zerial, M., and McBride, H. (2001). Rab proteins as membrane organizers. Nature reviews Molecular cell biology *2*, 107-117.

Zhai, S., Ark, E.D., Parra-Bueno, P., and Yasuda, R. (2013). Long-distance integration of nuclear ERK signaling triggered by activation of a few dendritic spines. Science *342*, 1107-1111.

Zhu, J.J., Esteban, J.A., Hayashi, Y., and Malinow, R. (2000). Postnatal synaptic potentiation: delivery of GluR4-containing AMPA receptors by spontaneous activity. Nature neuroscience *3*, 1098-1106.

Zhu, J.J., Qin, Y., Zhao, M., Van Aelst, L., and Malinow, R. (2002). Ras and Rap control AMPA receptor trafficking during synaptic plasticity. Cell *110*, 443-455.

Zoncu, R., Perera, R.M., Sebastian, R., Nakatsu, F., Chen, H., Balla, T., Ayala, G., Toomre, D., and De Camilli, P.V. (2007). Loss of endocytic clathrin-coated pits upon acute depletion of phosphatidylinositol 4, 5-bisphosphate. Proceedings of the National Academy of Sciences *104*, 3793-3798.

Zou, W., Yadav, S., DeVault, L., Jan, Y.N., and Sherwood, D.R. (2015). RAB-10-dependent membrane transport is required for dendrite arborization. PLoS Genet *11*, e1005484.

Zuo, Y., Lin, A., Chang, P., and Gan, W.-B. (2005). Development of long-term dendritic spine stability in diverse regions of cerebral cortex. Neuron *46*, 181-189.

Biography

Jie Wang

Birthplace

Yangzhou, Jiangsu Province, China January 18th, 1988

Education

Ph.D in Neurobiology

Duke University, Durham, NC, USA August, 2010 - December, 2016

B.S. in Biological Sciences

Tsinghua University, Beijing, China August, 2006 - July, 2010

Publications

- **Wang, J**., Szatmari, E.M., Liu, X., Nishiyama, J., and Yasuda, R. (2016) Rab4 and Rab10 oppositely regulate AMPA receptors exocytosis and structural plasticity in single dendritic spines.(in preparation)
- Shao, L., Shuai, Y., **Wang, J**., Feng, S., Lu, B., Li, Z., Zhao, Y., Wang, L., and Zhong, Y. (2011). Schizophrenia susceptibility gene *dysbindin* regulates glutamatergic and dopaminergic functions via distinctive mechanisms in *Drosophila*. *Proceedings of the National Academy of Sciences* 108, 18831-18836.

Honors and Awards

Duke University Graduate School Conference Travel Fellowship 2010 - 2012

POSCO Asia Fellowship 2007

Teaching Experience

TA in Neurobiology course, Marine Biological Laboratory 2014